Title

CVD-Assisted Carbon-Coating on Titanium-Based Silicate Anode Material for Lithium-Ion and Sodium-Ion Batteries

Author

Kong, Dejia

Publication Date

2020

UNIVERSITY OF CALIFORNIA

Los Angeles

CVD-Assisted Carbon-Coating on Titanium-Based Silicate Anode Material for Lithium-Ion and Sodium-Ion Batteries

A dissertation submitted in partial satisfaction of the
requirements for the degree Doctor of Philosophy
in Chemical Engineering

by

Dejia Kong

2020

ABSTRACT OF THE DISSERTATION

CVD-Assisted Carbon-Coating on Titanium-Based Silicate Anode Material for Lithium-Ion and Sodium-Ion Batteries

by

Dejia Kong

Doctor of Philosophy Candidate in Chemical Engineering

University of California, Los Angeles, 2020

Professor Yunfeng Lu, Co-Chair

Professor Philippe Sautet, Co-Chair

The communication between humanity and energy sources reflects the evolution of human society. As the landmark of history, from the awe of the prehistoric man about the fire to the steam's popularization in the industrial revolution, different kinds of energy play an unparalleled role in the development of technology. Up to time now, electricity, the ultimate energy source in existence, powers the development of civilizations. Meanwhile, with the more urgent request for

improving the quality of life, higher energy consumption, and more diverse forms of energy storage systems (ESS) are integrated into the world.

Among all the various ESS, the battery received considerable attention because of its high theoretical energy density, the feasibility of current technology, and applicability for different fields. Whereas, the significant issues rest on the sluggish reaction kinetics of electrode materials during fast charging and discharging process. For instance, graphite is the most used anode material for lithium-ion batteries because it has economical production cost and considerable energy density (theoretical capacity: 372 mAh g^{-1}, discharge plateau: ~ 0.1 V *vs*. Li^+/Li). When employed as high-power batteries, however, graphite shows inadequate endurance with rapid fading of its capacity and delivers reduced capacity. The uncontrollable growth of lithium dendrite will also cause safety problems, particularly at high charging current density.

In order to fill the vacancy of the desired high-rate anode candidate, titanium-based materials acquire numerous studies. The most representative candidate is $Li_4Ti_5O_{12}$ (LTO), which has been widely studied and commercialized. In respect that LTO has “zero strain” physical property, its cycling stability is exceptionally long, compared with other carbon-based anodic materials. However, low electronic conductivity (10^{-8} S cm^{-1}), slow ionic diffusivity, low theoretical capacity (175 mAh g^{-1}), and high operational voltage (1.55 V *vs*. Li^+/Li) limit its performance and further development in the matter of power batteries. By contrast, another member from titanium-based materials, lithium titanium silicate (Li_2TiSiO_5, LTSO), offers an intriguing theoretical capacity of 308 mAh g^{-1} and a low potential of 0.28 V *vs*. Li^+/Li.

Nevertheless, inherent properties like low electric and ionic conductivity are still tangling the growth of such materials in power lithium-ion batteries. For the improvement of these drawbacks, using carbon composites and nanocrystallizations is simple and effective.

Nevertheless, they bring new issues like low tap density, low initial coulombic efficiency, and complex synthesis. In brief, there is a conflict between the total amount of carbon materials (for conductivity enhancement), particle size (for ionic diffusivity improvement), and tap density (effect on volumetric energy density), initial coulombic efficiency (related to specific surface area).

In this dissertation, we first designed a chemical vapor deposition (CVD)-assisted synthetic strategy to achieve conductive carbon-coating over the surface of fumed-silica and transform the catalysts to LTSO for high-rate anode material of lithium-ion batteries. The application of CVD allows the steerable carbon content and uniform surface carbon growing to compensate for the low conductivity. With optimized carbon content (2.35 wt.%), the obtained LTSO carbon composite could deliver desirable high-rate performance (~ 100 mAh g^{-1} at 15 C, where 1 C = 300 mA g^{-1}), which is comparable with commercialized LTO.

In consideration of using nanosized particles (fumed-silica, with 20-30 nm primary structure), the current state needs to advance regarding the tap density and initial coulombic efficiency. Thereupon we proposed a novel tactic for CVD-assisted *in-situ* graphitic carbon-coating by employing the dual functional material, LTSO, with both catalytic and electrochemical activity. The catalytic ability of LTSO render the hierarchical structural design with microsphere particulate, which guarantees the tap density at 1.3 g ml^{-1}. The optimized thin layer (15 nm) conductive carbon-coating, with only 3.5 wt.%, dramatically improves the conductivity form ~ 10^{-7} S m^{-1} to ~ 10^{3} S m^{-1}. After incorporating all the advantages, carbon-coated LTSO reveals a superior graphite-like volumetric capacity of 441.1 mAh cm^{-3} and $Li_4Ti_5O_{12}$-like rate capability (120.1 mAh cm^{-3} at 4.5 A g^{-1}).

Based on the attained understanding of LTSO, we then started the exploration of relative titanium-based silicate in sodium-ion batteries (Na_2TiSiO_5, NTSO) as anode candidate. By using inexpensive materials (fumed-silica and P-25) and facilities (ball milling), the obtained NTSO is very practicable for large-scale production. Benefited from the similar catalytic ability as it of LTSO, NTSO carbon composite shows promising performance with excellent cycling stability (100 mAh g^{-1} at 100 mA g^{-1} and 90% capacity retention after 3000 cycles).

The dissertation of Dejia Kong is under review by,

Vasilios Manousiouthakis

Yang Yang

Yunfeng Lu, Committee Co-Chair

Philippe Sautet, Committee Co-Chair

University of California, Los Angeles

2020

To my stunning wife S. Zhang, my lovely son Ryan, my parents J. Qian and L. Kong, and the future of myself

Table of Contents

List of Figures

List of Tables

Acknowledgment

Recalling my past several years at UCLA, I feel a strong sense of achievement. It is not because I will accomplish my program and acquire a doctorate, but I have gone through the journey, learned a lot, and experienced a lot. When I was pursuing my goal on this trip, I can see the light, but far away from my beginning. The road is rugged, dim all around, and I do not know where this road will take me. I used to feel frustrated, unconfident and lost. I can get here today is not because I am tough, but the people who are helping me; are supporting me and always by my side.

The first and most important person I met on my journey is my advisor, Professor Yunfeng Lu. As a mentor, he taught me how to effectively and concisely demonstrate my idea, meticulously and adequately design the experiment, and scientifically and systematically solve the problem. These competencies are so critical that they will benefit me for the rest of my life. As a third parent, his sagaciousness, patience, inspiration, and encouragement, made me understand many truths about being a respectable person. He impressed me the most because trust is mutual, and you need to earn it by proving yourself, but not asking it without doing anything. Stop settling in your comfort zone, start trying, start failing, and start improving yourself. I was wet behind the ears until I met him and experienced the real world. I am indebted to him for his guidance and support. I want to express my heartfelt thanks here. No matter how far apart we are, I will bear in mind your edification.

I want to thank my committee members, Professor Philippe Sautet, Professor Vasilios Manousiouthakis, and Professor Yang Yang, for their practical advice on my research and dissertation.

I want to present a special thanks to Dr. Li Shen and Dr. Runwei Mo for their guidance on my projects. It would be pretty tough for me to overcome all the hardships without your support and help. I also like to express appreciation to Dr. Gen Chen, Dr. Haobin Wu, Dr. Lu Zhang, Dr. Zhuang Liu, Dr. Fang Liu, Dr. Duo Xu, Dr. Gurong Shen, Dr. Zaiyuan Le, and Dr. Xiangyang Li for their helpful advice and support. Professor Bin Xu, Dr. Haiping Wu, Dr. Xiao Zhu, Dr. Seung Ho Choi, Dr. Zhiyong Wang, and Dr. Hui Liu, thank you for accompanying me through your visit. It is my pleasure to meet you and work with you at UCLA.

I want to take the opportunity to thank my peers in our lab, Dr. Shengxiang Ma, Dr. Ran Tao, Dr. Wenyue Shi, Chen Zhang, Xing Lu, Xinru Li, Jinhui Xu, and Xinyi Tan, for their assistance on various experiments and helpful discussions. I also want to thank all other colleagues in our lab, Pengcheng Xu, Jie Ren, Dr. Jesse Baucom, Dr. Fan Li, Roxanne Castillo, Zheng Cao, Shilin Chen, Bowen An, Qingyang Yin, and Tong Qi, for their efforts of creating a relaxing and friendly atmosphere.

I am deeply grateful for everything my parents have done for me. They give their all to create better conditions for my growth and future. They never asked for anything in return, but keep giving me their time and their love. This dissertation is dedicated to my family.

Furthermore, above all, I want to thank Shuting, the love of my life. Without your support and love, I would not be here today. I appreciate your patience, silently waiting, the long waiting, waiting for my triumph. I will remember all you have done for me. I shall stake all I have to fend you and our lovely Ryan. I love you.

VITA

2010 – 2014	B.S., College of Chemistry Dalian University of Technology, China
2014 – 2016	M.S., Chemical Engineering Department Columbia University in the City of New York, USA
2016 – 2020	Graduate Researcher, Teaching Assistant, Graduate Division Award Department of Chemical and Biomolecular Engineering University of California, Los Angeles, USA

Publications

1. **D. Kong**, L. Shen*, R. Mo, J. Liu, R. Tao, W. Shi, S. Ma, C. Zhang, Y. Lu*. CVD-Assisted Fabrication of Hierarchical Microparticulate Li_2TiSiO_5-Carbon Nanospheres for Ultrafast Lithium Storage. *Nanoscale*, 2020, 12, 13918-13925.
2. R. Mo, X. Tan, F. Li, R. Tao, J. Xu, **D. Kong**, Z. Wang, B. Xu, X. Wang, C. Wang, J. Li, Y. Peng*, Y. Lu*. Tin-graphene tubes as anodes for lithium-ion batteries with high volumetric and gravimetric energy densities. *Nature Communications*, 2020, 11, 1374.
3. H. Wu, X. Lu, **D. Kong**, L. Shen,* Y. Lu*. Facilitating Lithium-Ion Conduction in Gel Polymer Electrolyte by Metal-Organic Frameworks. *ACS Material Letter*. (Under review)
4. L. Shen,* X. Li, X. Lu, **D. Kong**, A. Fortini, C. Zhang, Y. Lu*. Semiliquid Electrolytes with Anion-Adsorbing Metal-Organic Frameworks for High-Rate Lithium Batteries. *Chemical Communication*. (Under review)

Chapter 1. Introduction and background

1.1 Energy and energy storage systems

1.1.1 History of energy

Energy plays a critical role in human history as a source of energy, a sense of safety, and a historic milestone of evolution. With the development of technology, people are relying more on energy and using it to explore the universe further, seeking the truth of life.

Three hundred thousand years ago, when the Homo sapiens became distinguished from Homo erectus, the first energy era started. The era sustained until the beginning of stable societies nearly 10,000 years ago.[1] Throughout prehistory, all efforts to control higher energy flows were plugged by the low power of humans and by the ineffective use of fire. Acclimatization of draft animals and utilizing of fire for producing metals and other durable materials instituted the first excellent energy transition: reliance on these extra somatic energies had raised energy quantity of preindustrial societies by ten times higher.[2]

The second transition got underway only several thousand years later; it was not as general as the initial one, and its impacts made a thoughtful, and relatively early, the variance only in some places: it came as some outdated societies replaced large shares of their human resources by waterwheels and windmills, ingenious but straightforward inanimate prime movers that were designed to convert the two typical renewable energy flows with growing power and efficiency.[1,2]

The third admirable energy transition (substitution of animate prime movers by engines and biomass energies by fossil fuels) began only several centuries ago in a few European countries, and all industrialized nations accomplished it through the 20th century. That transition is up till now to run its course in most low-income economies, particularly in Africa. The latest energy transition has been underway since 1882 when the world's first electricity-generating stations were established in London, New York, and Appleton, Wisconsin (the first hydroelectric station).[1] From then on, all modernizing countries have been consuming increasing shares of their fossil fuels circuitously as electricity and introducing new methods of primary electricity generation to increase the overall production of this most adaptable and most expedient form of energy. The second key feature of this transition has been a firm relative withdrawal of coal reflected by the rise of hydrocarbons, first crude oil and later natural gas.[2]

Refining the quality of life has been the primary individual benefit of this pursuit for higher energy use that has brought augmented food harvests, a more significant accumulation of personal possessions, the profusion of educational opportunities, and massively enhanced personal mobility.[1] The increase of the world's population, the growing economic might of nations, the extension of military abilities, the development of world trade, and the globalization of human affairs have been the vital joint consequences of the quest.[2]

1.1.2 Energy storage systems

Energy systems play a crucial role in garnering energy from various sources and converting it to the energy forms required for applications in various divisions, e.g., utility, industry, building, and transportation.[3] Energy sources like fossil fuels can be used to provide energy according to customer demand, i.e., they are readily storable when not required. However, other sources such as solar and wind energy need to be harvested when available and stored until needed. Employing energy storage can provide several advantages for energy systems, such as permitting increased penetration of renewable energy and better economic performance. Also, energy storage is essential to electrical systems, allowing for load leveling and peak shaving, frequency regulation, damping energy oscillations, and improving power quality and reliability.

Energy storage systems have been used for centuries and undergone continual improvements to reach their present levels of development, which for many storage types, is mature. So far, there are a lot of different types of energy storage systems on the stage, which can be classified as multiple categories. For instance, features of electrochemical energy storage types, according to specific energy and power, are often summarized in the “Ragone plot,” which helps recognize the potentials of each storage type and contrast them for applications requiring varying energy storage capacities and on-demand energy extraction rates.[4] The plot also helps to pick the most suitable energy storage for particular applications or demands (**Figure 1-1**). Energy density means the amount of energy stored for a given system or space, and power density is the energy transfer rate per unit volume or mass. When produced energy is over demands and will not be consumed in the short term, an energy storage device with a high energy density that can store excess power is required. When the charging/discharging current is high, and charge/discharge fluctuations over short periods are frequent, a high-power density device is desired. Energy storage systems also can be classified based on the storage period. Short-term energy storage typically involves the storage of energy for hours to days, while long-term storage refers to the storage of energy from a few months to a season (3 to 6 months). For instance, long-term thermal energy storage retains thermal energy in the ground over the summer for use in winter. It should be emphasized that only a few types of energy storage systems are shown in Figure 1-1 since the Ragone plot is commonly used for capacitors, batteries, and fuel cells.

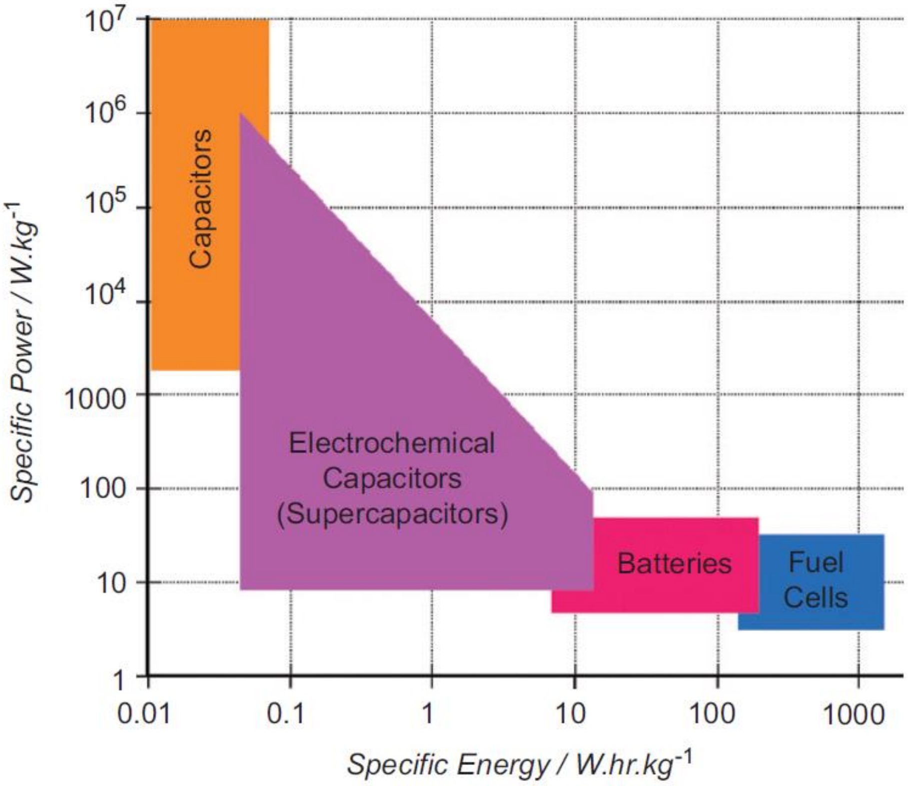

Figure 1-1. Energy-storage Ragone plot.[5]

The various types of energy storage can be divided into many categories, and here most energy storage types are categorized as electrochemical and battery energy storage, thermal and thermochemical energy storage, compressed air energy storage, flywheel energy storage, pumped energy storage, magnetic energy storage, and hydrogen energy storage. In the current dissertation, the electrochemical and battery energy storage will be discussed in detail.

1.1.3 Electrochemical and battery energy storage

Electrical energy can be stored electrochemically in batteries and capacitors. Batteries are developed energy storage technique with has high energy density and high working potential. Various types exist, including lithium-ion, sodium-sulfur, nickel-cadmium, lead-acid, lead-carbon batteries, as well as zebra batteries and flow batteries. Capacitors store and deliver energy electrochemically and can be classified as electrostatic capacitors, electrolytic capacitors, and electrochemical capacitors. Among these three types, electrochemical capacitors, also called supercapacitors or ultracapacitors, have the highest capacitance per unit volume due to having a porous electrode structure.

Several new electrode materials and electrolytes have been reviewed and suggested to improve the cost, energy and power density, cycle life, and safety of batteries. Hall and Bain[5] provide a review of electrochemical energy storage technologies, including flow batteries, Li-ion batteries, sodium-sulfur, and the related zebra batteries, nickel-cadmium, and the related nickel-metal hydride batteries, lead-acid batteries, and supercapacitors. Baker et al.[6] also viewed some of these electrochemical energy storage technologies, while Hou et al. provide performance information for supercapacitors and Li-ion batteries.[7] Nitta et al.[8] review fundamental properties, opportunities, challenges, and recent progress of anode and cathode material research for lithium batteries. As strategies to improve the performance of Li-ion batteries, Nitta et al. suggest (1) reducing dimensions of active materials, (2) formation of composites, (3) doping and functionalization, (4) tuning particle morphology, (5) formation of coatings around active materials, and (6) modification of the electrolyte.

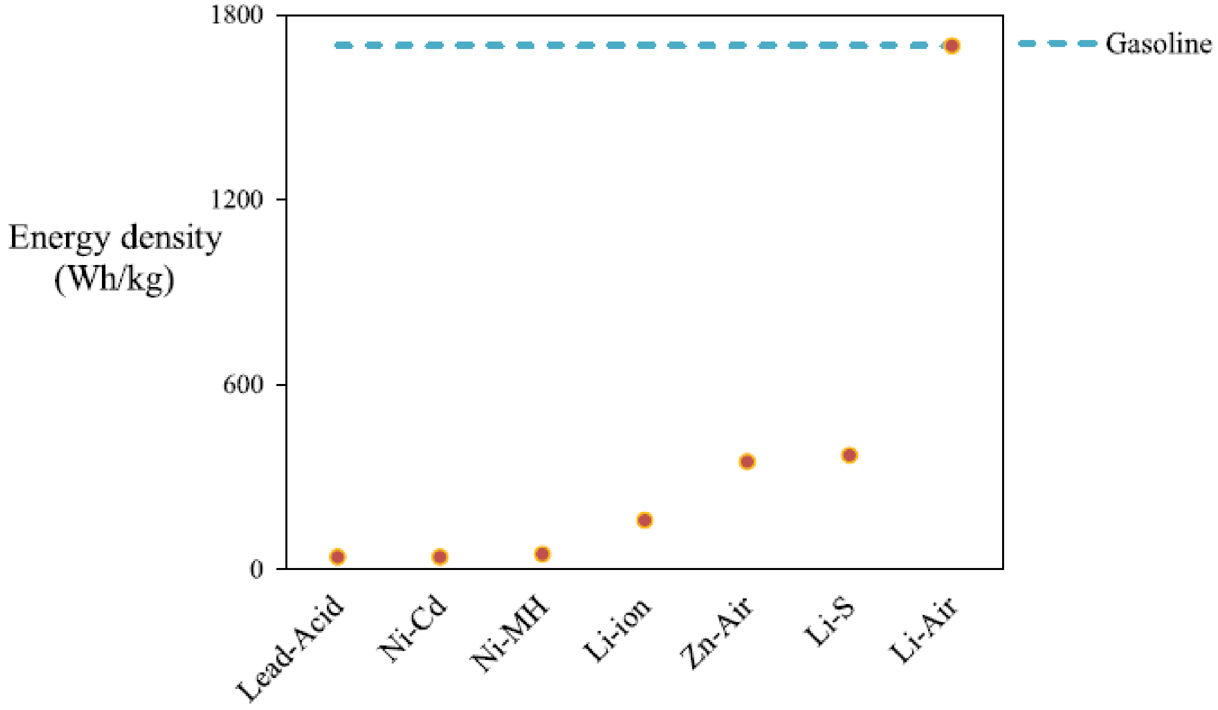

Figure 1-2. Energy densities for various types of rechargeable batteries compared to gasoline.[8] Note: Ni-Cd: Nickel-Cadmium; Ni-MH: Nickel-metal hydride; Li-ion: Lithium-ion; Zn-Air: Zinc-air; Li-S: Lithium-Sulphur; Li-Air: Lithium-air.

Among the various battery types, lithium batteries are playing an increasingly important role in electrical energy storage because of their high specific energy (energy per unit weight) and energy density (energy per unit volume). A fully charged Li-air battery is competitive with gasoline concerning the practicable energy density that can be delivered for powering the electric vehicles (**Figure 1-2**). The fundamental battery chemistry during discharge is the electrochemical oxidation of lithium metal at the anode and the reduction of oxygen from the air at the cathode. In order to enable the high performance and commercialization of Li-air batteries, plenty of technical challenges have to be addressed: designing structures of electrodes, optimizing electrolyte compositions and explicating the storage mechanisms during charging and discharging process.[8-10] The most significant developments, the main limiting factors for Li-air batteries, and the current understanding of their chemistry have been summarized in the following content.[8,9] The Li-ion battery is a type of lithium battery that uses an intercalated lithium compound as an electrode material. Bruce et al. examine the energy that can be stored in Li-air (based on aqueous or non-aqueous electrolytes) and lithium-sulfur (Li-S) batteries and compare it with that for Li-ion batteries, and discuss cell operation and development challenges.[11] They suggest that both batteries offer improved energy density compared to Li-ion batteries and could also be more cost-competitive than Li-ion batteries. However, they suggest that more research on the fundamental chemistry involved in the Li-O_2 and Li-S cells is needed before they can reach markets. Thackeray et al. provide a historical overview of Li-ion batteries, the status of current ones, and a description of advances in lithium-air batteries.[12] The performance of Li-ion batteries is affected by the solid electrolyte interphase, a protecting layer formed on the negative electrode of the battery due to electrolyte decomposition during the first charge-discharge cycle. Verma et al. discuss factors that affect the solid electrolyte interphase and how they impact battery performance.[13] Janek and Zeier[14] propose that the energy density of conventional Li-ion batteries will soon reach a physicochemical limit, and solid-state batteries that use solid electrolytes rather than liquid ones could meet the need for higher energy and power densities, although technical issues such as slow kinetics limit commercialization of solid-state systems.

Due to the extensive availability and low price of sodium, and the similarity of Li and Na insertion chemistries, Na-ion batteries could become the future low-cost batteries for smart electric grids that integrate renewable energy sources. A mountain of work has to be finished in the Na-ion field to get closer to Li-ion technology. Cathodic and anodic materials have to be optimized, and new electrolytes will also be the key for Na-ion accomplishment. Palomares et al.

describe Na-ion battery materials to provide a broad view of already explored systems and a platform for future research. Among the Na insertion cathodic materials, the authors suggest phosphates and fluorophosphate as promising options, but only after structural characteristics and Na insertion-extraction mechanisms are further studied and well understood.[15] They also suggest several electrolytes as promising for Na-ion batteries, including sodium β-alumina solid electrolyte and gel polymer electrolytes. Watanabe et al. review the various application of ionic liquids, i.e., liquids consisting entirely of ions, and focus on their use as electrolyte materials for Li/Na-ion batteries, Li-sulfur batteries, and Li-oxygen batteries.[16] They focus on the characteristic features of ionic liquids, including non-volatility, high thermal stability, and high ionic conductivity, to provide solutions to some current barriers for further developing the batteries. Ru et al. propose Al-ion batteries as the alternative candidate for Li-ion batteries because of their plentiful materials, desired cost performance, environmental friendliness, the potential for high-rate application, and long service life.[17] Such advantages could allow them to support power generation from renewable energy sources. However, their energy density, cell capacity, and cycle stability may still need to be improved before commercialization. Ru et al. review development challenges for such batteries, such as a selection of the most suitable electrolyte and positive electrode materials; these challenges result in the batteries remaining in the conceptual stage.

1.2 Overview of lithium-ion batteries

Li-ion batteries (LIBs) have an unbeatable combination of high energy and power density, making it the technology of choice for portable electronic equipment, electric tools, and hybrid/full electric motorcars.[18] Greenhouse gas emissions will be dramatically diminished if electric automobiles powered by Li-ion batteries replace most engine vehicles.[19] The high power efficiency of Li-ion batteries may also permit their purpose in miscellaneous electric power grid applications, including enhancing the quality of energy gathered from solar, wind, geothermal, and other renewable energy sources, thus dedicating to their more extensive use and establishing an energy-sustainable economy. Therefore Li-ion batteries are of intense interest from both industry and government funding agencies, and research in this field has teemed in recent years.

Nevertheless, looking to the future, many suspect that Li-ion batteries will be able to power the world's desires for portable energy storage in a long time. For some applications at the current stage, for example, transportations and transmission grids, Li-ion batteries are uneconomic, and the insufficient Li sources and some of the transition metals currently applied in Li-ion batteries may one day become an issue.[20] At the same time, Li-ion batteries have convinced essential advantages over other systems. Firstly, Li has the lowest reduction potential over other elements, allowing Li based batteries to have the highest possible working voltage. Also, Li is the lightest metallic element and has the smallest ionic radii in any single charged ions. These advantages allow Li-based batteries to acquire high volumetric and gravimetric energy density and power density. Lastly, although multivalent cations afford for higher charge capacity, the additional charge severely decreases their mobility. Known that ionic diffusion in the solid electrodes is often the rate-limiting issue for power performance, this offers a giant obstacle for the further development of such alternative chemistries.

A significant shortage of Li is unlikely presently.[21,22] Similar statements have been made about peak oil but have yet to arrive as world oil reserves and resources remain to grow with increasing prices and the progress of exploration and mining development. Following absolute quantities, the amount of Li available on the Earth is sufficient to power a global fleet of automobiles.[23] Rising prices, though, can be problematic for Li-ion batteries because the cost is the primary factor inhibiting its expansion into renewable energy applications. Even so, Li is not a significant factor in the cost of Li-ion batteries at present. Li is used in the cathode and electrolyte, which make up only a small portion of the overall cost.[24] Within these considerations, the cost of processing and the cost of cobalt in cathodes are the major influencing factors.[25] Given its fundamental advantages, Li-ion batteries will possibly continue to dominate portable electrochemical energy storage for many years to come. Since Li-ion batteries are the preferred supplier of the moveable electrochemical energy storage system, improving their cost and performance can markedly extend their applications and empower new technologies that rely on energy storage systems. A large number of research in Li-ion batteries has yet been in electrode active materials. With higher rate aptitude, higher energy capacity, and adequately high voltage window, electrodes can expand the energy and power densities of Li-ion batteries and allow them to be smaller and cheaper. However, this is only referable if the material itself is not too expensive or rare.

(a) Availability

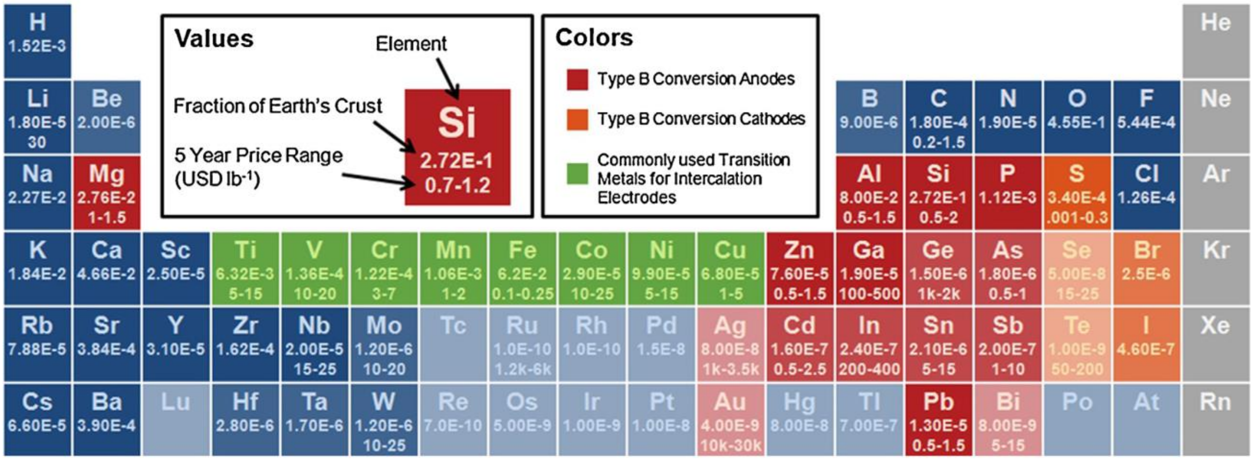

(b) Charge Capacity

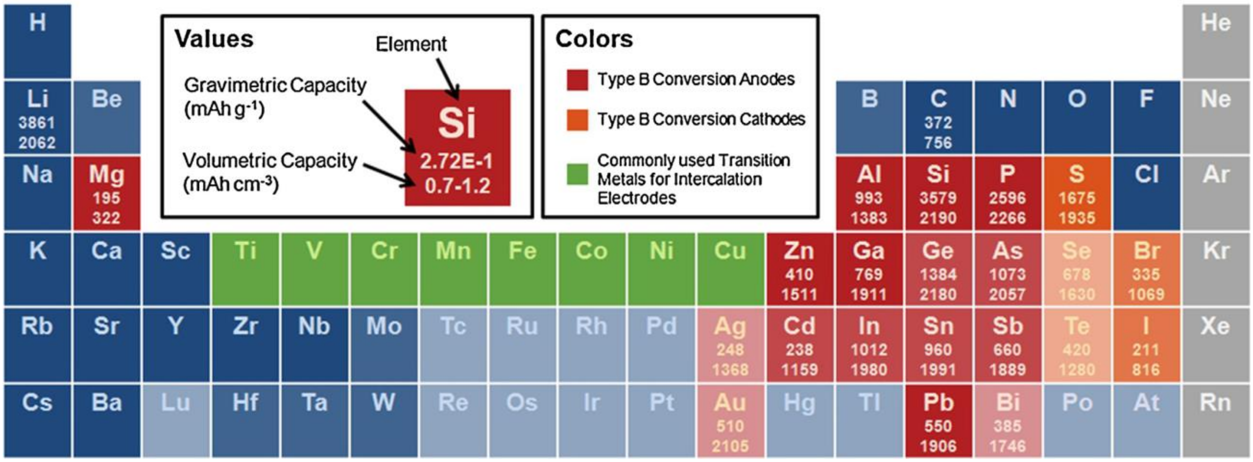

Figure 1-3. a) Availability, and b) capacities of elements that may host Li as electrodes. Elements with abundance (as the fraction of Earth's crust) below 10^5 are slightly faded, and elements below 10^7 are faded further. Prices are approximate 5-year ranges of metal prices (except Ge, which is a three years range), 80-100 mesh natural graphite for carbon, and the Vancouver/USGS prices for sulfur.[8] Gravimetric and volumetric capacities are theoretical values calculated based on de-lithiated mass and lithiated volume.

Figure 1-3 shows the wholesale price of various metals and the abundance of elements as a fraction of the Earth's crust.[26] Although the electrodes are not manufactured from pure metal bars, the prices illustrate the relative differences. Mn is much cheaper than Co, which elucidates the cost difference in the cathodic active materials prepared from them. The abundance of elements signifies a restriction on the obtainability of the element. While actual availability also depends on supply and demand, this chart shows the superiorities of some elements. Finally, the theoretical specific and volumetric capacities of the elements which undergo conversion reactions with Li are shown in Figure 1-3b.

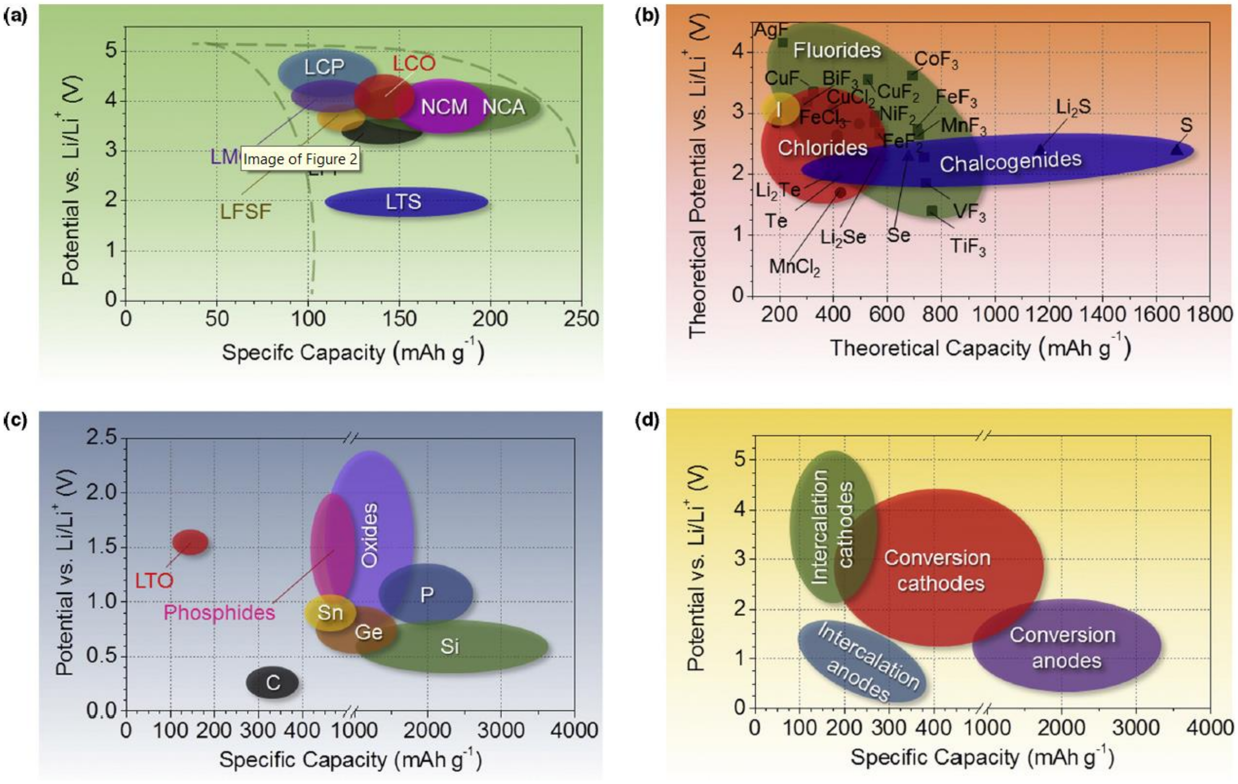

Figure 1-4. Approximate range of average discharge potentials and specific capacity of some of the most common: a) intercalation-type cathodes (experimental); b) conversion-type cathodes (theoretical); c) conversion type anodes (experimental), and d) an overview of the average discharge potentials and specific capacities for all types of electrodes. Note: LCO: lithium cobalt oxide, LMO: lithium manganese oxide, NCM: nickel cobalt manganese oxide, NCA: nickel cobalt aluminum oxide, LCP: lithium cobalt phosphate, LFP: lithium iron phosphate, LFSF: lithium iron fluoro-sulfate, LTS: lithium titanium sulfide.[8]

Inappropriately, as valuable as the periodic table is, most cathodic materials are chemical compounds and are not suitable for this chart. **Figure 1-4** is a relatively comprehensive form of a simplified chart, representing average electrode potential compared to experimentally accessible (for anodes and intercalation cathodes) or theoretical (for conversion cathodes) capacity. This map allows the reader to estimate different combinations of anode and cathode, and their theoretical voltage window, energy density, and total capacity. The chart can also be used to recognize proper additives, electrolytes, and current collectors for the electrode materials of choice.

For a more compendious illustration, the evolution of Li-ion batteries (working electrodes) from conventional technologies into advanced, state-of-the-art, and hybridized technologies, is shown in **Figure 1-5**.

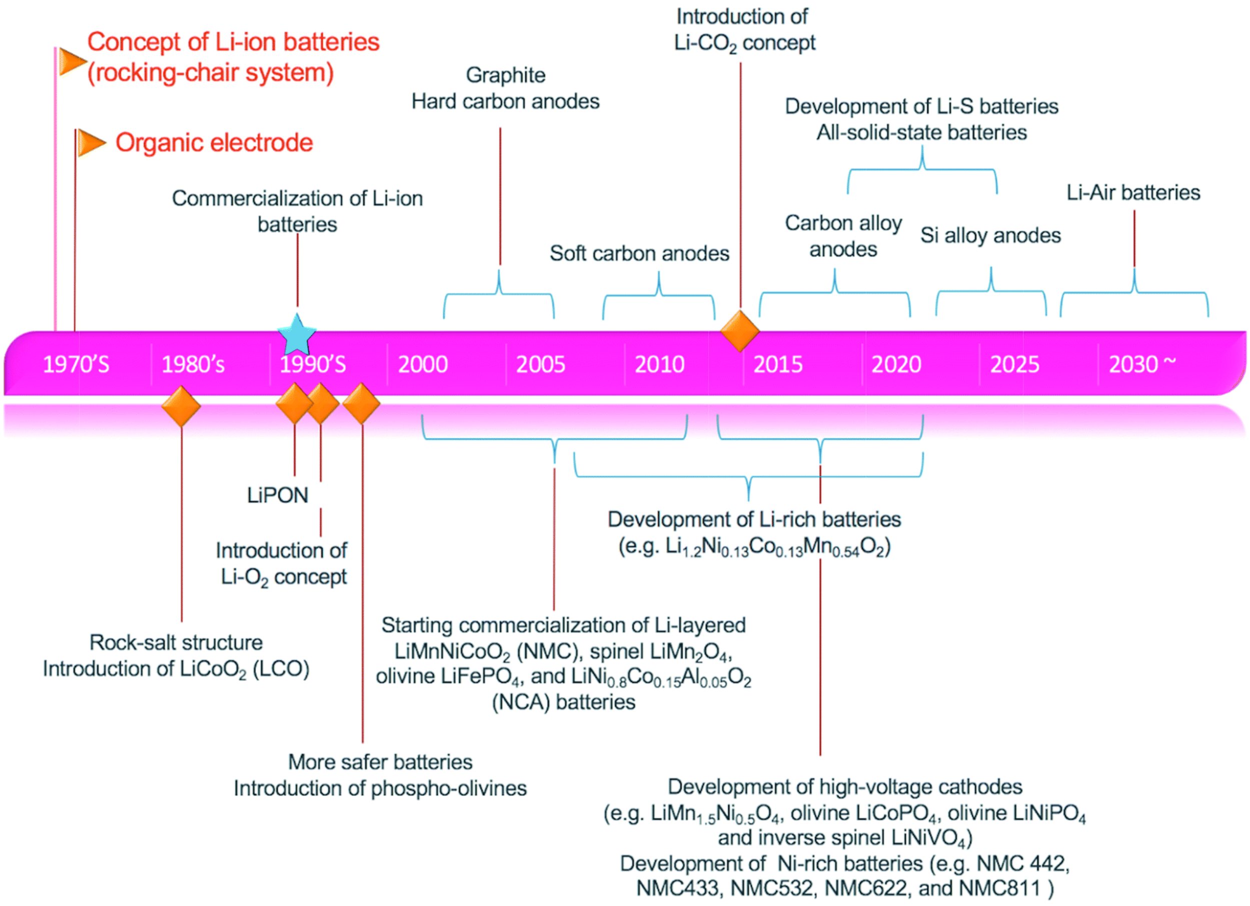

Figure 1-5. Historical evolution and advances of Li-ion battery technologies.[27]

1.3 High-rate anode material for lithium-ion batteries

With the growing demands of electric vehicles, portable electronics, and ESSs, the rechargeable batteries with high power density are obbligato requirements for their extensive applications.[28-34] Fast charging, as one of the core technology of rechargeable batteries, has drawn extensive interests and exhibited an excellent market prospect.[29,30,35-38] The data analysis of all charge points through Ireland and Northern Ireland shows that the fast charging substructure is the most prevalent and becomes commercially feasible because of its time saving and handiness.[37] **Figure 1-6a** compares the required travel time from Salt Lake City to Denver, of internal combustion engine vehicles, conventional charging electric vehicles, and extremely fast-charging electric vehicles. Conventional charging electric vehicles consume 29% more time than internal combustion engine vehicles because of the long charging duration and frequent charging cycles during the journey. By comparison, high-speed charging requires equal time to internal combustion engine vehicles due to its short charging time. Thus, the fast charging technology is the kernel to solve the extended mileage issue of electric vehicles, and it is critical to lessening consumer range concerns.[39,40]

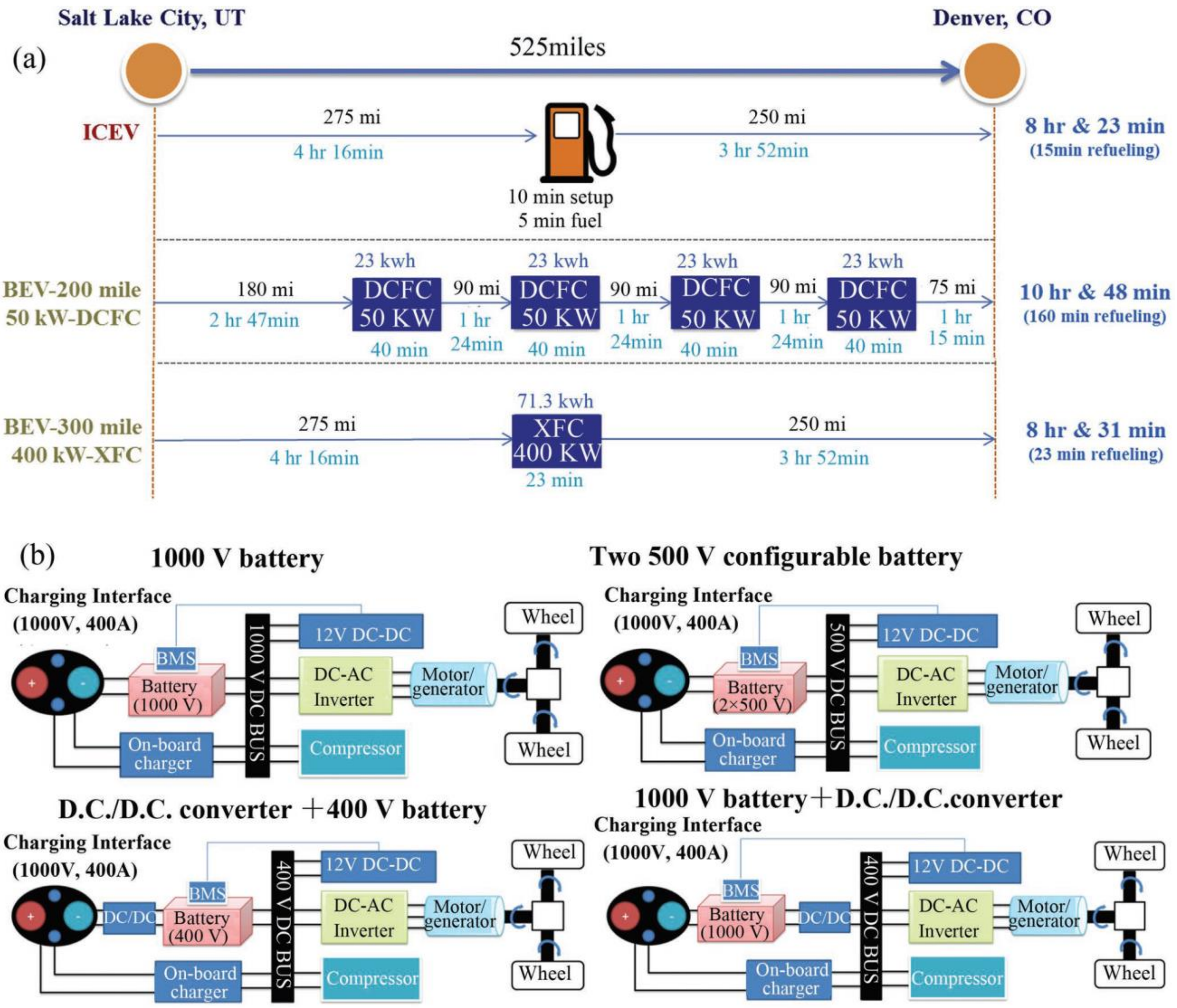

Figure 1-6. a) Drive from Salt Lake City to Denver with different strategies. b) Four 1000 V battery electric vehicles architectures to support extreme fast charging. ICEV, BEV, DCFC,

XFC, BMS, DC represent internal combustion engine vehicles, battery electric vehicles, direct current fast charger, extreme fast charging, battery management system, and direct current, respectively.[40]

The fast charging ability for Li-ion batteries has raised rigorous requirements for their core components, including electrodes, electrolytes, and external equipment.[41,42] The achievable charge/discharge rate of a Li-ion battery depends critically on the mobility rate of the Li-ions and electrons within the batteries, including electrodes, electrolytes, and their interfaces.[43,44] Fast charging typically involves high fluxions, which result in lithium dendrites growth and the repeated formation of solid-electrolyte interface (SEI) film, further contributes to the reduced coulombic efficiency, increased voltage polarization, and safety risks.[45,46] Worse still, organic liquid electrolytes in conventional Li-ion batteries are combustible and reactive, fast charging cause the increase of temperatures for batteries, increasing the possible risks of explosion or ignition after exposure or leakage of liquid electrolytes.[47] While solid electrolyte benefited from its intrinsic stability and safety has aroused full attention for the applications in next-generation Li-ion batteries.[48-50] Simultaneously, with the development of high ionic conductivity solid-state electrolytes, it is possible to realize fast charging in solid-state lithium batteries.

1.3.1 The requirements of electrodes for fast charging

The rate performances of lithium batteries depend mostly on the mobility of the ions and electrons transportation within the electrolytes, composite electrodes, and their interfaces. The sluggish ion and electron transportation of the electrode is considered as the rate-limiting step in batteries. Thus, these two particular factors that should be satisfied for electrodes for fast charging technology are a) high ionic conductivity, and b) excellent electronic conductivity. The criterion for fast charging is to return 60% of the state of charge (SOC) of the battery within 6 min. **Table 1-1** lists the Li-ion battery performances with different electrodes at 10 C. It is worth noting that when the ionic or electric conductivity is less than ≈ 10^{-5} S cm^{-1}, it will be difficult for the battery to attain 60% of the SOC at 10 C. Therefore, ≈ 5×10^{-5} S cm^{-1} is believed as the critical threshold of ionic and electronic conductivity for fast charging electrode. When the ionic or electronic conductivity of the electrode is lower than this threshold, the electrode is not suggested to be applied in the fast-charging application. The higher intrinsic conductivity is necessary for an electrode with a high areal loading or large size particles. The approaches include developing novel electrode materials with high ion and electron mobility,[43,51-53] designing hierarchically structured electrode with high ion and electron transport rate through coating or doping,[36,44,54] reducing the length of transportation path for electrons and Li-ions through structural unification,[41,55] and modifying the ion diffusion channels by controlling crystal structure.[44,54]

Table 1-1. The ionic and electronic conductivity of different electrodes.[56]

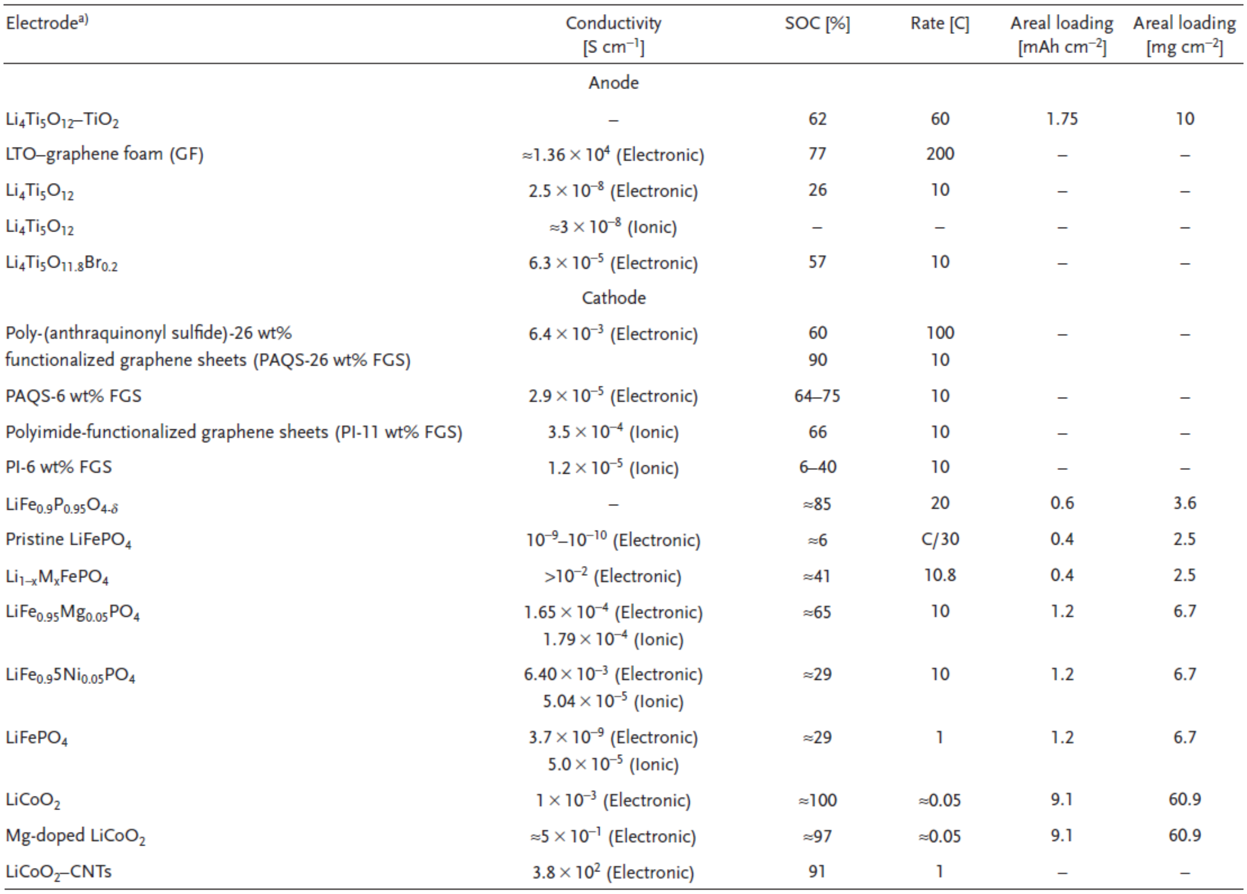

Electrode[a)]	Conductivity [S cm^{-1}]	SOC [%]	Rate [C]	Areal loading [mAh cm^{-2}]	Areal loading [mg cm^{-2}]
	Anode				
$Li_4Ti_5O_{12}$–TiO_2	–	62	60	1.75	10
LTO–graphene foam (GF)	≈1.36×10^4 (Electronic)	77	200	–	–
$Li_4Ti_5O_{12}$	2.5×10^{-8} (Electronic)	26	10	–	–
$Li_4Ti_5O_{12}$	≈3×10^{-8} (Ionic)	–	–	–	–
$Li_4Ti_5O_{11.8}Br_{0.2}$	6.3×10^{-5} (Electronic)	57	10	–	–
	Cathode				
Poly-(anthraquinonyl sulfide)-26 wt% functionalized graphene sheets (PAQS-26 wt% FGS)	6.4×10^{-3} (Electronic)	60 90	100 10	–	–
PAQS-6 wt% FGS	2.9×10^{-5} (Electronic)	64–75	10	–	–
Polyimide-functionalized graphene sheets (PI-11 wt% FGS)	3.5×10^{-4} (Ionic)	66	10	–	–
PI-6 wt% FGS	1.2×10^{-5} (Ionic)	6–40	10	–	–
$LiFe_{0.9}P_{0.95}O_{4\text{-}\delta}$	–	≈85	20	0.6	3.6
Pristine $LiFePO_4$	10^{-9}–10^{-10} (Electronic)	≈6	C/30	0.4	2.5
$Li_{1-x}M_xFePO_4$	$>10^{-2}$ (Electronic)	≈41	10.8	0.4	2.5
$LiFe_{0.95}Mg_{0.05}PO_4$	1.65×10^{-4} (Electronic) 1.79×10^{-4} (Ionic)	≈65	10	1.2	6.7
$LiFe_{0.9}5Ni_{0.05}PO_4$	6.40×10^{-3} (Electronic) 5.04×10^{-5} (Ionic)	≈29	10	1.2	6.7
$LiFePO_4$	3.7×10^{-9} (Electronic) 5.0×10^{-5} (Ionic)	≈29	1	1.2	6.7
$LiCoO_2$	1×10^{-3} (Electronic)	≈100	≈0.05	9.1	60.9
Mg-doped $LiCoO_2$	≈5×10^{-1} (Electronic)	≈97	≈0.05	9.1	60.9
$LiCoO_2$–CNTs	3.8×10^2 (Electronic)	91	1	–	–

a) Calculation of the SOC [%]: $Li_4Ti_5O_{12}$ and $LiFePO_4$ based materials are compared with their theoretical capacity, 175 mAh g^{-1}, and 170 mAh g^{-1}, respectively. $LiCoO_2$ based materials are compared with 150 mAh g^{-1}. The others are compared with their capacity at 0.1 C rate.

1.3.2 Anodic electrode materials for high-rate application

Graphite is one of the most widely recognized anode material in Li-ion batteries due to its good reversibility, safety, and low cost.[31] However, the poor high-rate intercalating capability dramatically confines its practical applications in fast charging.[57] The slow lithium-ion diffusion mainly causes the reduced rate performance of graphite within the bulk carbon-based materials.[58] Therefore, porous carbon anode has been applied to shorten the Li-ion diffusion pathway in the bulk phase and increase channels for transporting ions.[59,60] Maier and co-workers prepared hierarchically porous carbon monoliths, which exhibited a high-rate capacity of 145 mAh g^{-1} at 30 C.[61] Besides, surface modification is another tactic to enhance the rate performance of the carbon-based anode material. The existence of heteroatoms on the surface of carbon-based material can efficiently enhance the reaction kinetics and electronic conductivity. Cheng et al. described that the N-doped graphene and B-doped graphene exhibited a high capacity of 199 mAh g^{-1} and 235 mAh g^{-1} at 25 A g^{-1}, respectively.[62] Huang et al. suggested that the combination of porous structure and heteroatoms doping improved the high rate performances of carbon-based material in lithium batteries. The as-prepared nitrogen-doped porous carbon nanofiber networks provided a reversible capacity of 226 mAh g^{-1} at a current density of 20 A g^{-1} for about 40 cycles.[63]

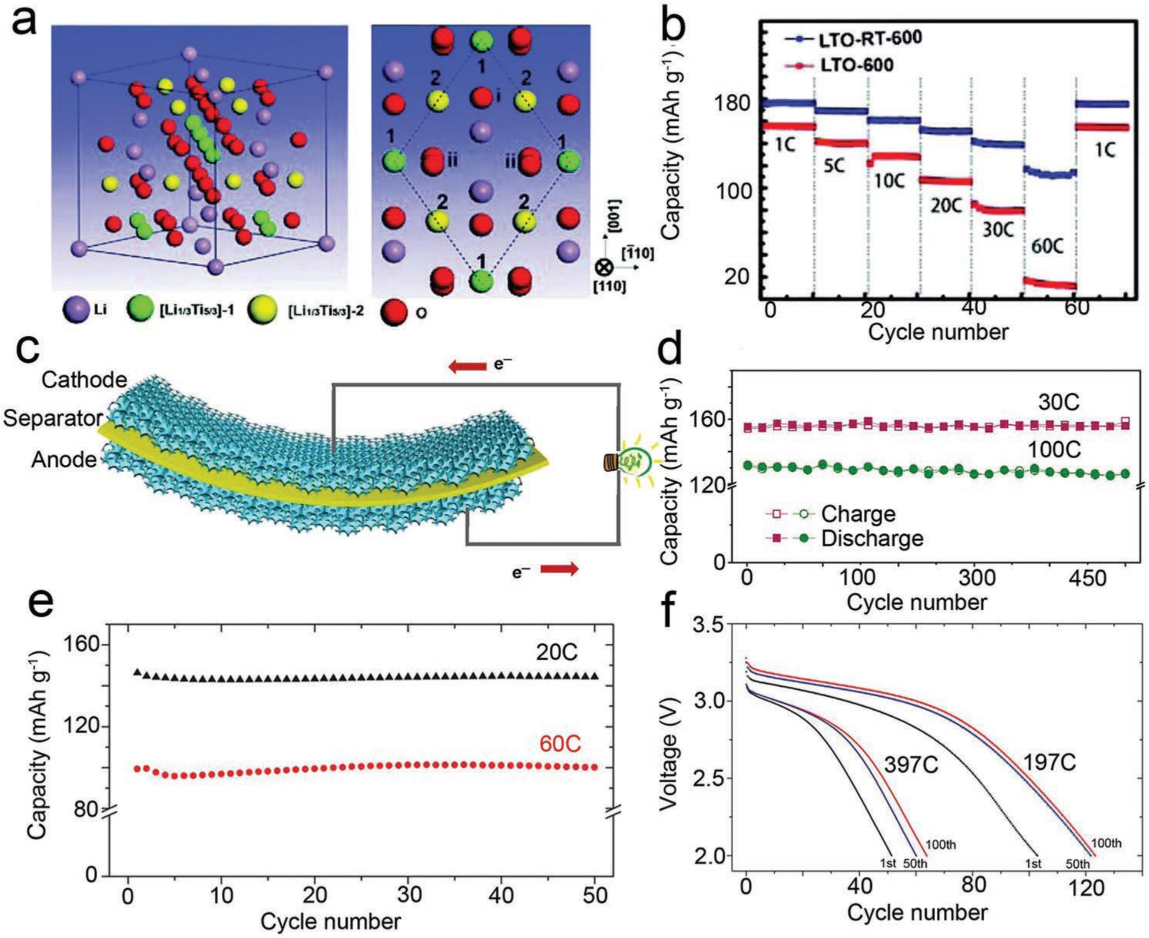

Figure 1-7. Electrode for fast charging: a) the spinel structure of LTO (left) and its projection along with the (1 1 0) direction (right). b) Rate performance of the LTO nanosheets. LTO-600 represents Li/Ti molar ratio is 4.5:5, LTO-RT-600 represents Li/Ti molar ratio is 4:5. c) Schematic of a flexible battery containing a cathode and an anode made from 3D interconnected graphene foam (GF).[43] d) Cyclic performance of the LTO/GF at 30 and 100 C.[43] e) Cyclic capability for $LiFe_{0.9}P_{0.95}O_{4-\sigma}$ synthesized at 600 °C at 20 and 60 C. f) Discharge capability for $LiFe_{0.9}P_{0.95}O_{4-\sigma}$ at different rate.[56]

Alternatively, immense efforts have been dedicated to seeking for novel anodic materials to acquire better high rate performance. As the most promising anodic candidate for high rate lithium batteries, $Li_4Ti_5O_{12}$ (LTO) has been extensively researched because of its excellent structural stability during the Li-ion intercalation/deintercalation process and higher safety.[64-66]

However, both the poor electrical conductivity and sluggish Li-ion diffusion leave an unfulfilled rate capability of pure LTO. In order to overcome these essential drawbacks, approaches have focused on enhancing the electronic conductivity by doping or reducing the ion diffusion pathway by fabricating nanostructured particles.[67,68] Xia et al. pronounced that the carbon-coated nanoporous microsphere LTO revealed a capacity of 126 mAh g^{-1} at 20 C.[69] **Figure 1-7a** exhibits the well-defined spinel structure of LTO. The projection of (1 1 0) crystal face confirms that the rutile-TiO_2 is at the edges of the LTO nanosheets.[70] Such rutile-TiO_2 terminated LTO nanosheets show a reversible capacity of 110 mAh g^{-1} at 60 C charging/discharging rate, with an areal loading of 10 mg cm^{-2} (Figure 1-7b).[64] LTO/graphene foam composite anode (Figure 1-7c) exhibits a capacity of 130 mAh g^{-1} at 100 C (Figure 1-7d).[43] This remarkable rate performance is credited to the porous structure and superior electronic conductivity of the composite electrode.

Furthermore, the high content of other high-performance anodes for fast charging has been explored. Cho et al. prepared disordered graphene-like and enlarged interlayered distance of 0.69 nm MoS_2 nanoplates, which provided a reversible capacity of 700 mAh g^{-1} at 50 C.[71] Luo et al. pronounced that the mesoporous Fe_3O_4 loaded on 3D graphene foams exhibited a capacity of 190 mAh g^{-1} at 60 C.[72] Wu et al. discovered the mesoporous Co_3O_4 nanowire arrays anode with a considerable capacity of 350 mAh g^{-1} at 50 C.[73] Cui et al. demonstrated a notable Si-SiO_x double-walled silicon nanotube anode, in which the ion-permeable outer wall of SiO_x can sufficiently avert the reaction between inner silicon and electrolyte, and thus deliver a very high capacity of 540 mAh g^{-1} at 20 C.[74]

1.3.3 Titanium-based materials for high-rate anodic electrode

So far, the dominating and commercial anode materials for electrochemical energy storage are carbon-based. To be specific, graphite and activated carbon have dominated the LIBs anodes.

Although the carbon materials show significant advantages of low cost and excellent cycling stability, the increasing requirements for higher energy density and power density of energy storage fields put forward higher demands on the electrode materials. Based on these requirements, various metal oxides have been proposed and gradually employed as anode materials for LIBs due to the high energy density or power density.[75]

Generally, the electrochemical lithiation mechanism of metal oxides used as anode materials can be divided into four categories. 1) Intercalation/deintercalation reaction: lithium ions can be intercalated into the lattice vacancy sites with no volume change or little volume expansion, such as TiO_2, Nb_2O_5, $Li_4Ti_5O_{12}$, and $TiNb_2O_7$, etc.[76,77] 2) Alloying/dealloying reaction: lithium ions can be alloyed and formed to Li_xM alloy and Li_2O in the first discharge process, and then the Li_xM participate reaction as the only active component in subsequent cycles, accompanied by a vast volume expansion/shrinkage. The typical representative oxides are SnO_2, Sb_2O_3, SiO, and Li_2SnO_3, etc.[78,79] 3) Conversion (Redox) reaction: lithium ions can participate in the conversion reaction with the M_xO_y process directly and generate metal M and Li_2O, which will participate in reaction in the subsequent cycles together with small volume change. The typical representative oxides are NiO, Co_3O_4, Fe_3O_4, and MnO_2, etc.[80-82] 4) Both alloying/dealloying and conversion reaction: that is, lithium ions participate the electrochemical reactions through the two mechanisms at the same time, such as ZnM_2O_4 (M = Co and Fe), $CdFe_2O_4$, M_2SnO_4 (M = Co, Mn, Mg, and Zn) and metal carbonates, etc.[83,84] 5) Both intercalation /deintercalation and conversion reaction: lithium titanium silicate (Li_2TiSiO_5) has hybrid lithium-ion storage mechanism which includes two intercalations and one conversion process within different voltage window.[85] Due to the conversion reaction mechanism and noticeable volume change, the (2), (3), and (4) oxides generally deliver weak cycle stability. On the contrary, the (1) oxides, described as insertion-type electrodes, show excellent rate capacity and cycle stability due to the stable crystalline structure for Li-ion intercalation and deintercalation. Primarily, they can exhibit significant pseudocapacitive effects during the fast Li-ion intercalation process, which further elevates the rate capability and can be applied as the anode materials for nonaqueous Li-ion capacitors.[86] However, (5) oxide is a little bit special because its cycling stability depends on the discharge cutoff which is essentially because of the occurrence of conversion reaction.

Ti-based oxides, including TiO_2, $Li_4Ti_5O_{12}$, Li_2TiSiO_5, $Na_2Ti_3O_7$, $TiNb_2O_7$, etc., are the most representative insertion-type anode materials for electrochemical energy storage. Lately, massive efforts have acknowledged the vast potential of Ti-based oxides for Li-ion batteries. The significant advantages of Ti-based oxides could be summarized as the following aspects. 1) Excellent intrinsic safety due to the high working potential (1.2-1.7 V *vs.* Li^+/Li). 2) Stable crystalline structure during repeating lithium intercalation/de-intercalation based on the reaction mechanism (1). 3) Superior rate capability over traditional carbon materials. 4) Resource abundant and low cost. Inspired by that, titanium oxide-based materials have been extensively investigated and considered as alternatives for the traditional carbon-based anode materials in the LIBs. Besides, exploring novel Ti-based oxides for applications such as the sodium-ion batteries and hybrid pseudo-capacitors is another intriguing approach that has bright prospects. Unfortunately, some issues and challenges, such as low electrical conductivity and lithium diffusion coefficient, still limit its electrochemical performance. In order to overcome these drawbacks, understanding the electrochemical mechanism of Ti-based oxide anodes for a different energy storage system and making targeted modification are imperative for future applications in electrochemical energy storage devices.

1.4 Carbon composites in lithium-ion batteries

Because of the low electronic conductivity of most electrode materials, various carbon composites have been widely used to achieve superior electrochemical performance.

1.4.1 Porous carbon materials

Because of the high surface area, large pore volume, and unique pore size distribution, porous carbon materials are considered having great potential for many applications and therefore, attracted tons of attention.[87-89] Activated carbon, with a broad pore size distribution, however, has many limitations, such as low conductivity, low mass transportation, and low structural stability, which confines its commercialization in catalytic and electrochemical applications. Many efforts have been attempted to overcome these drawbacks and produce high-quality porous carbon materials with tuneable pore size, narrow pore size distribution, high specific surface area, and high conductivity from increased graphitization.[90] On the other hand, the morphology control has also been developed to prepare different structures, which are beneficial to enhance the performance as catalysts or electrode materials.[91-93] Nevertheless, the expectation of pure carbon materials in energy storage fields is still shadowy due to their disadvantageous intrinsic properties. For example, the theoretical capacity of carbon-based material (e.g., graphite, meso-carbon microbeads) is only 372 mAh g^{-1}, which is much lower than other types of active material, especially Sn/SnO_x and silicon, as anodes for lithium-ion batteries.[88] For lithium-oxygen batteries, carbon has sluggish dynamics in the oxygen reaction and oxygen evolution reactions, leading to low charge/discharge round-trip efficiency. Furthermore, non-aqueous electrolytes decompose on carbon catalyst, and side reactions produce by-products on the cathode side, resulting in poor cycling stability of lithium-oxygen batteries.[94]

Porous carbon materials have been incorporated with other active materials to explore novel electrode materials with satisfying catalytic or electrochemical properties. The porous carbon-based composites have many special features to achieve enhanced properties. For instance, the carbon frameworks always provide superficial electron transportation to achieve high electronic conductivity. Therefore, the porous carbon composite electrodes, with high operating current condition, is valuable for high-power energy supply systems. The active materials, embedded in the carbon substrate, induce enhanced performance, which can be credited to the synergistic effect. The porous structure of the composites results in a more adequately infiltrating effect of electrolyte, which allows the enhanced electrode/electrolyte interface. The higher interface means more active sites for promoting electrochemical and electrocatalytic reactions. Therefore, the porous carbon-based composites have many favorable characteristics and can achieve outstanding performance for energy storage and catalysis.[95]

Many strategies have been constructed to fabricate porous carbon substrates.[96,97] Generally, for “bottom-up” strategies, there are three typical synthesis methods: hard templating, soft templating, and mixed templating (hard and soft templating) methods.

1) Hard templating methods have been extensively used to prepare porous carbon substrates with a wide range of pore sizes from microporous to macroporous by nano casting carbon precursors to different kinds of hard-templates. The structures of the as-prepared porous carbon material are the replicas of their templates. Explicitly, carbon structure will fill the void space between template particles, and the porous structure will replace the template after the removal. Therefore, the structure of porous carbon materials is controllable by selecting proper templates with specific synthetic route.[98]

Figure 1-8a shows a diagram of the synthetic route for Co_3O_4 in CMK-5 nanotube arrays, forming a peapod-like tubular composite by nano casting a Co precursor in CMK-5/SBA-15 precursor.[99] In this manner, Co_3O_4 nanoparticles can be restricted within the intratubular pores of the nanotube arrays. This specially designed anode architecture is efficient to overcome massive volume changes during the Li^+ insertion and extraction process. The interspace between the nanotubes, inherited from the structure of SBA-15, is accessible (similar to CMK-3), which leads to efficient electrolyte contact. A similar strategy can also be applied to construct SnO_2/CMK-5 composite.[100] As shown in Figure 1-8b, the SnO_2-80@CMK-5 presents an excellent electrochemical performance of 1039 mAh g^{-1} after 100 cycles, at a discharging current density of 200 mA g^{-1} between 0.005 and 3 V. The ultrafine SnO_2 NPs with average diameters of 4-5 nm offer a high reactivity and shorten electronic and ionic transport lengths, leading to a superior capacity and excellent rate capability. The walls of the carbon nanotubes suppress the expansion and aggregation of SnO_2 nanoparticles. The hollow area of the mesopores between nanotubes can compensate for the volume change of SnO_2 and provide efficient electrolyte flow. During Li intercalation, nanoparticles of tin-lithium alloy grow along the meso-channels of CMK-5, which simultaneously increases the sufficient contact between active particles and carbon structure, promoting the electronic transportation within the active material, and enhancing the conductivity of the composite. Hence, the SnO_2-80@CMK-5, because of its remarkable reversible capacity, high coulombic efficiency, stable cycling performance, and decent rate capability, is considered as an applicable anode candidate for LIBs.

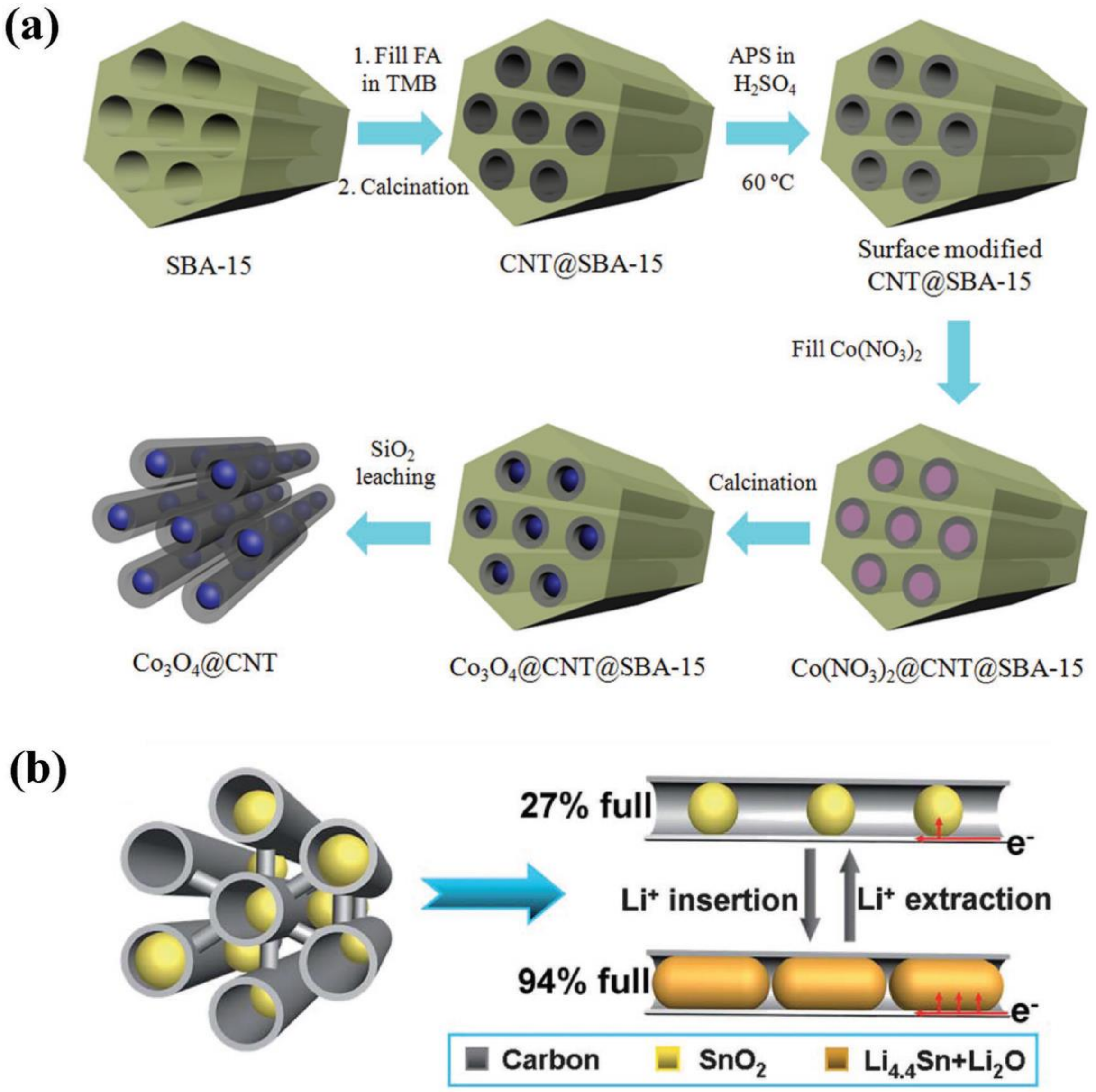

Figure 1-8. a) Schematic illustration of the formation process of mesoporous peapod-like Co_3O_4@carbon nanotube arrays. b) Schematic illustration of volume change during Li^+ insertion/extraction processes in SnO_2/CMK-5 composite.[95]

2) Soft templating methods have a milder requirement of preparation than the hard templating methods since the templating surfactant has a lower decomposition barrier during the heating treatment. In a soft templating strategy, guest species are self-assembled in nano/mesostructures by the self-assembly. For such a spontaneous process, it is crucial to

generate micelles from the communication between surfactants and guest species. The curvature of micelles determined by the hydrophilic/hydrophobic ratio significantly affects the symmetry of closed packed micelles (e.g., 2D hexagonal or 3D bicontinuous cubic structure). During high-temperature calcination, the surfactant molecules can be removed, and the carbon frame can be obtained.[101-103]

Liu et al. reported a versatile route to prepare hollow TiO_2/graphitic carbon (H-TiO_2/GC) spheres with superior electrochemical performance for lithium-ion batteries.[104] The schematic illustration of the preparation and functioning of H-TiO_2/ GC anodes is summarized in **Figure 1-9**. Typically, mesoporous amorphous TiO_2 shells can be uniformly deposited onto the surface of SiO_2 nanospheres via a versatile kinetics-controlled coating method.[105] The as-prepared SiO_2@TiO_2 core-shell structured spheres were hydrothermally treated in a glucose solution to form SiO_2@TiO_2/C spheres. Along with the hydrothermal reaction, glucose was decomposed and filled in the void space of the polycrystalline TiO_2 networks, forming a TiO_2/C core-shell structure. During the heating process, the amorphous TiO_2 core and carbon shells could be converted *in-situ* to crystalline TiO_2/graphitic carbon composite. This mesoporous H-TiO_2/GC composite offers a high specific surface area (298 m^2 g^{-1}), a large pore volume (0.31 cm^3 g^{-1}) and size (≈ 5 nm), distinct hollow structure (monodispersed particle size of 600 nm, and the inner diameter of around 400 nm, with a shell thickness of 100 nm), and small anatase TiO_2 nanocrystals (≈ 10 nm) uniformly encapsulated in thin layers of graphitic carbon. Therefore, the H-TiO_2/ GC hollow spheres could achieve excellent electrochemical performance with decent stability as a candidate for anode material of Li-ion batteries.

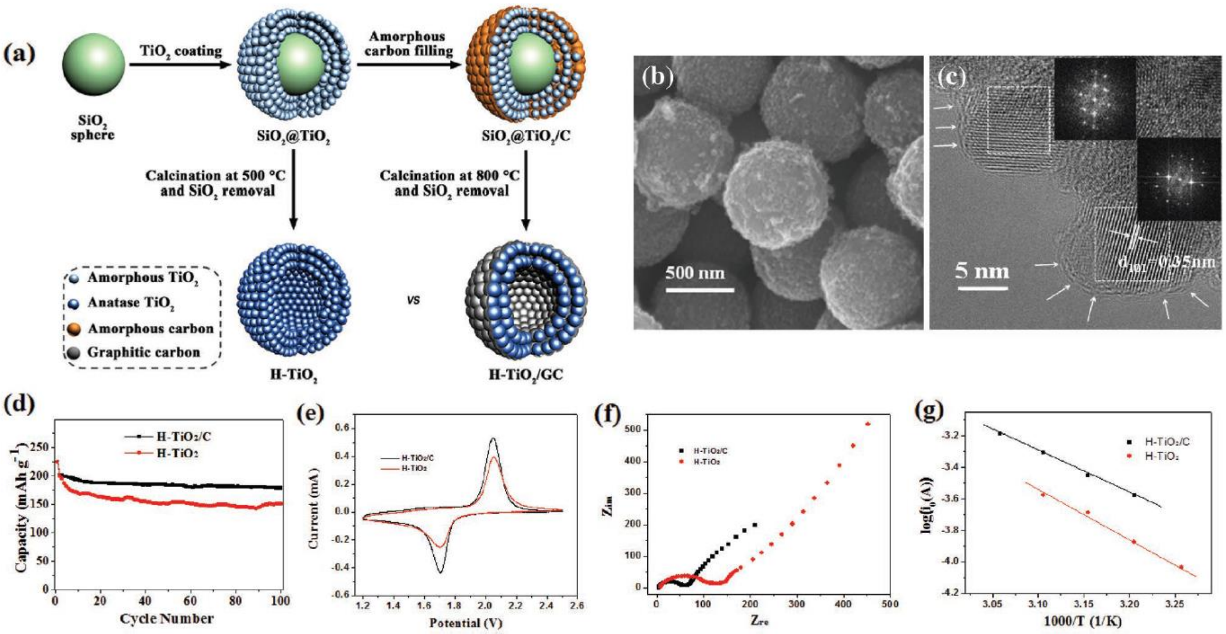

Figure 1-9. a) Schematic illustration of the formation of conformal graphitic carbon coating of mesoporous hollow TiO_2 (Denoted as H-TiO_2/GC) spheres. b) SEM and c) TEM images of the mesoporous H-TiO_2/GC hollow sphere d) Cycling performance of H-TiO_2/GC and H-TiO_2 spheres at a constant current density of 0.1 A g^{-1} (approximately 0.5 C). Inset images show the structural evolution of H-TiO_2 and H-TiO_2/GC spheres upon cycling. e) Cyclic voltammetry (CV) curves of H-TiO_2/GC and H-TiO_2 sphere electrodes with a scanning rate of 0.5 mV s^{-1}. f) Nyquist plots of H-TiO_2/GC and H-TiO_2 spheres at room temperature. g) Activation energy and corresponding Arrhenius plots of log i_0 versus 1/T for fresh electrodes of H-TiO_2/GC and H-TiO_2 spheres collected at 2 V at different temperatures from 35 to 55 °C.[95]

3) Mixed templating methods, namely, hard and soft templating combination methods, are smart methods to produce hierarchical porous materials, which provide multi-sized pores for secure transportation of electrolyte and lithium ions. Several templates can be applied to form the microporous structure, including colloidal, foam, anodic aluminum oxide, and biological templates. Simultaneously, mesostructured can be generated in situ by surfactant. After final calcination and template removal, hierarchically porous carbon materials can be obtained.[106] Subsequently, active materials can be loaded into the cavity of porous carbon with desirable

nano casting and heat treatment procedures to obtain the final porous carbon composites for lithium-ion battery materials.

Kim et al. reported mesoporous Si@carbon core-shell nanowires with a diameter of ≈6.5 nm that were prepared by using mesoporous silica SBA-15 as a rigid template and an organic silicon source as a precursor.[107] The as-synthesized nanowires demonstrate an excellent first charge capacity of 3163 mAh g^{-1} with high Coulombic efficiency of 86% at a rate of 0.2 C (600 mA g^{-1}). Furthermore, around 87% capacity is retained after 80 cycles, and the rate performance at 2 C is 78% of it at 0.2 C. On account of carbon modification, mesoporous Si@carbon core-shell nanowires exhibit superior electrochemical performance, which also implies the excellent structural stability. Similarly, mesoporous SnO_2/C composites can be obtained by impregnating organic tin salt in SBA-15 hard-template with calcination at 400 °C (**Figure 1-10a**).[108] The SnO_2 nanostructure can be uniformly coated by a thin layer of carbon, which improves its stability and conductivity (Figure 1-10b-d). Therefore, the mesoporous SnO_2/C composites present amended electrochemical properties (Figure 1-10e).

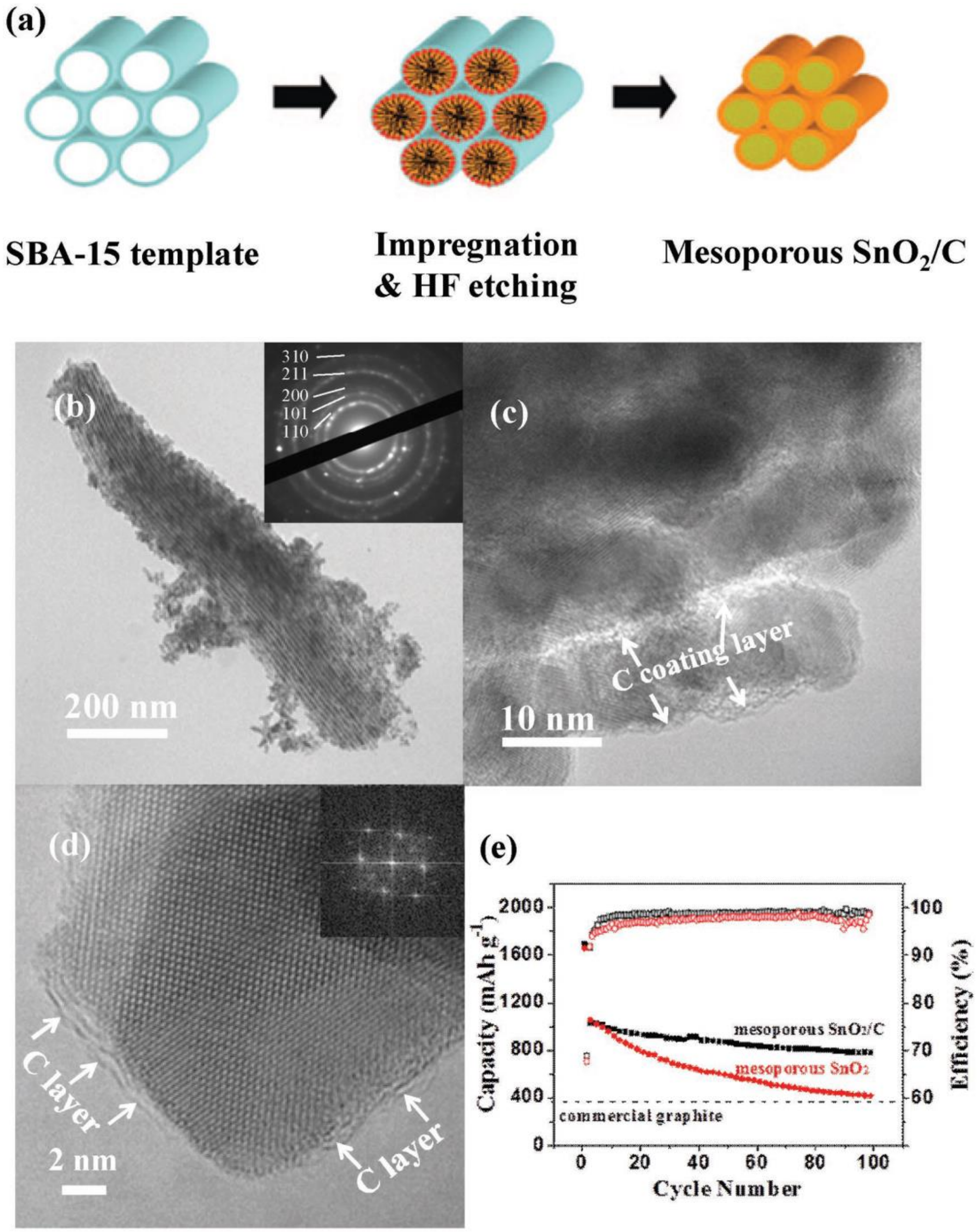

Figure 1-10. a) Schematic view of the preparation of mesoporous SnO_2@carbon core-shell nanowires. b) TEM image of the SnO_2@carbon core-shell structure and (c) enlarged TEM image of (b), showing the carbon-coated core-shell structure. d) HRTEM image of a mesoporous SnO_2@ carbon core-shell structure with graphitic carbon coated on SnO_2 crystalline.[95]

1.4.2 Graphite-derived materials

Carbon-based materials are progressively playing increasingly critical roles for energy storage in lithium-ion batteries (LIBs).[109] Graphite-derived materials, in particular, are appropriate for energy storage devices and especially for LIBs, owing to their layered structure and the reversible reaction between these materials and the lithium-carbon compounds used as electrolytes.[110] Graphite is extensively used as the anode material in LIBs due to its unique electrochemical and physical properties.[111,112] Despite its widespread use, the low theoretical capacity (372 mAh g^{-1})[113,114] and reduced rate capability[115] of graphite still restricts LIB performance. Theoretical research has indicated that reducing the dimensionality of routine anode materials via nanotechnology can realize higher energy capacity. Thus low dimensional carbon materials have been investigated as a replacement for graphite in LIB anodes.[116,117] Graphene, the carbon-based two-dimensional (2D) material discovered in 2004, has generated excitement among LIB researchers because of its atomic thickness, unique electronic properties, high mechanical strength, high thermal conductivity, and large surface area.[118,119] Graphene, along with its leading derivatives, has promoted rapid developments in LIB commercialization.[120,121] Graphene oxide (GO) can be easily synthesized on a large scale via the chemical oxidation and exfoliation of graphite. GO contains oxygen functionalities (epoxy, hydroxyl, carboxyl, and carbonyl groups) on its surfaces and edges, which help in the attachment of metal oxide nanomaterials for energy-related applications. Several techniques, such as chemical treatment, thermal annealing, microwave heating, and laser irradiation, can be applied to obtain the reduced GO (rGO). **Figure 1-11** presents a schematic illustration of the possibilities for the application of graphene/rGO and their derivatives in LIBs.

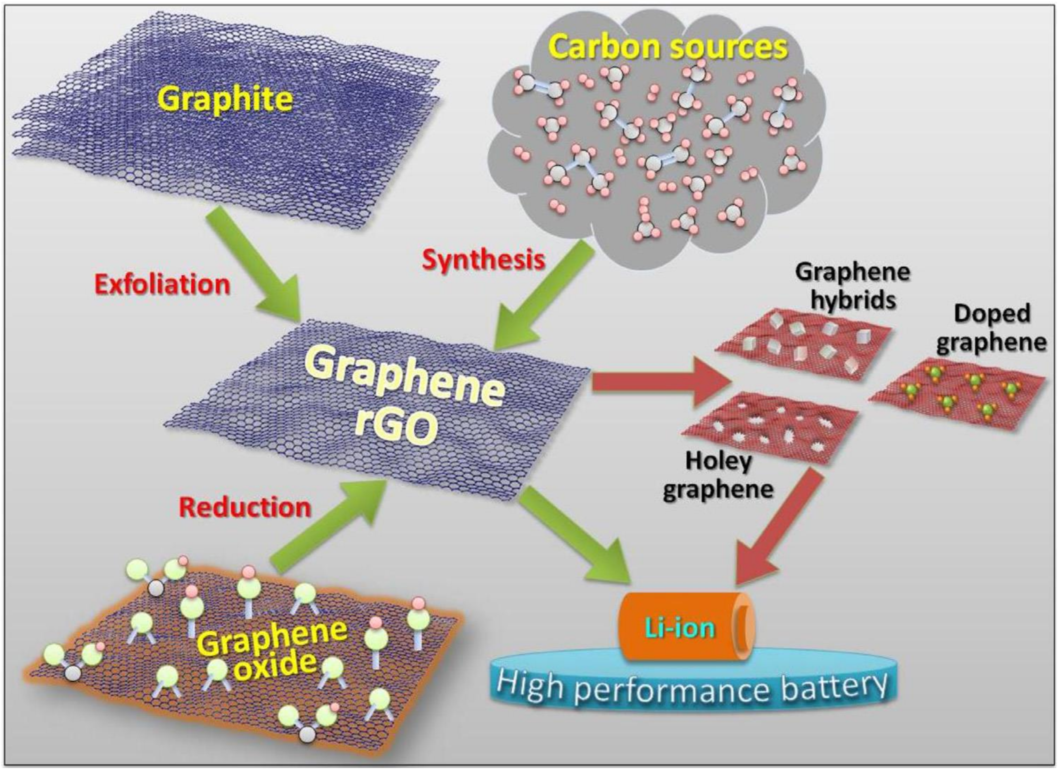

Figure 1-11. Graphene/GO and derived structures for application as electrode materials in LIBs.[122]

The main paths for the synthesis of graphene can be classified into two major categories: top-down and bottom-up methods.[123] In the top-down methods, bulk size materials are converted into their smallest compositional components.[124] Some of the main top-down methods to produce graphene from graphitic sources are mechanical/chemical exfoliation,[125-127] laser ablation,[128,129] plasma etching,[130] and unzipping of carbon nanotubes (CNTs).[131,132] In the bottom-up methods, the synthesis of graphene is accomplished from liquid or gaseous carbon-containing precursors.[133] Molecules/atoms are decomposed from carbonaceous precursors and in-situ arranged to form the hexagonal structure of graphene layers. CVD,[134,135] pyrolysis,[136] and epitaxial growth[137] are some of the main paths in this approach for the synthesis of graphene.

Figure 1-12 shows a schematic representation for the synthesis of graphene by both bottom-up and top-down routes.

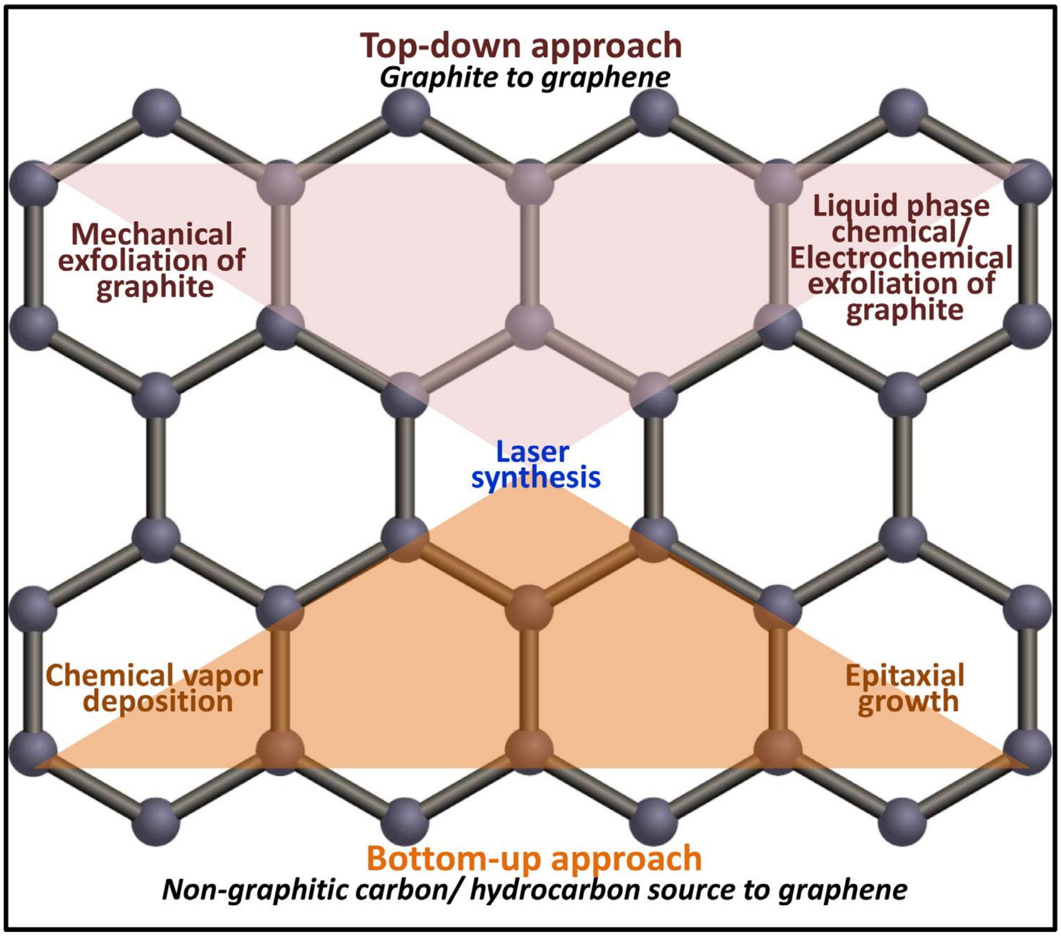

Figure 1-12. Schematic representation of graphene synthesis by different approaches.[122]

Reduced graphene oxide (rGO) has physical and chemical properties similar to those of graphene. The high electrical conductivity of rGO is of particular importance for application in nano-devices. Several GO/graphite oxide reduction methods have been employed to minimize the amount of oxygen present on the surfaces of GO, thus increasing its conductivity. Some of the essential reduction strategies involve chemical, thermal, microwave, or laser treatments (**Figure 1-13**).

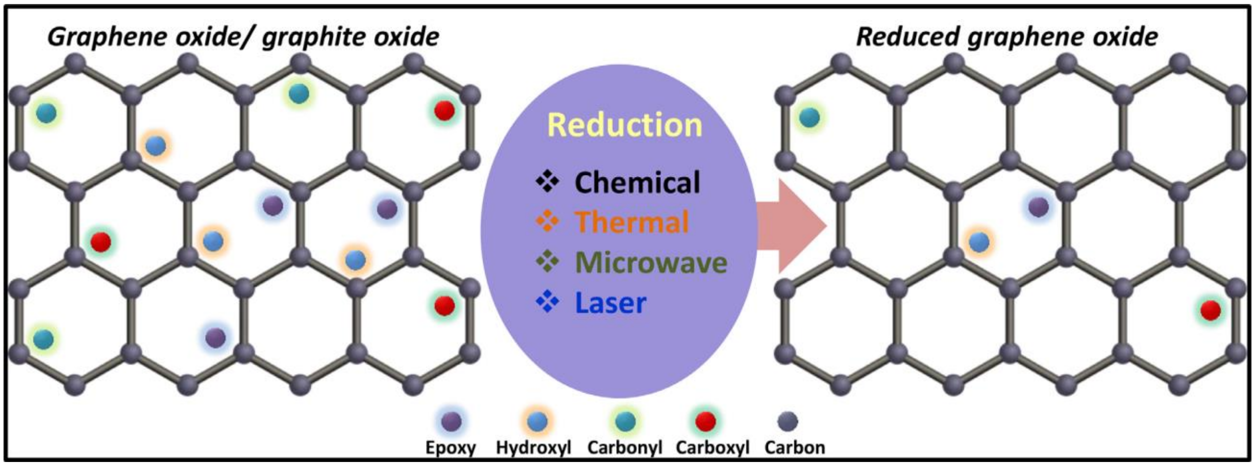

Figure 1-13. Reduction of GO/ graphite oxide into rGO using various methods.[122]

The GO contains many oxygen-containing groups, including epoxy, carboxyl, and hydroxyl groups. By changing the concentration of these oxygen-containing groups, GO can be turned into a material with tunable electrical properties. It is also important to note that GO can provide large numbers of active sites for anchoring electroactive materials. Overall, graphene/GO-based materials modified with metal oxides exhibit better electrochemical performance for LIB applications. Several C/metal oxide hybrid structures, with widely varying morphologies, have been proposed by Raccichini et al. as shown in **Figure 1-14**.[138]

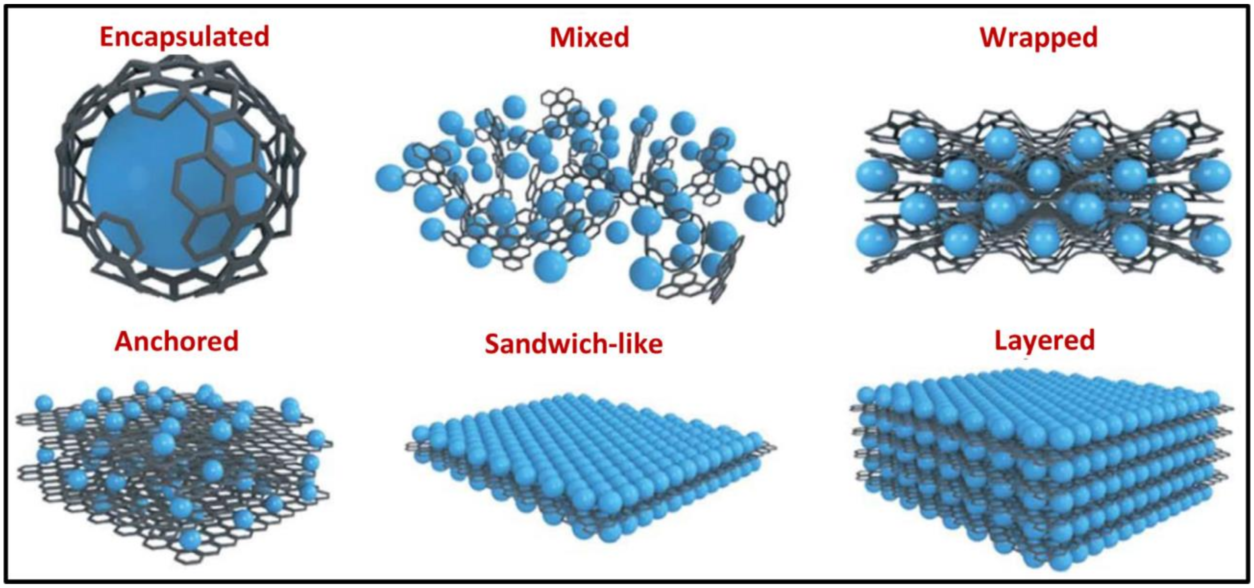

Figure 1-14. Structural models of different graphene-based composite electrodes.[138]

Kim et al. fabricated self-assembled ZnO nano-aggregates, using GO as the template, which exhibits superior electrochemical performance (**Figure 1-15**).[139] With the reduction of GO, the ZnO-based nanohybrids showed a high discharge capacity (752.8 mAh g^{-1}) after 65 charge/discharge cycles. The rGO-based electrode also displayed a capacity of 400 mAh g^{-1}, even when subjected to a current density of 2 A g^{-1}. According to the authors, the hierarchical self-assembled structure is the main reason for tremendous electrochemical performance.

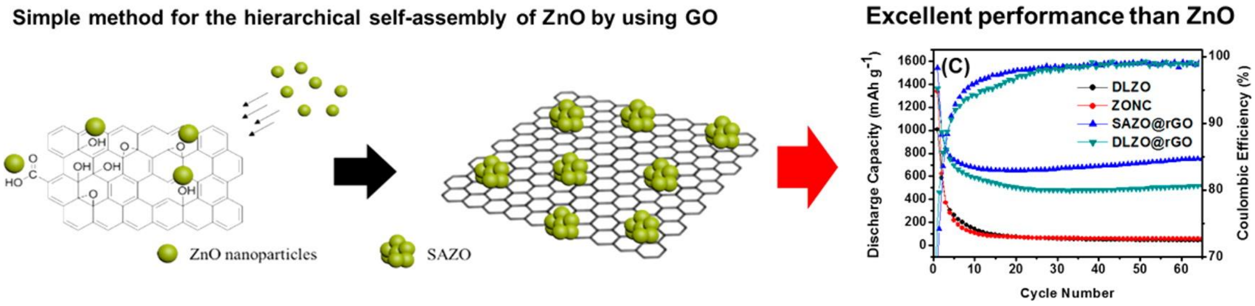

Figure 1-15. Illustration Depicting the Preparation of SAZO and GO Nanocomposite.[139]

Sun et al. synthesized a Co_3O_4-graphene core-shell composite by a solvothermal method (**Figure 1-16**).[140] This graphene-wrapped composite revealed enhanced electrochemical performance with a vast potential range of 0.01-3 V. With high surface area and synergistic interactions between Co_3O_4 and graphene. The hybrid electrode achieved high discharge and charge capacities of 1609 and 1115 mAh g^{-1}, respectively. The low CE for the initial cycle was caused by the formation of SEI, which is one of the common problems in LIBs. With 23.8 wt.% of graphene loading, the Co_3O_4-based nanohybrid maintained a high reversible capacity of 600 mAh g^{-1} up to 500 cycles.

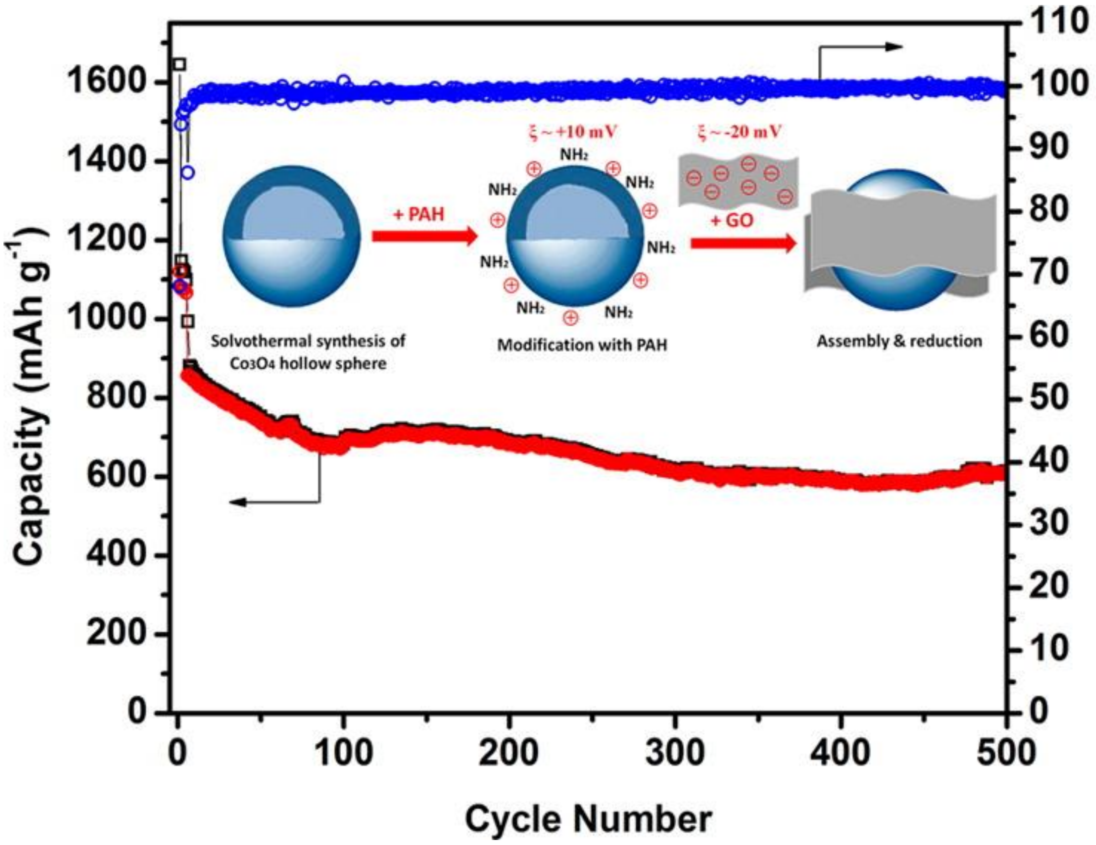

Figure 1-16. Scheme of the fabrication process of Co_3O_4@G core-shell composites.[140]

Liu et al. reported the sol-gel synthesis of LTO/graphene composites, which exhibited a capacity of 170.7 mAh g^{-1} at 1 C.[141] The specific capacity was lower than the ones for conventional metal oxide-based composites. However, the electrode retained ~99% of the specific capacity after 100 cycles. In another similar study, LTO/rGO exhibited a capacity of only 131.6 mAh g^{-1}, but no capacity fading was observed up to 500 cycles.[142] On the other hand, the rate capability was quite impressive, being higher than the one for pristine LTO. With a minimal graphene loading (3 wt.%), the nanohybrids exhibited long cycle life because of the more accessible transport of Li^+ ions.

Nonetheless, there are still many challenges to entirely surmount the inadequacies of carbon-based anode materials such as low initial coulombic efficiency, low tap density, and unsatisfactory cycling stability.[143]

1.5 Application of chemical vapor deposition in lithium-ion batteries

Chemical vapor deposition (CVD) is the most widely used method for synthesizing graphene because it fulfills the requirements for electronic applications (large area, high-quality graphene), which are frequently not achieved by exfoliation.[144,145] Another advantage of CVD is the flexible choice of carbon precursor materials.[146,147] On the other hand, the cost of CVD synthesis of graphene is higher than that of mechanical and liquid-phase exfoliation. In the CVD method, various types of carbon-containing substances are decomposed at high temperature in the absence of oxygen on metallic substrates for large-area graphene growth. Examples of carbon sources may be solids (camphor, sucrose, polymers), liquids (ethanol, benzene, hexane, turpentine oil), or gases (C_2H_2, C_2H_4, CH_4). Appropriate substrates are Cu, Ni, Au, Co, Pd, Pt, Ir, Ru, Re, Rh Ge etc..[148-152]

As shown in **Figure 1-17**, the growth mechanism involves several steps for final graphene formation. Depending on the substrate material, these steps may include decomposition, adsorption, dissolution, dehydrogenation, diffusion, nucleation, segregation, and precipitation (**Figure 1-18**).[153,154] Carbon has a relatively high solubility in Ni at high temperatures, so carbon dissolved in Ni diffuses, segregates, and precipitates to form graphene (few to multi-layers).[155] On the other hand, carbon has very low solubility in Cu, so it adsorbs on the surface and diffuses to form single, bi, and trilayer graphene.[155,156] For this reason, Cu is presently the most extensively used catalyst material, which offers reasonable control over the number of graphene layers formed.

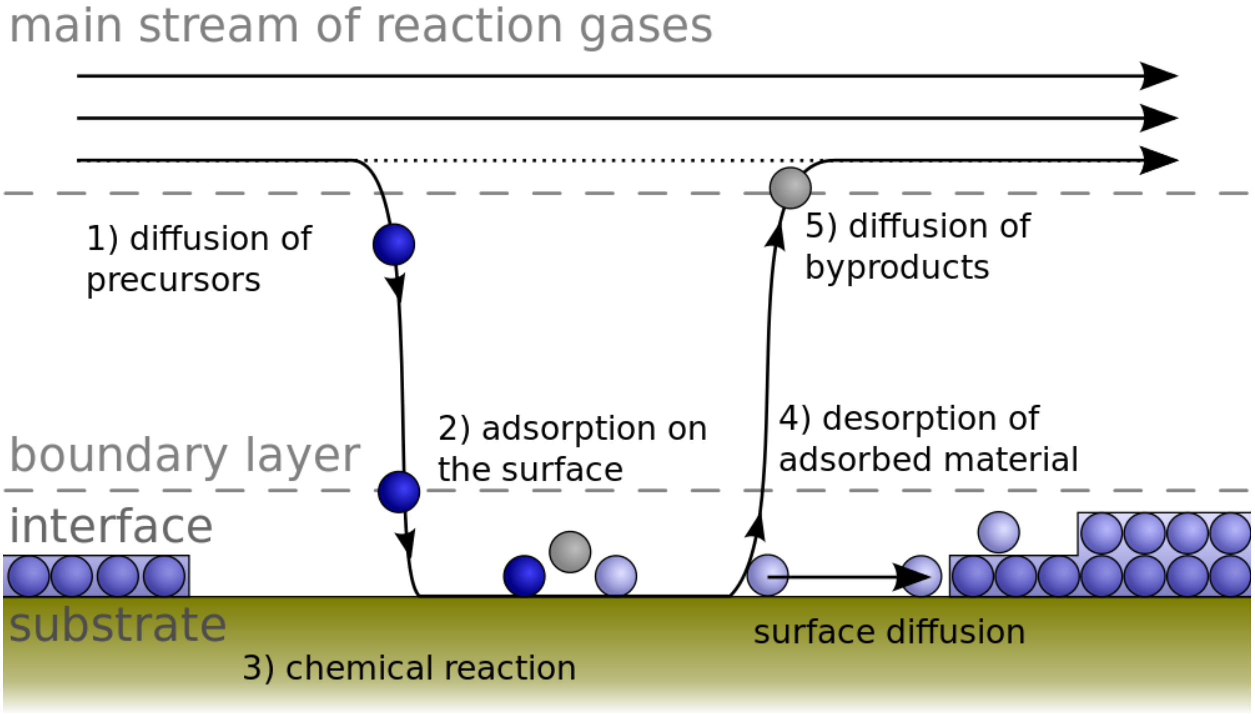

Figure 1-17. Scheme of a general process for chemical vapor deposition.

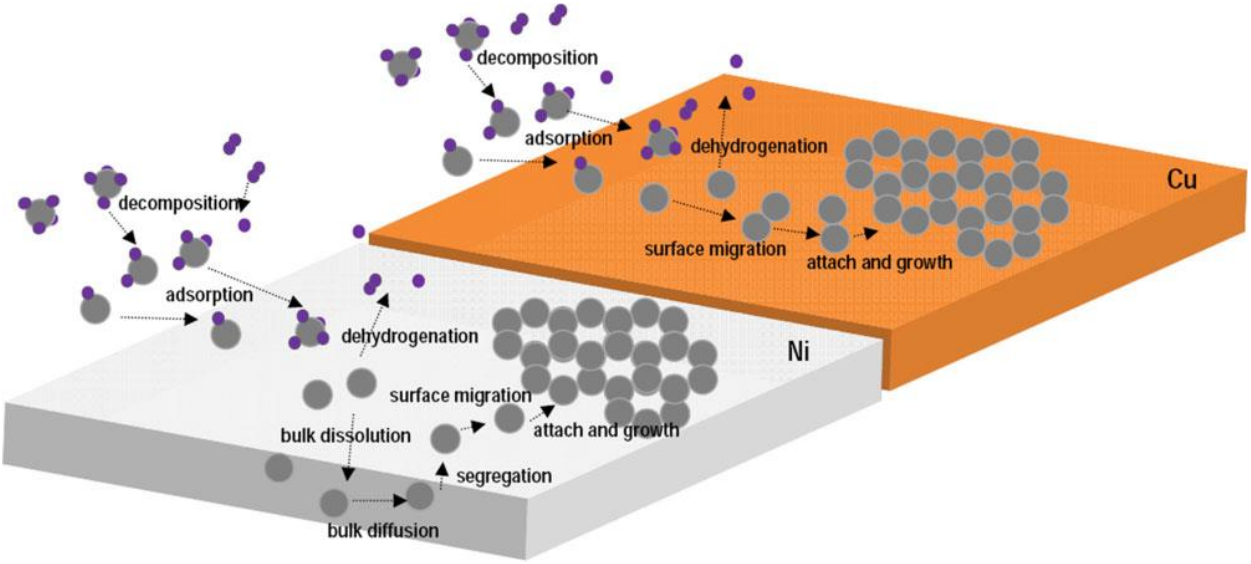

Figure 1-18. Growth kinetics in CVD-produced graphene on various catalysts: Case of CH4 on Ni and Cu.[157]

Hydrocarbon-based reactants, the most mentioned being methane (CH_4), are commonly used as C source. Due to strong C-H bonds in the methane molecule (440 kJ mol^{-1}), its thermal (non-catalytic or non-plasma-activated) decomposition occurs at very high temperatures (>1200 °C).[158] This high temperature is not easily obtained in a typical thermal CVD set-up. Different transition metal catalysts (e.g., Fe, Co, Ni, Cu) are widely used to reduce the temperature of the decomposition of methane. Such catalytic behavior is also confirmed during low-temperature (< 900 °C) graphene growth on metals, with assistance from CVD. Therefore, non-catalytic activation can be considered negligible when working in thermal systems.[159]CVD-assisted graphene material is usually relocated onto the particular substrate for further employment. Therefore, seeking specific dielectric substrates, such as BN, Si, SiO_2, Al_2O_3, GaN, MgO, and Si_3N_4, with the ability to endow direct growth of continuous graphene films is entirely worth exploring. Considerable efforts were made to grow graphene films on these substrates directly, but so far continuous and highly conductive films have been challenging to synthesize.[160-164]

1.6 Overview of sodium-ion batteries

Among the diverse available energy storage systems, the Li-ion battery, which has dominated the portable electronic market, has become the primary contender to power the next generation of electric vehicles (EV) and plug-in electric vehicles. Li-ion cells offer a sufficient energy density and output voltage of all rechargeable battery technologies in use. Moreover, Li-ion technology relies on rich and versatile chemistry leading to an extensive range of potential electrode materials for both cathodic ($LiCoO_2$, $LiMn_2O_4$, $LiFePO_4$) and anodic electrodes (C, Sn, Si, etc.).[15]

After that, so far, Li-ion batteries have attracted all the attention in energy storage. However, recently, Na-based compounds have made a comeback because of controversial debates regarding the size of reserves and higher cost to obtain Li.[165] Recently, worries have emerged about the availability reserve of lithium and hence future price, given the projected orders of exponential growth in lithium usage of batteries for hybrid or fully electric vehicles (EV). Though the mild extension of Li production can supply 1 MM 40 kW h vehicle batteries, to fulfill a long-term target with 100 MM 40 kW h Li-based EV batteries per year, a dramatic enlargement of annual production will be inevitable.[166] The issue is not deficient lithium reserves on a global scale, but what fraction can be used and still be economically practical.[167] Most untapped lithium reserves occur in remote or politically sensitive areas. Aggrandizement will necessitate an extended lead period, also involve massive capital investment in mining, and may require the extraction and refining of resources with inferior quality, which could lead to higher extraction costs. Currently, high costs remain a critical obstacle to the prevalent scale-up of battery energy storage. Concerning the long-term “stock” objective of 1 billion 40 kWh vehicle batteries, the available quantity of several Li-based materials is satisfactory but close to the boundary of what is accessible. Indeed, if following such a route, Li recycling will be obligatory. Although the argument over the viability and environmental influence of lithium carbonate production remain, sodium-based compounds are under consideration as options for abundant scale energy storage combined to renewable energy sources. Expansion of battery research regarding alternative materials may accelerate the ability to complete both the scaling and cost challenges of long-term planning for battery energy storage. Therefore it is urgent to search for low-cost replacements that have massive reserves.[166]

Table 1-2. Main characteristics of Na and Li materials.[15]

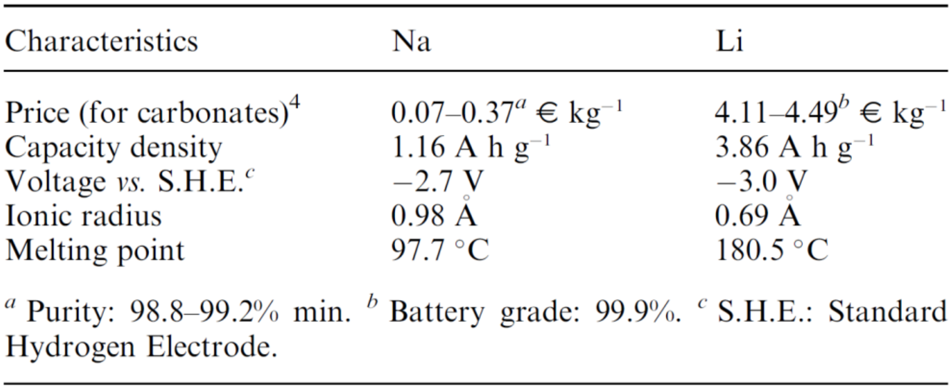

Characteristics	Na	Li
Price (for carbonates)[4]	0.07–0.37[a] € kg^{-1}	4.11–4.49[b] € kg^{-1}
Capacity density	1.16 A h g^{-1}	3.86 A h g^{-1}
Voltage *vs.* S.H.E.[c]	−2.7 V	−3.0 V
Ionic radius	0.98 Å	0.69 Å
Melting point	97.7 °C	180.5 °C

[a] Purity: 98.8–99.2% min. [b] Battery grade: 99.9%. [c] S.H.E.: Standard Hydrogen Electrode.

The use of Na in place of Li in batteries could alleviate the available shortage of lithium economically, due to the unlimited sodium sources, the ease to recover it, and its lower price (**Table 1-2**). Furthermore, sodium intercalation chemistry of positive electrode materials is very comparable to lithium, hence making it possible to practice very similar compounds for both systems. Moreover, if a rechargeable sodium-ion battery with excellent performance features could be developed, it could have the benefit of using electrolyte systems with lower decomposition voltage, since the higher potential of half-reaction for sodium concerning lithium. This low operating voltage would make Na-ion batteries more economical because water-phase electrolytes could be applied instead of organic electrolytes. The Na has already been successfully used in Na/S and Na/$NiCl_2$ Zebra batteries.

It has to be indicated that Na-ion batteries will always fall short of meeting requirements of specific energy densities, if compared to Li-ion batteries, for the following reasons. 1) The molecular weight of sodium is much higher than lithium. 2) The ionization potential rises from 3.893 eV to 5.390 eV as it goes from Cs to Li in the sequences of alkali metal elements. The lower the ionization potential, the faster the electron shifts from the alkali metals to the anode. For example, graphite is used as a typical anode material. Consequently, the potential energy could be harvested based on the charge transfer becomes smaller in the order of Cs > Rb > K > Na > Li. 3) Though it looks inconsistent with what occurs with lithium intercalation. The smallest ionic diameter of Li can explain this fact. Therefore, Na-based batteries will have difficulties competing with Li-based batteries in terms of energy density. Nevertheless, they can be considered for use in applications which have mild requirement on the weight and footprint, for example, storage of off-peak and substantially fluctuating renewable energies, such as wind and solar farms. Despite these considerations, there exists an increasing interest in the Na-ion energy storage system. Recent computations by Ceder et al. on stability, potential, and diffusion barrier of Na-ion and Li-ion materials designate that Na-ion systems can be competitive with Li-ion systems.[168] In any case, Na-ion batteries would be impressive for keeping down the cost for grid storage, which could make renewable energy an essential source of energy rather than just a standby.

The search for commercially feasible Na-ion batteries requires discovering and adjusting new electrode materials and electrolytes for more economical, safer, and more lasting battery systems. One of the ways to get more economical systems would be exploring the aqueous-phase electrolyte, which would not exact ultra-dry fabricating conditions and would not apply higher-cost organic electrolytes. Another subsidiary saving could be the use of cheaper materials for assembling the battery, for instance, the current collectors.

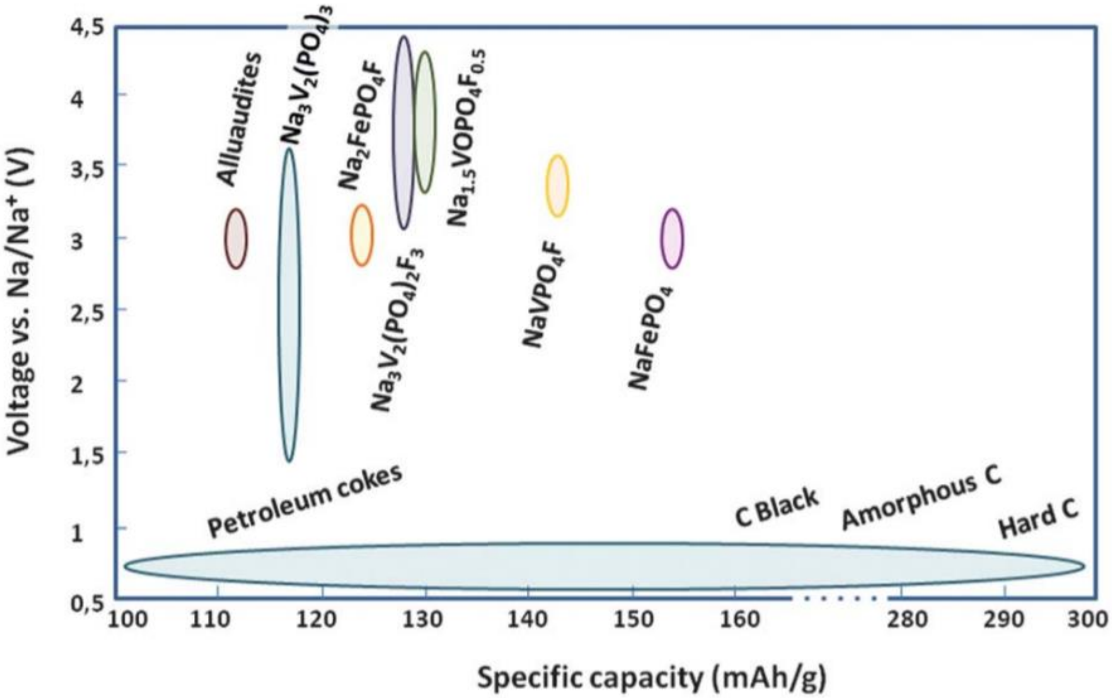

Figure 1-19. The most critical cathode and anode materials studied for their application in sodium-ion batteries, represented by their specific capacity and operating voltage versus a sodium metal anode.[15]

Figure 1-19 depicts the most essential cathodic and anodic materials for sodium-ion batteries, indicating their specific capacity and operating voltage. It is not hard to see that many materials have been reported in the literature as potential cathodic candidates for Na-ion batteries. In contrast, only some carbon-based anodes have been pointed out for this storage technology.

The favorite family of cathodic materials in a Na-ion battery is phosphate-based materials, die to their decent thermal stability and higher voltage window. It is worth mentioning that olivine $NaFePO_4$ has the highest theoretical specific capacity among $NaVPO_4F$, $Na_3V_2(PO_4)_2F_3$, Na_2FePO_4F, and $Na_3V_2(PO_4)_3$.[14] Still and all, these phosphates require conductive coating and nano-crystallization for realizing the improvement of electrochemical performance.

As for the anodic materials, the use of metallic sodium is not practical due to the formation of the dendrite, and aging problems happen in the interface. Furthermore, alternative anode materials must be explored to fabricate aqueous-phase Na-ion batteries.

1.7 Anode material for sodium-ion batteries

The exploration of proper anode materials for Na-ion batteries is sophisticated. Although a great diversity of phases that can potentially be used as cathode electrodes which have been identified, very few valuable materials have been reported for anode electrodes.[15]

1.7.1 Carbon-based anodic materials

Graphite, the anode of choice in LIBs with a high theoretical specific capacity of 372 mAh g^{-1}, operates at a flat and low potential of ≈ 0.15 V *vs*. Li^+/Li and is stable over many cycles. When applied to the SIB system, the electrochemical insertion of sodium into graphite results in NaC_{64}, corresponding to the deficient theoretical capacity of only 35 mAh g^{-1}.[169,170] It was initially proposed that the more significant Na^+ ion mismatches the graphite interlayer distance of 3.35 A, and results in less favorable formation energy for binary graphite intercalation compounds (b-GIC).[171-173] However, this could not explain the fact that other b-GIC such as MC_6 and MC_8 (where M is the alkali metal) are readily formed with heavier alkali metals such as K, Rb, and Cs.[174] It is therefore evident from the above that the ionic radii of the alkali metals are, at least, not the only inhibiting factor.

Expanded graphite (EG) is yet another carbonaceous anode material that has been proposed for SIB application.[172] The charge insertion mechanism in EG is illustrated in **Figure 1-20a**, where pure intercalation is therein assumed. Further explorations in the role of the oxygen-containing surface groups in the insertion mechanism are, however, needed. A comparison between the voltage profiles obtained in EG and the typically observed voltage profiles in rigid carbon-based electrodes (see Figure 1-20b,c) reveals that the voltage profiles reported in EG only show a sloping profile and do not manifest a plateau region. This fundamental difference could be a result of the modification of the distribution of intercalation sites due to the function of heteroatoms, such as the oxygen-containing surface groups.

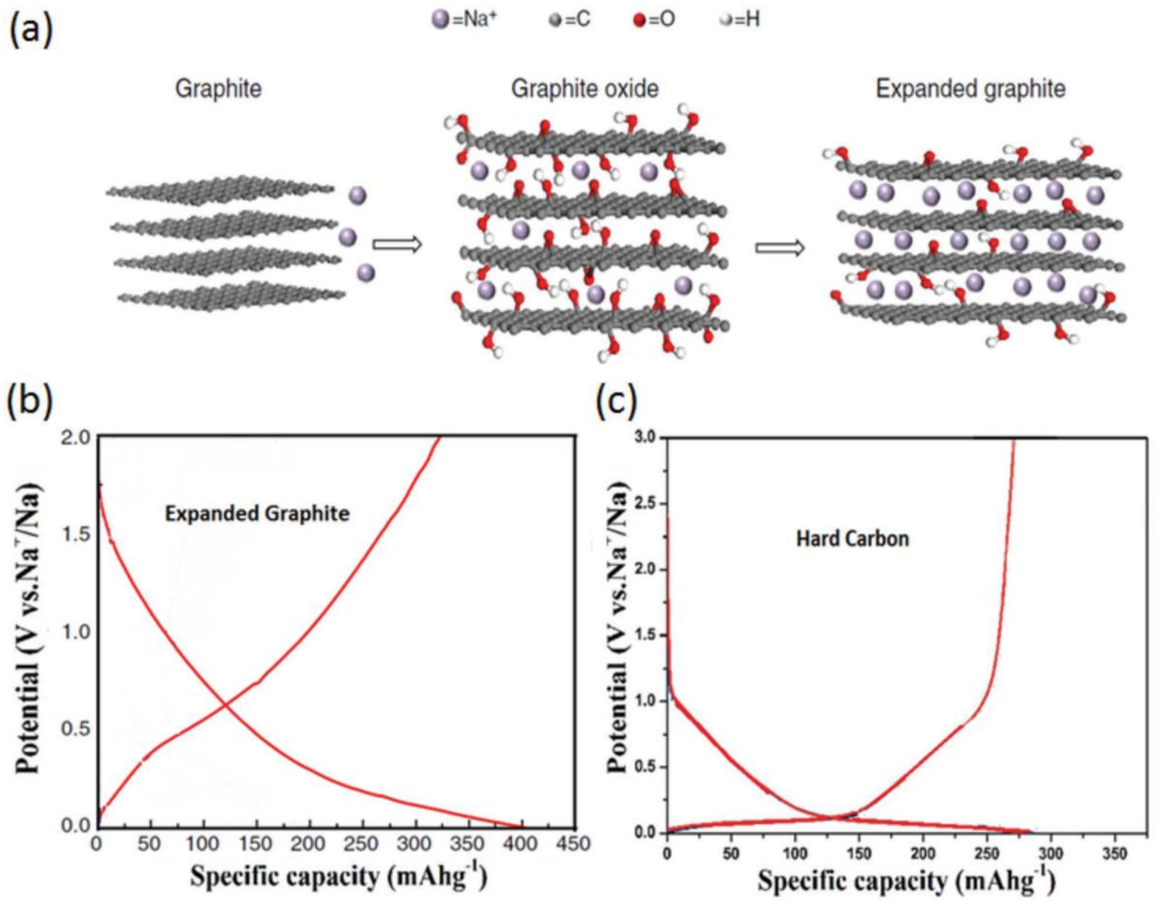

Figure 1-20. Overview of sodium storage in hard carbon and expanded graphite. a) Illustrative figure showing sodium intercalation in graphite, graphite oxide, and expanded graphite. b) Voltage profile in expanded graphite showing a sloping potential. c) Typical voltage profile in hard carbon.[14]

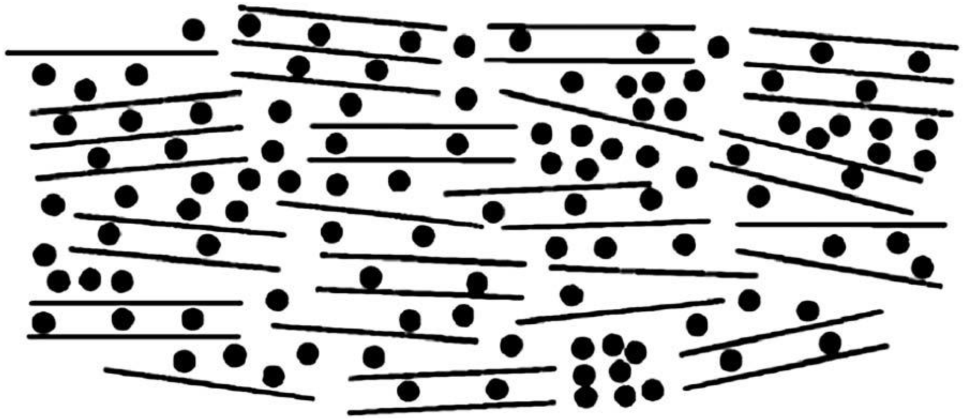

Figure 1-21. “House of cards” model for sodium/lithium filled hard carbon.[15]

The state-of-the-art anode material for SIBs is hard carbon, prominent since its inception in the year 2000.[171] Hard carbons are usually prepared by high-temperature carbonization of solid-phase organic and polymer precursors such as cellulose,[175] glucose,[176] sugar,[177] and poly-pyrrole.[178] The complex microstructure of HC is composed of graphene-like parallel layers embedded in a microporous amorphous phase. This structure is frequently exemplified by the "house of cards" model, which is here shown in **Figure 1-21**. The charge and discharge voltage profile of HC is also shown in **Figure 1-22**. From these results, two characteristic features are evident: i) a sloping region from ≈ 1 V, and ii) a long plateau region commencing from about 0.1 V until reaching 0 V (*vs*. Na^+/Na).

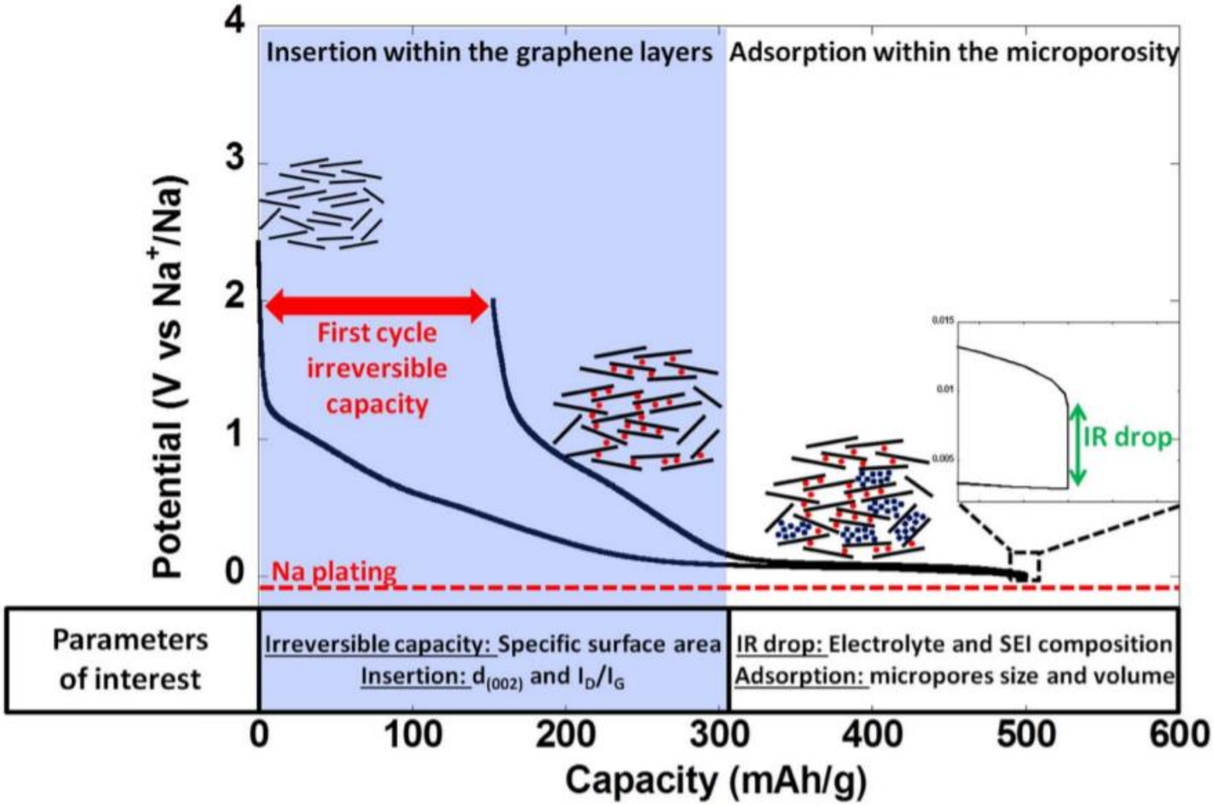

Figure 1-22. Typical potential vs. capacity profile for hard carbon when tested against sodium metal counter electrodes.[179]

Doeff et al. discussed the electrochemical insertion of sodium into a petroleum-coke carbon and observing a reversible capacity of 85 mAh g^{-1}.[180] They evidenced the highest value reported for electrochemical "intercalation" of Na-ion on carbonaceous materials (NaC_{15}) by using submicron particle-sized carbon powder (**Figure 1-23**).

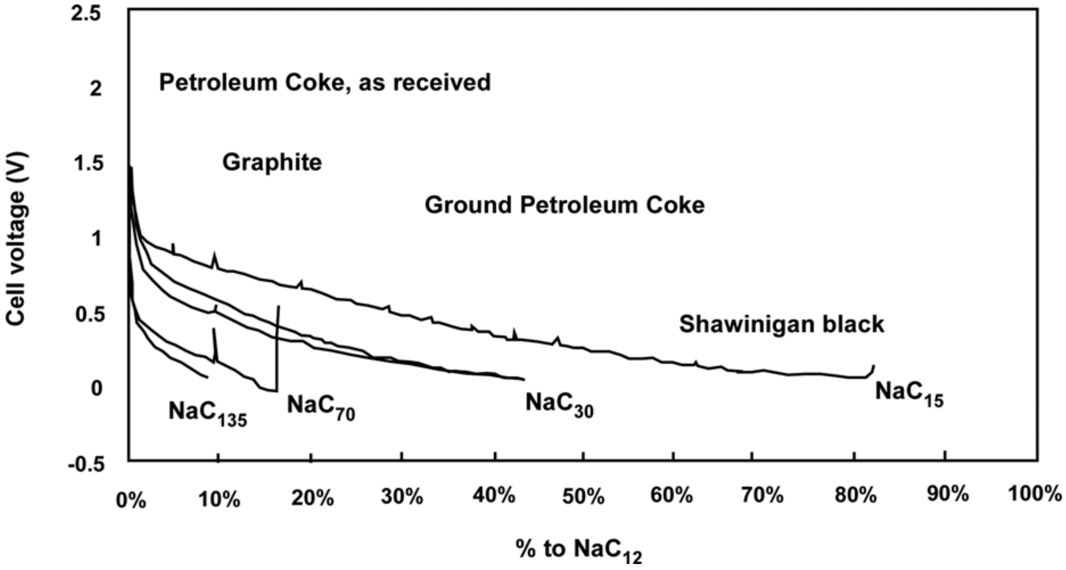

Figure 1-23. Discharge curves (50 mA cm^{-2}) of Na/P(EO)$_8$NaCF$_3$SO$_3$/C cells heated to 86 °C. The spikes in the profiles are due to periodic current interrupts to assess the cell polarization.[180]

Tirado's group presented the reversible capacity of 121 mAh g^{-1} and 200 mAh g^{-1} for the discharging of amorphous carbon black, where 0.0155 moles of Na could be inserted in 1 cm^3 of carbon material.[181] It was confirmed that sodium was stored between the graphene layers in the amorphous carbon black, and the accessibility of carbon surface was another limiting condition for the capacity contribution. The same research group, some years later, showed improvements by using amorphous carbon obtained from the pyrolysis of a polymeric resin forming microspheres with high surface area (**Figure 1-24**).[182] The reversible capacity for this material, through the insertion of Na-ion, was 285 mAh g^{-1}, which is also unaffected about the addition of different ether solvents in the electrolyte. As ether-type solvents are chemically reactive against metallic sodium than carbonate-based electrolytes, optimizing the additive amount of ether-based solvents in the liquid and solid electrolytes will be the key for the electrochemical efficiency of the batteries.

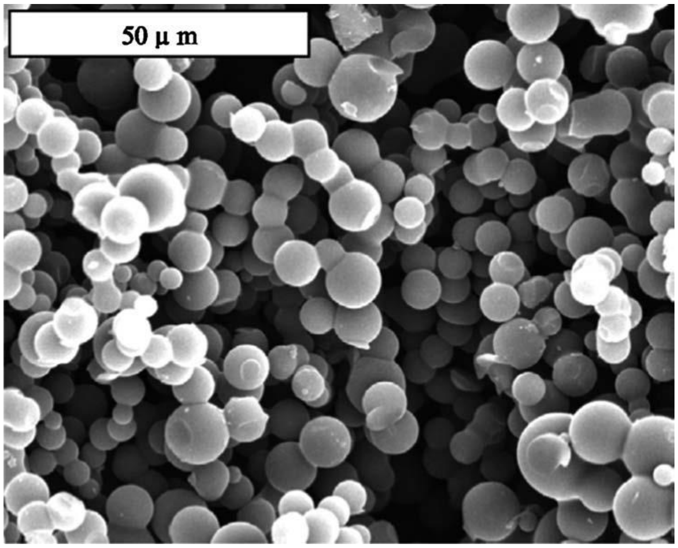

Figure 1-24. SEM of carbon microspheres.[182]

Prof. Janek's group has made a templated carbon which could provide 130, 120, and 100 mAh g^{-1} at C/5, 2 C, and 5 C rates, respectively.[183] They reveal the specific storage mechanism where at the first capacity value corresponds to a NaC_{17} nominal composition. Up to the present time, similar capacities but reduced cyclability could be reached only for carbon black at room temperature with a current density as small as C/75. This remarkable result is attributed to the hierarchical pore system in the material, which consists of interconnected pores in the macro- and mesopore range that enables fast ion transport and short diffusion lengths. This structure is produced from porous silica as a template and mesophase pitch as a carbon precursor, which develops into a well-defined and thus highly conductive carbon microstructure compared to other carbons.

1.7.2 Titanium-based anodic materials

Several titanium-based compounds are extensively studied as possible intercalation hosts in SIBs, and this is partly due to their promising applications in LIBs.[184-187] The first successful sodium intercalation in anatase-type TiO_2 occurred in its nanocrystal forms.[188] Nanocrystalline TiO2 has an impressive rate capability at a moderate gravimetric capacity of about 150 mAh g^{-1} and exhibits stable cyclability up to 1000 cycles.[188,189] Furthermore, an outstanding rate capability of 11 C rate is reported in carbon-coating free samples, the highest among either carbonaceous or Ti-based SIB anodes.[189] This is a phenomenal achievement, given the fact that TiO_2 has a low electric conductivity intrinsically. **Figure 1-25a** illustrates the crystal configuration in TiO_2. Figure 1-25b shows a high-resolution SEM image of pristine TiO2 nanoparticles. The electrochemical properties of TiO_2 are illustrated in Figure 1-25c-f, where a sizeable first cycle irreversible capacity loss is highlighted and based on the cyclic voltammetry analysis, the redox reaction appears to be kinetically limited. However, the cyclability and rate performance are outstanding.

Several disadvantages, however, persist in anatase TiO_2, some of which are illustrated in Figure 1-25c. The most evident being a sloping voltage profile that undermines the available energy density. Furthermore, a first cycle Coulombic efficiency of only 42% is rather unimpressive. In general, nanosized active materials come at a penalty of increased SEI formation and side reactions at the surface of the active material, and this results in the mostly irreversible capacity loss therein evidenced. However, despite these challenges, nanocrystalline TiO_2 remains a promising candidate anode material for high-power SIB applications.

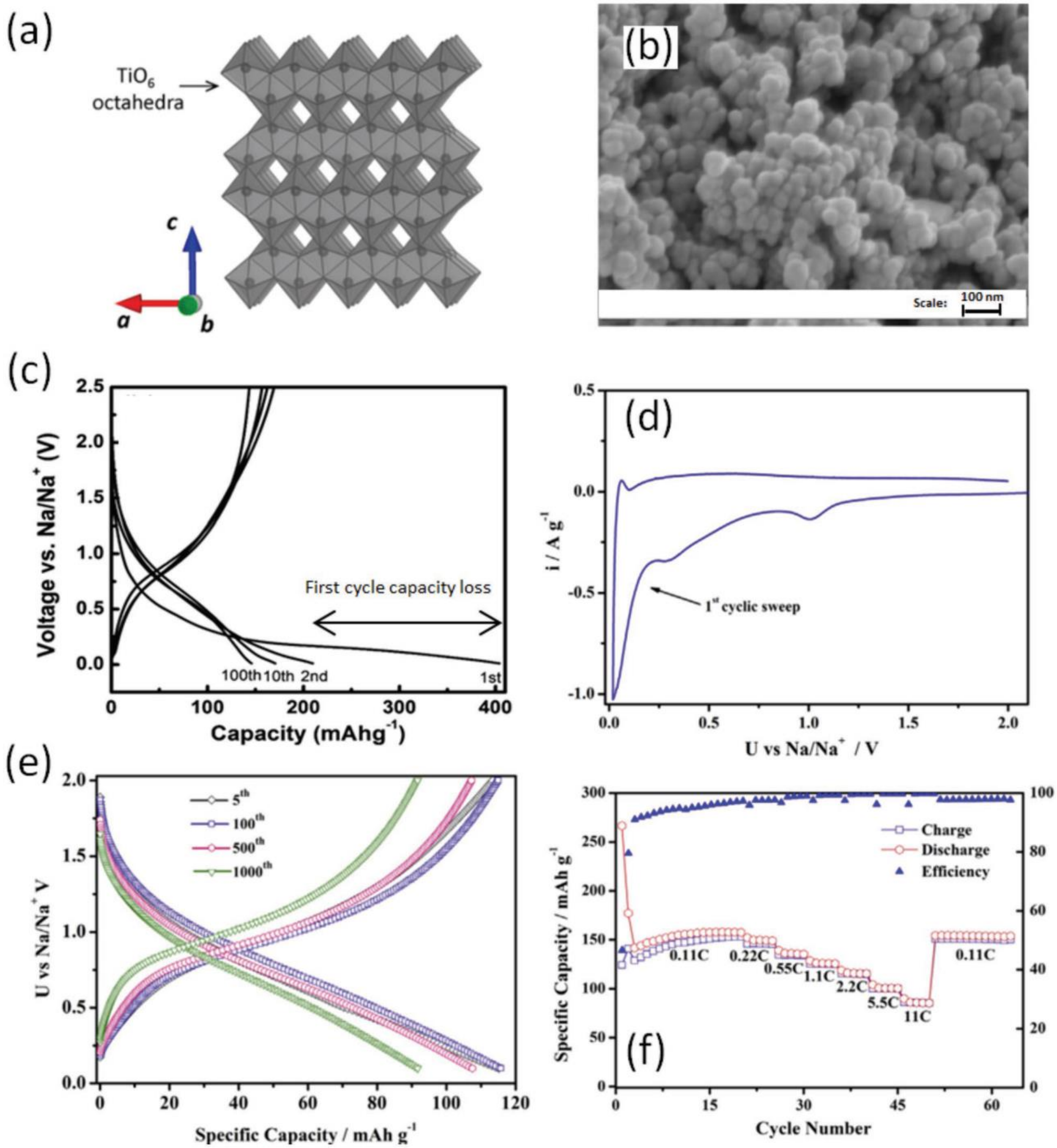

Figure 1-25. Properties of anatase-type TiO_2. a) Schematic illustration of the configuration of TiO_2 octahedra and b) SEM image of pristine TiO_2 nanoparticles. c) The first 100 charge/discharge voltage profiles of TiO_2 showing the first cycle irreversible capacity loss and d) cyclic voltammogram of TiO_2, illustrating the first cycle sweep. e) Extended cycling voltage profiles of TiO_2 showing 1000 cycles. f) Rate capability tests of TiO_2 and a high rate of 11 C is evidenced while a return to 0.11 C recovers the initial capacity.[14]

Sodium titanates, the compounds composed of Na_2O and TiO_2 with a general composition series of Na_2O-nTiO_2, have also been applied as anode materials in SIBs.[190] In 2011, Senguttuvan et al., in a quest for low-voltage transition metal oxides, investigated the electrochemical insertion of sodium in $Na_2Ti_3O_7$, [191] a compound which hitherto had been utilized for divers proposes such as photocatalysis and heavy metal removal from wastewater.[192] Surprisingly, $Na_2Ti_3O_7$ can reversibly insert up to 2 moles of Na^+ ions per formula equivalent, corresponding to ≈ 200 mAh g^{-1}, while $Li_2Ti_3O_7$ can only intercalate 1.4 moles of Li^+ ions.[193] An impressively low and plateau (flat) discharge potential of 0.3 V *vs*. Na^+/ Na was also evidenced, culminating in the lowest intercalation potential recorded in oxide electrodes of either LIBs or SIBs. **Figure 1-26a-c** illustrates the structure and electrochemical properties of $Na_2Ti_3O_7$.

While microsized $Na_2Ti_3O_7$ is electrochemically active, it suffers from a short cycle-life. On the other hand, nanosized samples of $Na_2Ti_3O_7$have a significantly improved cyclability, but due to the increase in surface area, the first cycle Coulombic efficiency is unimpressive. Several optimizations challenge to simultaneously reduce the first cycle irreversible capacity and increase the cyclability remain in $Na_2Ti_3O_7$. Interestingly, however, nanosized and carbon-coated $Na_2Ti_3O_7$samples, as shown in Figure 1-26c, exhibit longer cycle life. Carbon coating has thus proved to be a highly beneficial strategy to enhance the electronic conductivity and simultaneously reduce the SEI formation in such electrode materials.[194,195]

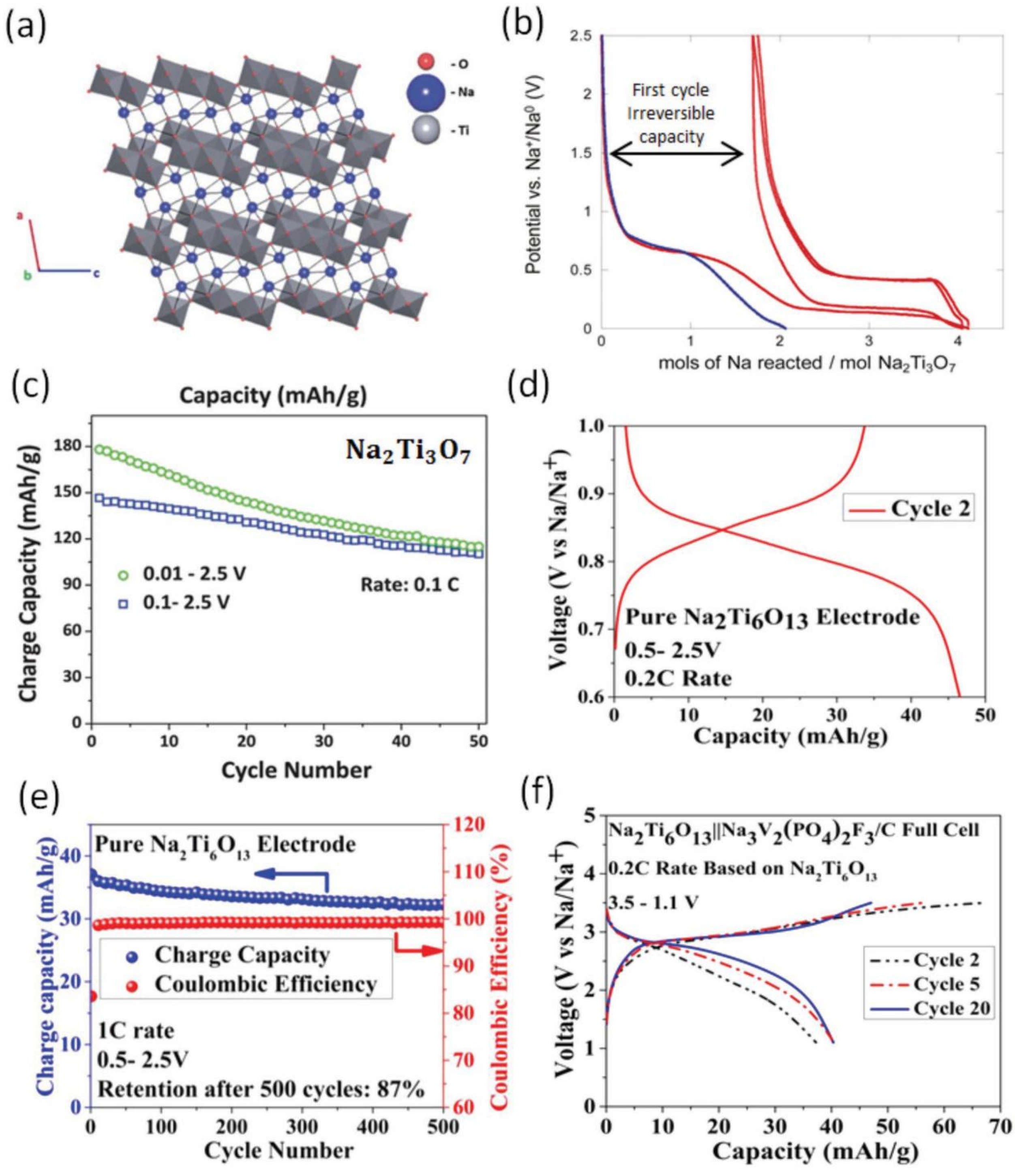

Figure 1-26. Structure and electrode performance of sodium titanates. a) The structure of $Na_2Ti_3O_7$ viewed along the b-axis. b) Charge and discharge cycles of microsized $Na_2Ti_3O_7$. c) Charge capacity versus cycle number of carbon-coated, nanosized $Na_2Ti_3O_7$/C. d) Second cycle

voltage profile of $Na_2Ti_6O_{13}$. e) Capacity versus cycle number for $Na_2Ti_6O_{13}$at 1 C rate. f) A pure $Na_2Ti_6O_{13}$// $Na_3V_2(PO_4)_2F_3$/C full cell cycled at C/5 rate.[14]

Sodium nano titanate $NaTi_3O_6(OH)\cdot 2H_2O$, and its dehydrated form, are another titanium-based anode material that was first reported by Shirpour et al. in 2013.[196] Although an attractively low voltage of 0.3 V *vs.* Na^+/Na is therein reported, the voltage curve exhibits a sloping profile and attribute of the solid-solution charge insertion mechanism. Furthermore, a severe loss in capacity in the first cycles points to the need for electrode optimization.

Even though a relatively flat voltage profile is observed in the charge/discharge profile, as illustrated in Figure 1-26d, the average voltage thereof is too high (0.8 V *vs.* Na^+/Na). It limits the energy density of SIB cells fabricated with a $Na_2Ti_6O_{13}$ anode material, also considering the low gravimetric capacity of the samples. Indeed, Rudola et al. prepared such a cell using a $Na_3V_2(PO_4)_2F_3$/C composite electrode in EC/PC and 1 M $NaClO_4$ electrolyte.[197] As expected, the resulting average cell voltage of 2.5 V and capacity for the weight of the anode of 41 mAh g^{-1} after 20 cycles were relatively low. In this study, they used an excess cathode in the balanced full cell, most likely as a strategy to overcome the anodic first cycle irreversible capacity loss.

Spinel $Li_4Ti_5O_{12}$ (LTO), a known “zero-strain” anode material for LIBs,[66] was first reported as a sodium host in 2012 by Liang et al..[198] As a SIB anode, $Li_4Ti_5O_{12}$ has an attractively high plateau voltage between 0.5 and 0.8 V *vs.* Na^+/Na and achieves a reversible capacity of 145 mAh g^{-1}. Three-phase structural evolutions upon Na insertion are also reported, wherein pristine $Li_4Ti_5O_{12}$ evolves to $LiNa_6Ti_5O_{12}$ and $Li_7Ti_5O_{12}$ upon Na insertion.[198] Early optimizations of LTO composite electrodes focused on binders.[199] Compared to conventional polyvinylidene difluoride binders, sodium alginate and carboxymethyl-cellulose sodium binders resulted in better cyclability and coulombic efficiency. Recently, Na-doped LTO has been reported to have an improved electrode capacity of 150 mAh g^{-1} and an enhanced cyclability of 800 cycles,[200] while a superior rate capability of 10 C rate and 15 C rate has been reported in carbon-coated nanosheets and LTO nanorods, respectively.[201,202] Although these electrochemical properties are desirable for a safe SIB, a general drawback for LTO is a relatively high operating electrode potential for application in high energy density cells.[171]

Chapter 2. The objective of this dissertation

As mentioned in the last chapter, electronic conductivity and lithium-ion diffusivity are two essential factors in improving the performance of lithium-ion batteries, especially at the fast charge and discharge aspects.

So far, forming carbon composites is the most used tactic for electronic conductivity enhancement because of its economical and practical. However, typical methods, such as blending with conductive carbon, carbide encapsulation, and *in-situ* growth on carbon materials, will also present new issues, such as low initial coulombic efficiency, reduced high-rate performance, weak cyclability, and low tap density. For the improvement of lithium-ion diffusion, nanosizing particles are the most direct way. However, small granules are usually unable to tolerate high-temperature treatment, which could cause particle aggregation and result in smaller solid/electrolyte contact area. Such property will severely affect available processing methods to promote battery performance, like high-temperature carbonization and chemical vapor deposition for carbon coating. It is also worth mentioning that nanoparticles will also lead to small tap density, which will dramatically lower the volumetric energy density for the battery, and then impede the further commercialization.

One of the essential high-power anodic family is the titanium-based materials, such as TiO_2 and $Li_4Ti_5O_{12}$, because of their remarkable structural stability in tolerating fast reaction kinetics. Unfortunately, the performance of these materials is severely constrained by the above issues.

Hence, the current dissertation will start the exploration of hybrid approaches by combining material and structural design to overcome both low electronic conductivity and slow ion diffusion topics and retain high volumetric energy density for titanium-based high-rate anode materials.

On the other hand, sodium-ion batteries, as the substitution of lithium-ion batteries, have relatively immature systems, particularly for anode electrode materials. The as-mentioned two principal elements are also perplexing further developments of sodium-ion batteries. In consequence, the current dissertation will also seek the appropriate titanium-based candidates through hybrid approaches to achieve superior cyclability and rate performance.

Chapter 3. Using silica as a catalyst for CVD-carbon-coating and precursor of silicate anode material of lithium-ion batteries

3.1 Introduction

As described above, chemical vapor deposition (CVD) has been mainly used as a technology to synthesize graphene in the battery field. It can form a high-quality surface carbon-coating on the catalyst, which is loaded on the substrate. Most of the catalysts are in the form of pure metal or metal oxides to conduce the catalysis with mild temperature (< 1000 °C). However, such form usually does not have electrochemical activity, which means they need to be removed by further treatment for utilization in the formation of the electrode material. Considering the cost of the CVD process is generally higher than other traditional methods of producing graphene material, the overall commercial value of employing CVD in large-scale production of electrode materials is not entirely favorable. Therefore, seeking the particular substrates which have both catalytic ability of the CVD process and electrochemical activity for batteries is very remunerative.

Recently, Hyuk et al. discovered the potential of silica for the synthesis of 3D graphene using methane-CVD treatment without a metal-based catalyst.[203] They demonstrated the reaction as $SiO_2 + CH_4 \rightarrow SiO_x + OH^- + 3H^+$ + carbon(graphene), where SiO_x provides catalytic sites for graphene growth, and OH^- serves as a mild oxidant to facilitate the graphitic carbon formation toward graphene and prevents the formation of silicon carbide (SiC) layer at the surface of SiO_x. They mentioned that for a 30 min treatment under 1000 °C with methane gas, a prominent growth of graphene was confirmed. With the increase of CVD duration, the silica particle started to break up. Then, instead of surface growth, the graphene carbon began to become unoriented and form a popcorn-like ball structure (**Figure 3-1**). However, they proceed with graphene coating to make carbon composite with commercial $LiNi_{0.6}Co_{0.1}Mn_{0.3}O_2$ powder.

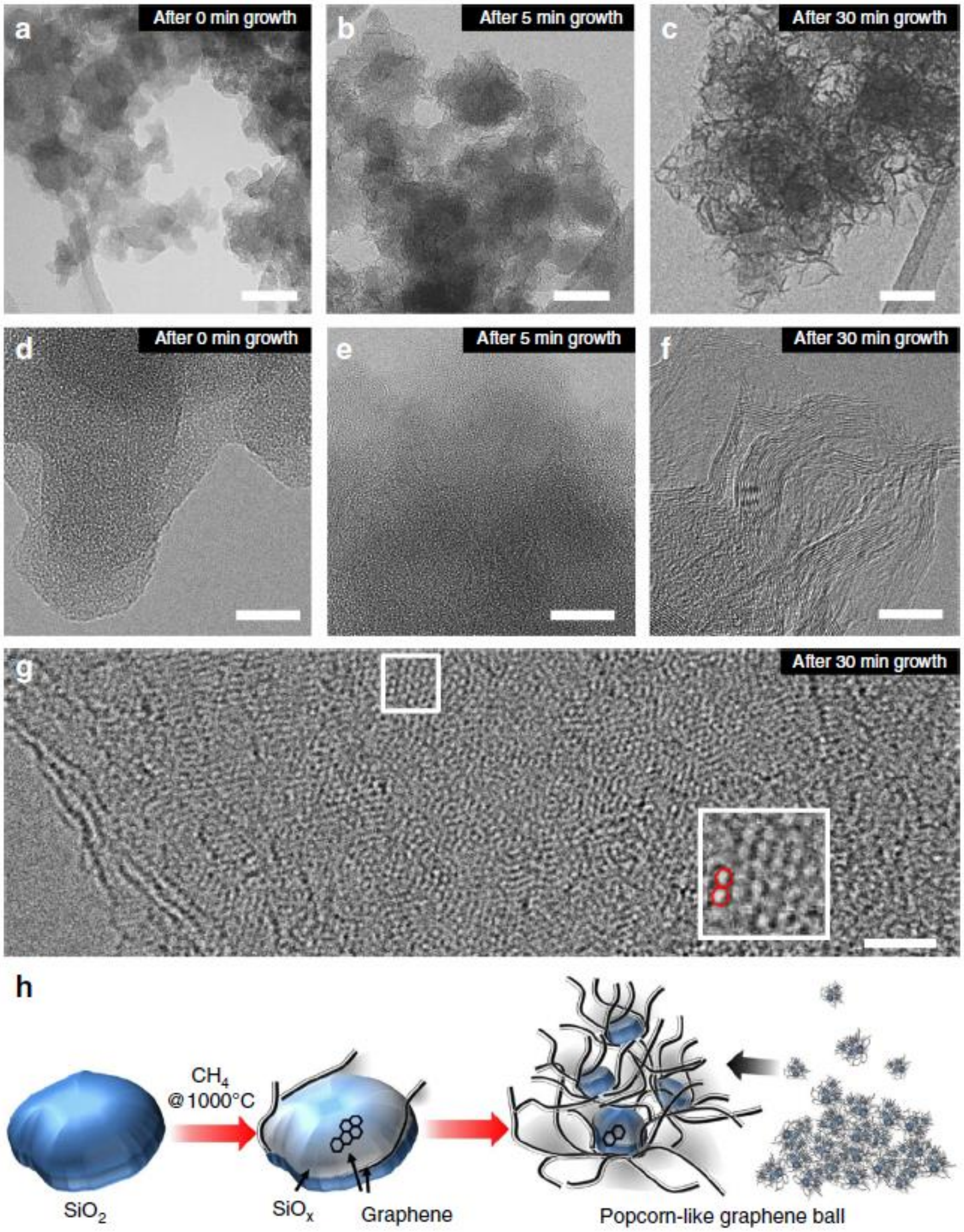

Figure 3-1. Graphene growth from SiO_2 nanoparticles. a-c) TEM characterization a before CVD growth, b after 5 min growth, and c after 30 min growth (scale bars, 50 nm). d-f) Their respective

magnified images (scale bars, 10 nm). g) Higher magnification image of graphene after 30 min growth and its atom-level view from the white box (inset)(scale bar, 2 nm). h) Graphical illustration of popcorn-like graphene growth from SiO_2 nanoparticles.[203]

The family of the titanium-based anode (such as TiO_2,[204] $Li_4Ti_5O_{12}$,[8] Li_2TiSiO_5,[85,205] and $TiNb_2O_7$[76]) serves as promising alternatives to carbonaceous materials due to their superior structural stability in tolerating fast reaction kinetics.[206] Of particular, the emerging Li_2TiSiO_5 (LTSO), a compound of Li_2O-TiO_2-SiO_2 ternary system, has spurred a growing interest in potential candidates for ultrafast anode materials.[207-209] Compared with the low theoretical capacity (175 mAh g^{-1}) and moderate operational potential (1.55 V *vs.* Li/Li^+) of well-researched $Li_4Ti_5O_{12}$,[210] LTSO offers an intriguing theoretical capacity of 308 mAh g^{-1} and a low potential of 0.28 V, simultaneously combining the merits of high-energy graphite and high-power $Li_4Ti_5O_{12}$.[85]

Inspired by In Hyuk Son et al.`s work, we started the further exploration based on silica and CVD treatment by transforming silica to the aforementioned titanium-based lithium silicate, Li_2TiSiO_5, for high-rate anode material of LIBs.

3.2 Experimental section

3.2.1 Preparation of graphene-coated silica nanoparticles (SiO_2/C), LTSO and LTSO carbon composite

SiO_2/C was synthesized through the methane-CVD process. 1 g fumed-silica was placed in a tube furnace and pre-heated to 1000 °C under Argon (Ar) gas flow (500 mL min^{-1}). Then, 200 mL min^{-1} CH_4 gas was introduced and hold for 30 min to yield Si/C powder.

LTSO and LTSO carbon composites were prepared by a sol-gel method and solid-phase reaction. A certain amount of lithium acetate hydrate was first dissolved in ethanol for forming solution A. Si/C powder (using pure fumed-silica for the synthesis of LTSO) was dispersed within ethanol as solution B. Solution C was prepared by diluting tetrabutyl titanate in ethanol. Then, blending solutions A and B with the help of an ultrasonic device. Solution C was then added in the mixture under intensely stirring. Subsequently, a few drops of water was slowly dropwise added. At the same time, keep stirring until the hydrolysis of tetrabutyl titanate was completed, where the mixture was uniformly scattered with gray-white particles. The amount of Li, Ti, and Si was kept as a stoichiometric ratio of LTSO where the molar ratio of Li:Ti:Si is 2:1:1. The volumetric ratio of water/ethanol is 0.5/30. The mixture was thoroughly dried at 80 °C under constant stirring and ground to powder, which was calcinated under Ar gas (using air gas for LTSO) at 870 °C for 8 hours, with a 5 °C min^{-1} heating rate, to form gray LTSO carbon composite (snow-white powder for LTSO).

3.2.2 Material characterization

Powder X-ray diffractometry (XRD) was performed using a Rigaku Miniflex II diffractometer with Cu-Kα radiation at 40 kV and 40 mA. The morphology and crystal structure of as-synthesized products were identified by a field scanning electron microscopy (SEM, Nova 230 Nano) with energy-dispersive X-ray spectroscopy (EDS), and a transmission electron microscopy (TEM, HRTEM, FEI-T12). Thermogravimetric analysis (TGA, Q600 SDT, TA Instruments) was performed in the air from 20 to 1000 °C with a heating rate of 10 °C min^{-1}. Raman spectrum was collected with a Renishaw 200 System. X-ray photoelectron spectroscopy (XPS) results were carried out using an AXIS Ultra DLD instrument. Powder electronic conductivity measurement was completed using the ST2722-SZ four-point probe resistivity tester.

3.2.3 Electrochemical measurements

The LTSO and LTSO carbon composite electrodes were prepared by the slurry-coating method. Solids containing activate materials (LTSO and LTSO carbon composite), Super P (carbon black), and polyvinylidene fluoride, were uniformly blended in a mass ratio of 70:20:10, correspondingly. The mixtures were subsequently dispersed in N-methyl-2-pyrrolidone, forming homogeneous slurry for doctor blade coating on a Cu foil. The as-prepared electrodes were assembled in the 2032-type coin cells with Li metal foils as the counter electrode and 1 M lithium hexafluorophosphate ($LiPF_6$) dissolved in a mixture of dimethyl carbonate (DMC), ethylene carbonate (EC), and diethyl carbonate (DEC) (1:1:1, by volume) as the electrolyte. The galvanostatic charge-discharge measurements were carried out using a Land CT2001A battery tester at room temperature. The electrochemical impedance spectra were taken in a frequency range of 0.1 to 10^6 Hz with an alternating-current voltage amplitude of 20 mV by using a Solartron 1860/1287.

3.3 Results and discussion

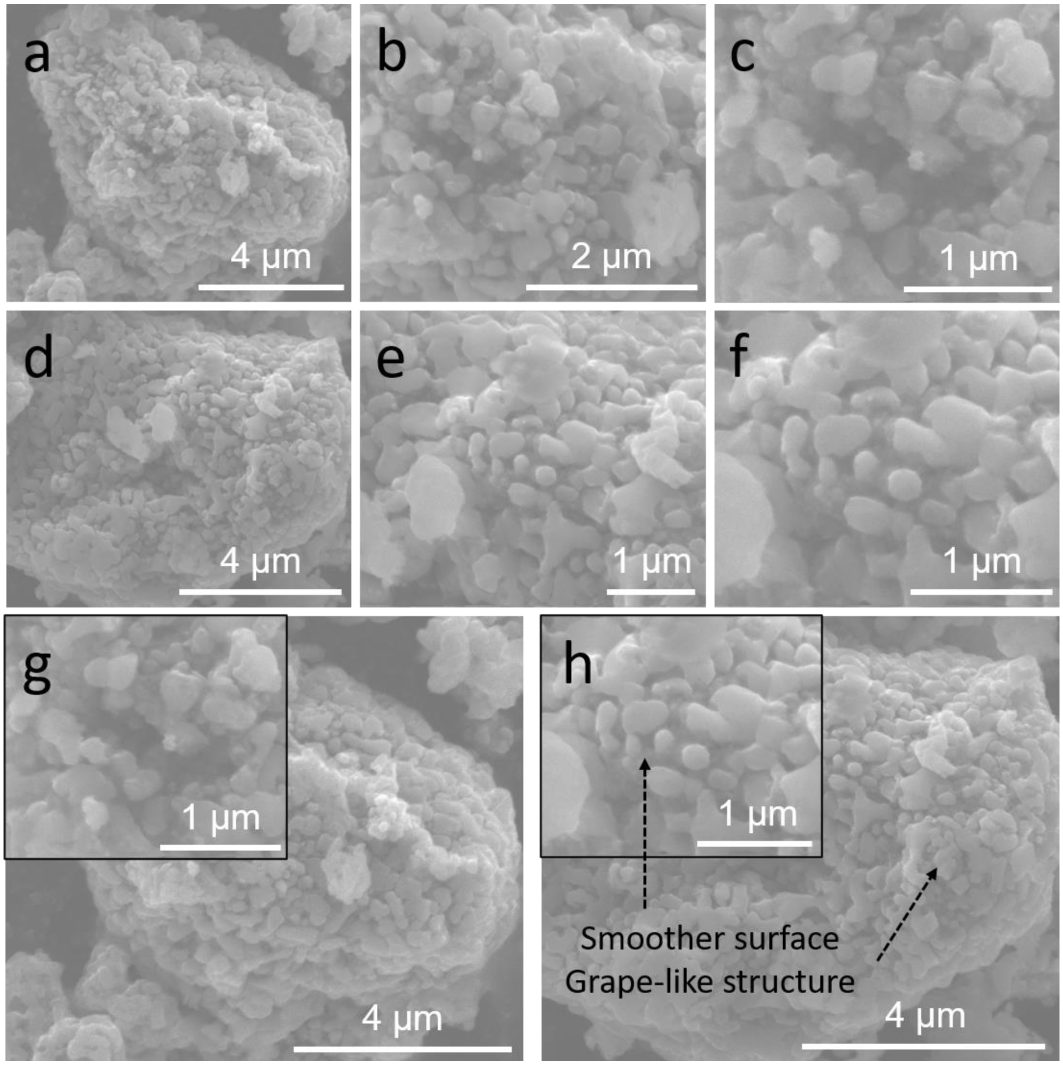

Figure 3-2. SEM images of a-c, g) LTSO and b-d, h) LTSO carbon composites.

As shown in **Figure 3-2**, the overall morphology of LTSO and LTSO carbon composites is semblable. Due to the high-temperature treatment, the fumed-SiO_2 nanoparticles aggregated and formed secondary structure as the larger chunks (Figure 3-1a,d). On the surface of aggregations, the primary structure with minor size was observed (Figure 3-2b-c, e-f). The particle surface becomes smoother after the formation of LTSO, compared with SiO_2/C, because of the solid-phase reaction (Figure 3-2g, h), and may imply the potential volume change during the solid-phase reaction.

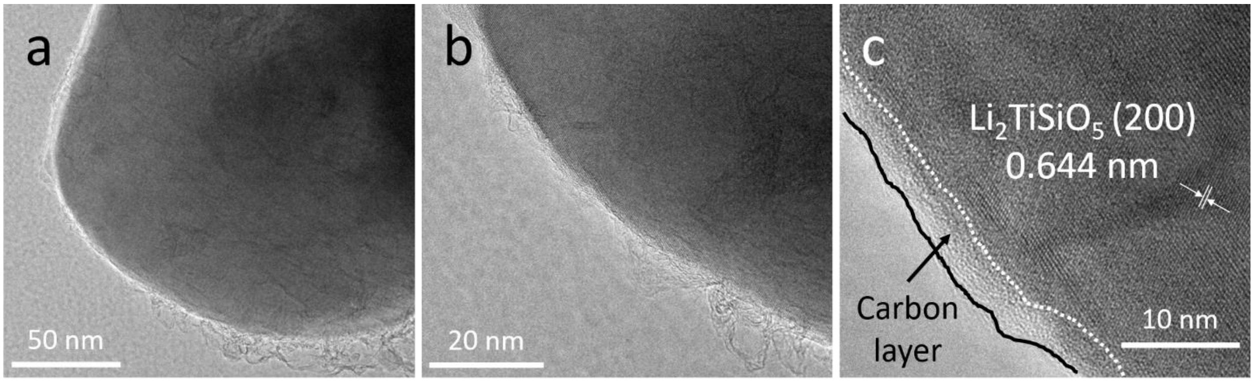

Figure 3-3. a, b) TEM images of LTSO carbon composites. c) HRTEM image with crystal spacing indication of LTSO carbon composites.

For a better understanding of the crystal structure of LTSO carbon composite, TEM and HRTEM images were captured and showed in **Figure 3-3**. From Figure 3-3c, it is confirmed that the internal crystal has ~0.644 nm for its crystal spacing, which was agreed with the reported literature as the LTSO. The outer layer is believed as the previous surface carbon-coating fumed-silica, with the help of methane-CVD, which has a thickness of around 5 nm. However, the coating layer is not entirely homogeneous, where branches are noticed in Figure 3-3a and b. This unidirectional carbon may be caused by volumetric change during the formation of LTSO and harm the tap density.

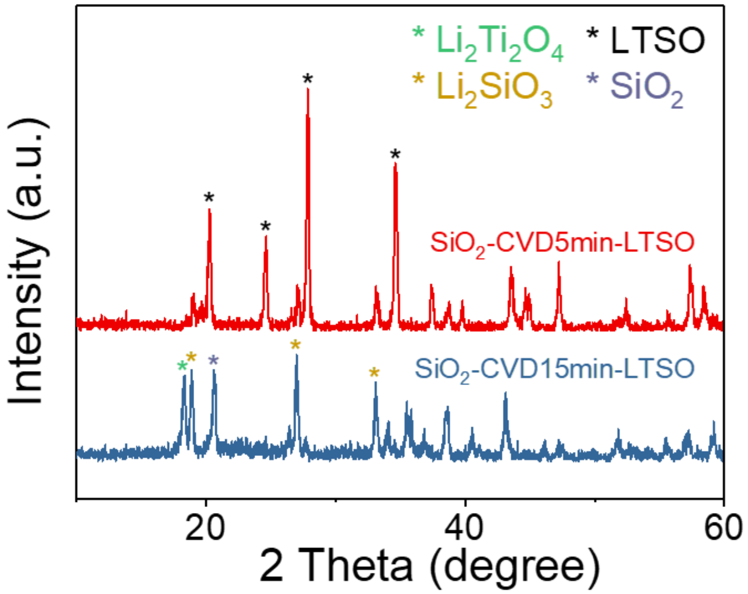

Figure 3-4. Comparison of XRD results for LTSO carbon composites with different duration of CVD treatment.

For optimizing the conductivity of the LTSO carbon composite, the maximum amount of carbon-coating needs to be specified. We applied different CVD duration on fumed-silica to achieve a different amount of carbon-coating since they are positively related. However, from **Figure 3-4**, we find out that when the treating time is increased from 5 min to 15 min, the purity of LTSO is severely affected. A lot of byproducts, such as $Li_2Ti_2O_4$, Li_2SiO_3, and unreacted SiO_2, are detected. This phenomenon is attributed to the restricted diffusion of Li and Ti source during the solid-phase reaction by the surface carbon-coating layer. Namely, when increasing the duration of CVD, the purity of LTSO will be reduced. Even so, the achieved carbon-coating still has a positive impact on the conductivity and performance of LTSO.

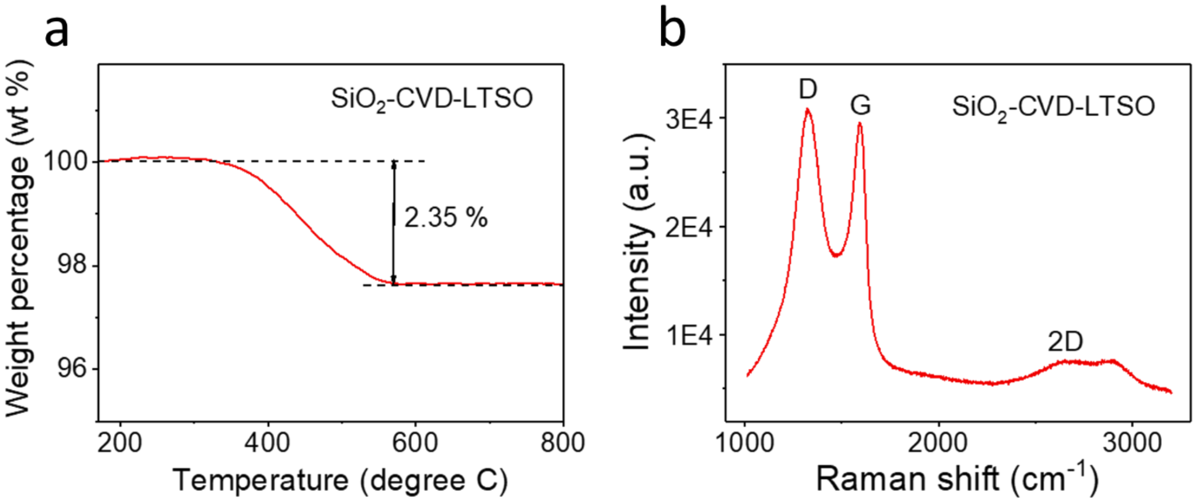

Figure 3-5. a) TGA, and b) Raman result of LTSO carbon composite with 5 min CVD treatment.

Figure 3-5 indicates the further characterizations of the carbon-coating layer. For 5 min CVD treatment, 2.35 wt.% carbon material is achieved (Figure 3-5a). Raman spectrum (Figure 3-5b) identifies the coated carbon structure has specific D (~1330 cm^{-1}), G (~1600 cm^{-1}), and 2D (~2665 cm^{-1}) peaks of conventional graphitized carbon material ($I_D/I_G = 1.1$). These characteristic vibrations prove the carbon-coating has both sp^2 and sp^3 hybridization of carbon bonds. Such results are in accord with the mentioned literature,[203] which also implies that the current approach can conduct the high-quality graphene carbon coating for assembling LTSO carbon composite.

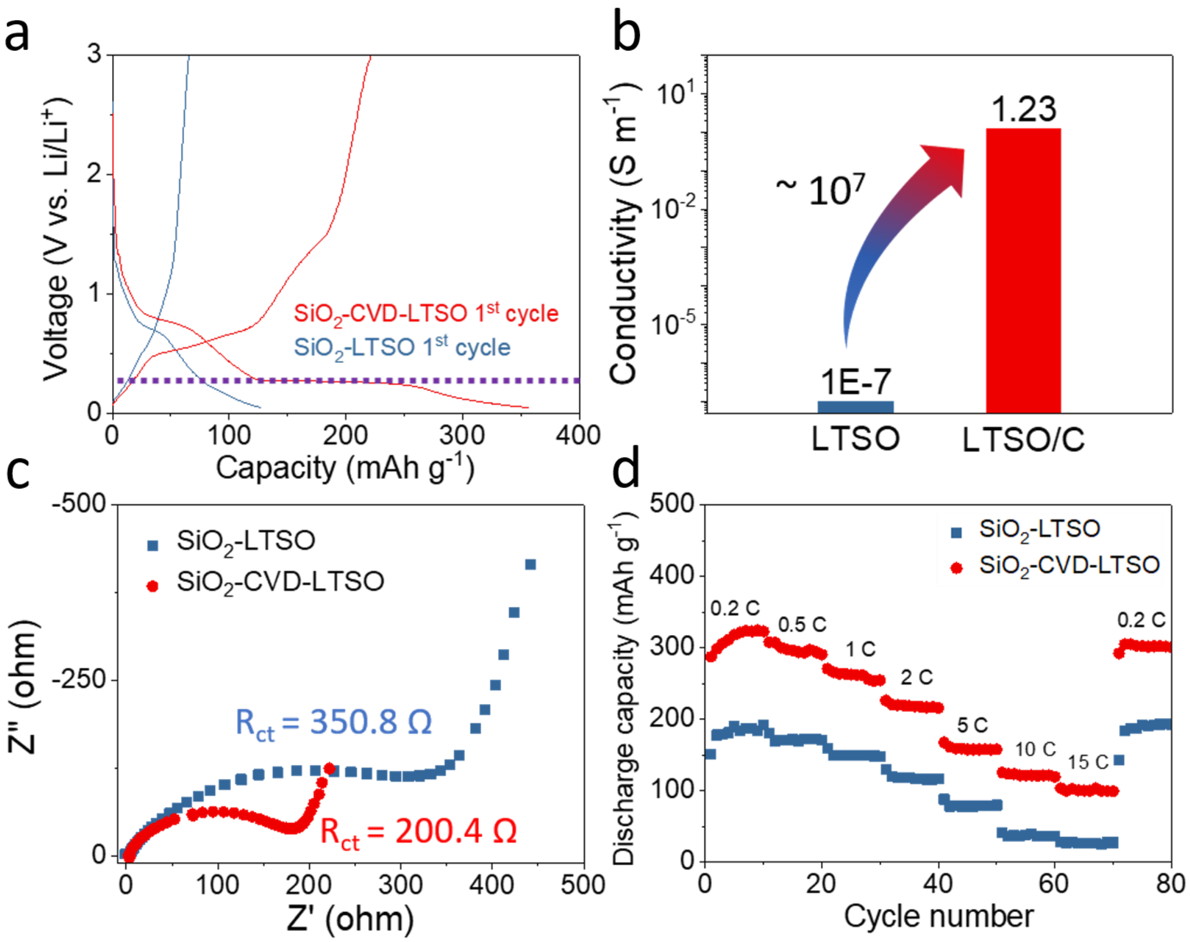

Figure 3-6. Electrochemical properties and performances comparasion of LTSO and LTSO carbon composite (LTSO/C): a) charge/discharge curves; b) electronic conductivity; c) electrochemical impedance spectrum (EIS);. d) multi-rate performance, 1 C = 300 mA g^{-1}.

To demonstrate the advantages brought by CVD-assisted carbon coating, we implemented different electrochemical measurements, as described in **Figure 3-6**. Charge/discharge curves (Figure 3-6a) show that LTSO carbon composite exhibits a distinct discharge plateau at around 0.3 V *vs*. Li^+/Li, especially compared with pristine LTSO. Such a consequence is on account of dramatic improvement in electronic conductivity from ~ 1 × 10^{-7} S m^{-1} to 1.23 S m^{-1},[208] with ~ 10^7 times higher (Figure 3-6b). Consistent with the conductivity measurement, the EIS result indicates the reduction of charge transfer resistance of LTSO carbon composite (200.4 Ω) compared with LTSO (350.8 Ω), which suggests the enhanced reaction kinetic from the facile carbon-coating. As a result, the LTSO carbon composite exhibits superior rate performance (~ 320 mAh g^{-1} at 2 C, and ~ 100 mAh g^{-1} at 15 C) that overmatches the pristine LTSO.

3.4 Conclusion

Hereto, we successfully achieved the combination of CVD-assisted high-quality carbon coating and *in-situ* transformation of catalyst (instead of the removal of catalyst) to novel anode electrode material, LTSO. The results indicate that 5 min CVD treating time is the optimum for ~ 10^7 times higher of the conductivity enhancement, considering the purity of LTSO. The yielded LTSO carbon composite could deliver desirable high-rate performance (~ 100 mAh g^{-1} at 15 C, where 1 C = 300 mA g^{-1}), which is comparable with commercialized LTO. However, there are still potentials of the current combination that could be explored, such as more considerable conductivity improvement, higher capacity at a low rate,[207-209] and higher tap density.

Chapter 4. Exploration of self-catalyzed silicate anode material for high power lithium-ion batteries

4.1 Introduction

In the previous chapter, the synthesis of LTSO and LTSO carbon composite from CVD-treated fumed-silica had been detailly studied. The duration of CVD was optimized as 5 min for the successful synthesis of LTSO carbon composite with decent purity. Even though using nano-sized particles would facilitate the diffusion of Ti and Li precursor during the solid-phase reaction, the thickness of the carbon coating layer is critical for limiting such process and then impact the purity of LTSO. Because of the threshold of thickness for the carbon layer, the further increasement of conductivity is also confined. Moreover, the employment of nanosized particles would result in infaust tap density, and the volumetric energy density of LTSO carbon composite would also be astricted. Therefore, another approach to accommodate the conflict between particle size, crystal purity, and optimal conductivity needs to be excavated.

Hitherto, using CVD as a carbon-coating tactic to accomplish *in-situ* growth of graphene carbon on the surface of electrode materials, especially for the anode side, has not been explored yet. It is essential because most of the electrode materials either do not have catalytic activity (such as LTO, TiO_2), or can not sustain the high-temperature (~ 1000 °C) process (such as LFP), or will react with carbon sources during the CVD process (such as Fe_3O_4). However, silicate, with similar Si-O crystal structure to it of SiO_2, may have the comparable catalytic ability for CVD carbon-coating. Besides, direct structural design on silicate itself will allow us to not only bypass the effect of carbon layer thickness, but the particle size and tap density.

Therefore, we initiated the investigation on LTSO for its potential of CVD-assisted *in-situ* growth graphene coating and the following benefits on its electrochemical performances.

4.2 Experimental section

4.2.1 Preparation of SiO_2 micro-sphere template, LTSO, and carbon-coated LTSO (LTSO/C).

The SiO_2 micro-sphere template was synthesized through the hydrolysis of tetraethyl orthosilicate.[211] 3.40 g of lithium acetate dihydrate dissolved in 30 ml of ethanol, and 5.73 g of tetrabutyl titanate in 20 ml of ethanol were blended and followed by the addition of 1.00 g SiO_2 template and 5 mL deionized water to produce LTSO precursor. The as-formed precursor was thoroughly dried at 80 °C under constant stirring and ground to powder, which was calcinated under air at 870 °C for 8 hours, with a 5 °C min^{-1} heating rate, to form white LTSO powder. The resulting LTSO was then placed in a tube furnace and heated to 1000 °C for 30 min with a gas flow consist of Ar (500 mL min^{-1})/CH_4 (200 mL min^{-1}) to obtain LTSO/C.

4.2.2 Material characterization

Powder X-ray diffractometry (XRD) was performed using a Rigaku Miniflex II diffractometer with Cu-Kα radiation at 40 kV and 40 mA. The morphology and crystal structure of as-synthesized products were identified by a field scanning electron microscopy (SEM, Nova 230 Nano) with energy-dispersive X-ray spectroscopy (EDS), and a transmission electron microscopy (TEM, HRTEM, FEI-T12). The N2 adsorption/desorption curves were collected by using the ASAP 2020 plus at 77 K, and the surface areas were calculated by the Brunauer-Emmett-Teller (BET) equation. Thermogravimetric analysis (TGA, Q600 SDT, TA Instruments) was performed in the air from 20 to 1000 °C with a heating rate of 10 °C min^{-1}. Raman spectrum was collected with a Renishaw 200 System. X-ray photoelectron spectroscopy (XPS) results were carried out using an AXIS Ultra DLD instrument. The XPS spectrums were analyzed using CasaXPS with the calibration of C 1s peak at 284.6 eV and Shirley-type background for fitting results. Powder electronic conductivity measurement was completed using the ST2722-SZ four-point probe resistivity tester. The tap density of LTSO/C was determined by tapping 4 g LTSO/C powder in a small glass vessel on the bench for 30 minutes by hand. The measured volume of tapped powder and its weight was used to calculate the tap density.

4.2.3 Electrochemical measurements

The LTSO and LTSO/C electrodes were prepared by the slurry-coating method. Solids containing activate materials (LTSO and LTSO/C), Super P (carbon black), and polyvinylidene fluoride, were uniformly blended in a mass ratio of 70:20:10, correspondingly. The mixtures were subsequently dispersed in N-methyl-2-pyrrolidone, forming homogeneous slurry for doctor blade coating on a Cu foil. The as-prepared electrodes were assembled in the 2032-type coin cells with Li metal foils as the counter electrode and 1 M lithium hexafluorophosphate ($LiPF_6$) dissolved in a mixture of dimethyl carbonate (DMC), ethylene carbonate (EC), and diethyl carbonate (DEC) (1:1:1, by volume) as the electrolyte. The galvanostatic charge-discharge measurements were carried out using a Land CT2001A battery tester at room temperature. The electrochemical impedance spectra were taken in a frequency range of 0.1 to 10^6 Hz with an alternating-current voltage amplitude of 20 mV by using a Solartron 1860/1287.

4.3 Results and discussion

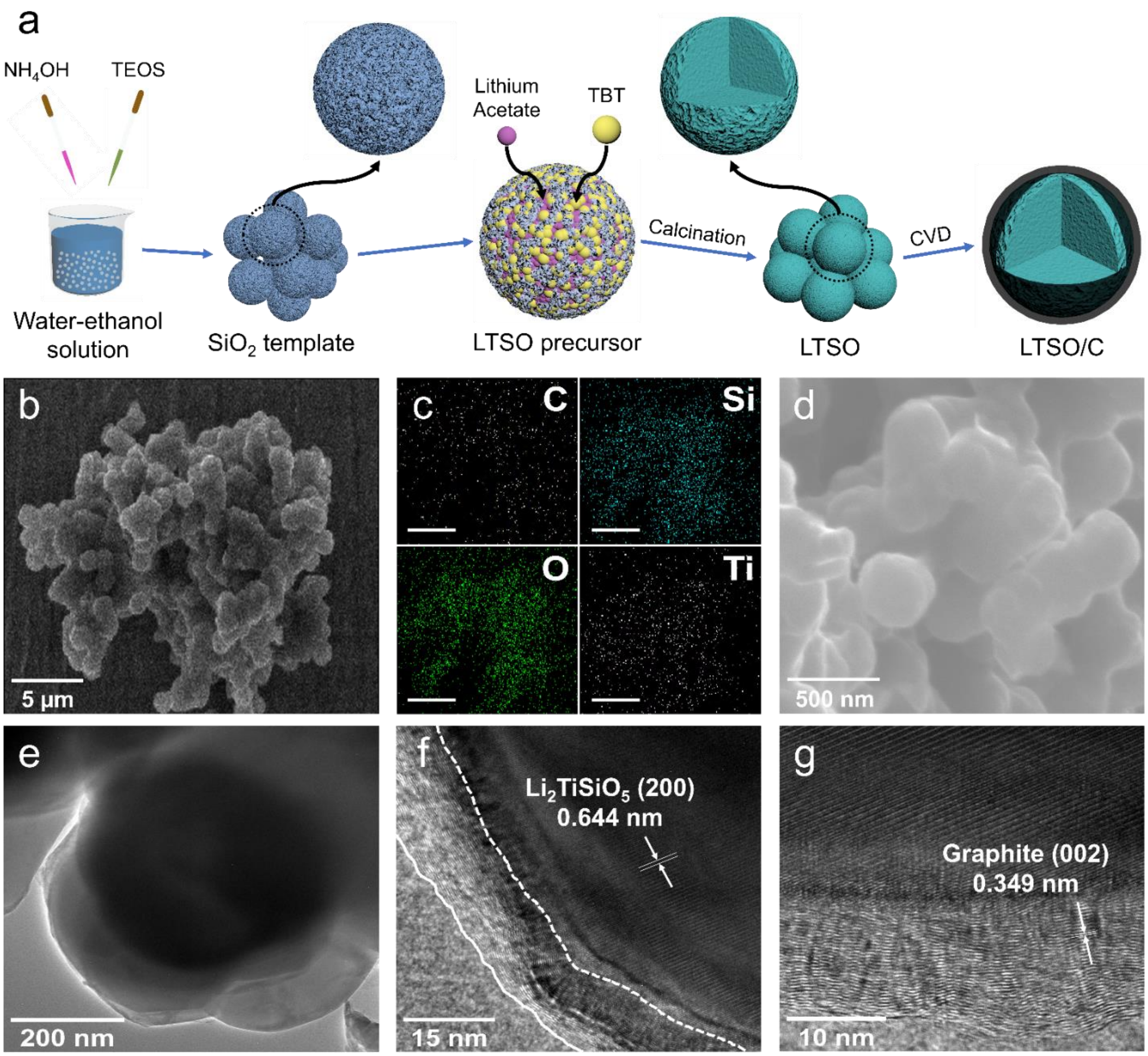

Figure 4-1. a) Schematic illustration of the synthetic route for LTSO and LTSO/C. Imaging of LTSO/C: b, c) SEM image coupled with EDS element mappings (C, Si, O, and Ti); d) Enlarged SEM image; e) TEM image; f, g) HRTEM images.

Figure 4-1a briefly illustrates the synthetic procedure for the LTSO/C composite. The Si source utilizes SiO_2 spherical templates that were prepared via hydrolysis of tetraethyl orthosilicate (TEOS) within an aqueous solution of ammonium hydroxide (NH_4OH).[211,212] The resulting SiO_2 templates were uniformly blended with lithium acetate (Li source) and tetrabutyl titanate (TBT, Ti source) in the ethanol-water mixture, leading to precipitated LiOH and TiO_2 on SiO_2 templates as LTSO precursor.[85] Calcinating the precursor in the air atmosphere at 870 °C produces the ternary Li_2O-TiO_2-SiO_2 compound (LTSO). A subsequent CVD treatment (1000 °C) of LTSO using methane (CH4) as carbon source (40% in argon by volume) catalyzes a conductive carbonaceous coating on LTSO.

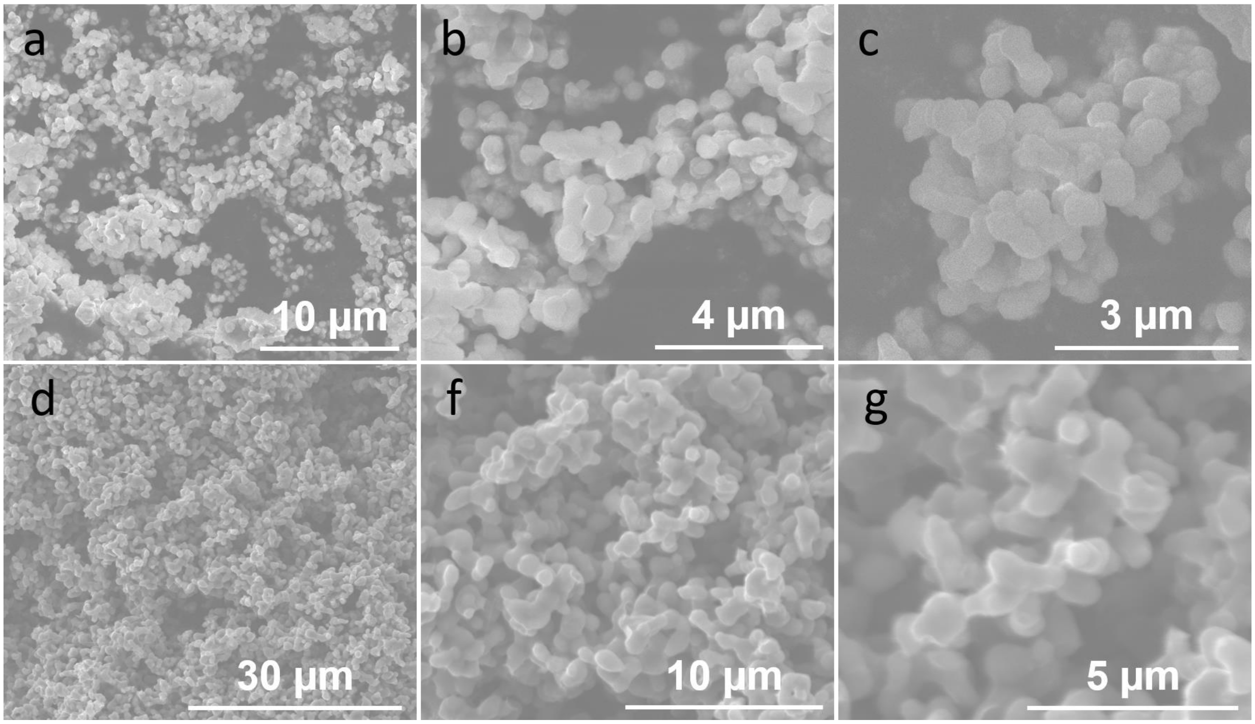

Figure 4-2. SEM images of a-c) LTSO, and d-g) LTSO/C.

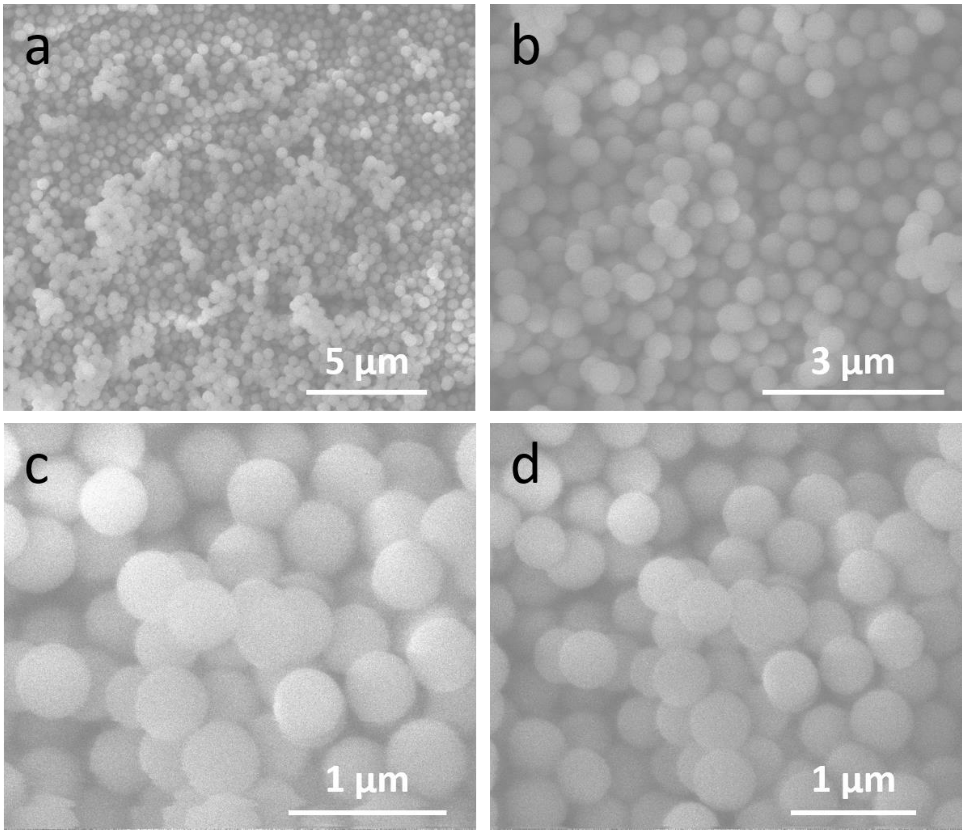

Figure 4-3. SEM images of the silica template.

Figure 4-1b-c, Figure 4-1d, and Figure 4-1e show a corresponding energy-dispersive X-ray spectroscopy (EDS) mappings, scanning electron microscope (SEM) image, and transmission electron microscope (TEM) image of LTSO/C, respectively. The SEM comparison of LTSO and LTSO/C shows in **Figure 4-2**. The primary particles templated from SiO_2 (**Figure 4-3**) show a uniform particulate size of ~ 400 nm, and they are partially agglomerated into secondary microsized assemblies. Such hierarchical architecture not only provides the fast lithium-ion diffusion at the nanoscale region (primary particle) but also contributes to the high tap density of the material at the microscale region (secondary structure).[206] The element mappings (C, O, Si, and Ti) from EDS (Figure 4-1c) support the uniform carbonaceous coating on LTSO particles. As shown in Figure 4-1f-g, high-resolution TEM (HRTEM) of LTSO/C was imaged to approximate the thickness of the carbonaceous layer. Two distinct domains differentiated by one crystal spacing of 0.349 nm and another spacing of 0.644 nm respectively originate from the (002) plane of graphitic structure and the (200) plane of the LTSO phase, thus yielding an average coating thickness of ~ 15 nm. Meanwhile, the spacing of 0.349 nm again suggests the presence of defects compared with the planar distance of 0.335 nm for perfect graphite. N_2 adsorption isotherms of SiO_2 template, LTSO, and LTSO/C show Brunauer-Emmett-Teller surface area of 11.6, 6.9, and 3.4 m^2 g^{-1}, respectively (**Figure 4-4**). The microsized secondary particle, along with the low surface area of LTSO/C, contributes to a high tap density of 1.3 g mL^{-1} (**Figure 4-5**).

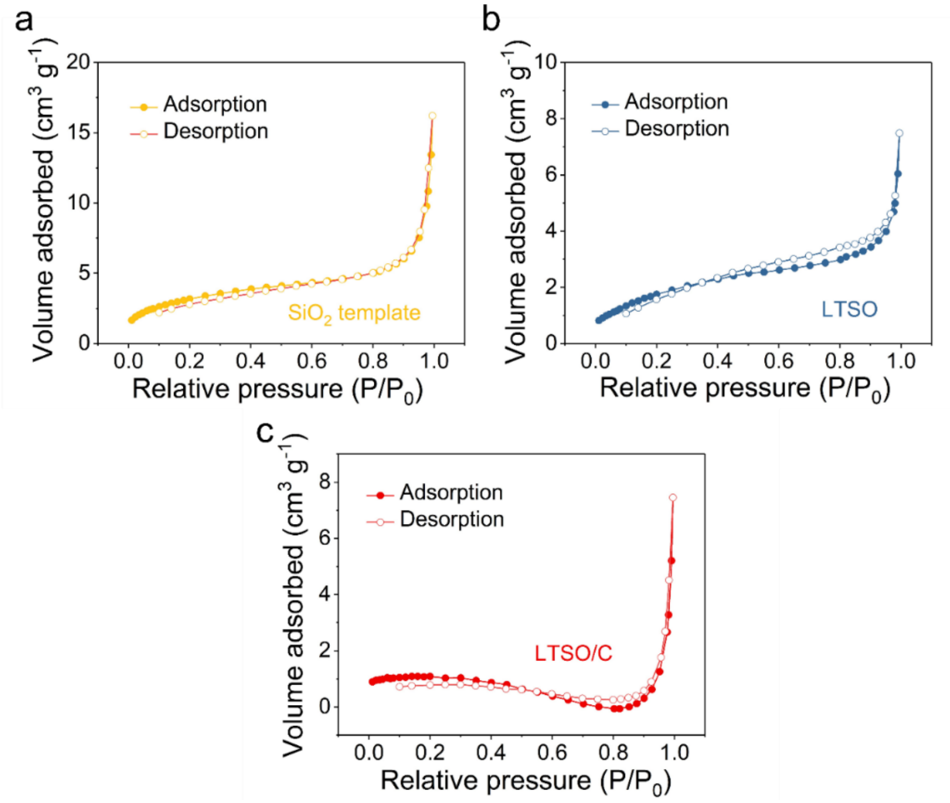

Figure 4-4. N_2 adsorption/desorption isotherms: a) SiO_2 template; b) LTSO and c) LTSO/C.

Figure 4-5. Illustration of tape density measurement of 2.5 g LTSO/C in a 4 ml glass vial.

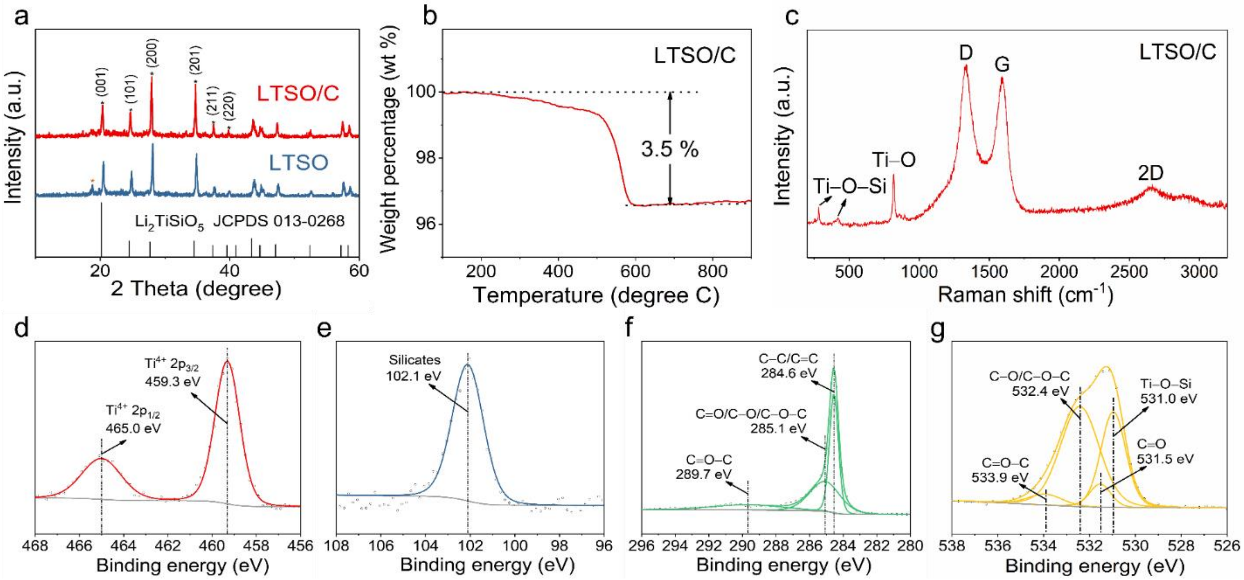

Figure 4-6. a) XRD patterns of LTSO and LTSO/C. Physical and structural characterizations of LTSO/C: b) TG curve; c) Raman spectrum; d) Ti 2p; e) Si 2p; f) C 1s and g) O 1s spectra of XPS.

The crystal structure of LTSO/C and LTSO was confirmed by powder X-ray diffraction (XRD). The pattern of LTSO/C indicates a crystalline phase and closely resembles the bare LTSO, both of which are in accord with the literature (straight bottom lines) (**Figure 4-6a**).[85] A minor impurity (Li_2SiO_3) peak at 19 degrees exhibits negligible intensity after the CVD process. The weight percentage of the coated carbon was determined by thermogravimetric analysis (TGA) of LTSO/C in air atmosphere. As shown in Figure 4-6b, the composite undergoes a total weight loss of 3.5% starting from 200 °C to 600 °C, which corresponds to the complete oxidation of coated carbon. Minimizing the content of carbonaceous coating in the composite is of practical significance for achieving a high tap density of parent material. The graphitic structure of coated carbon was investigated by Raman spectroscopy. As depicted in Figure 4-6c, the characteristic vibrations at 1331 cm^{-1} (D band), 1585 cm^{-1} (G band), and 2358 cm^{-1} (2D band) arise from the defect structure and sp^2 hybridization of carbon-carbon bonds in graphitic materials ($I_D/I_G = 1.08$), which imply the successful coating of graphitized carbon.[203,213] The additional peaks at 283.7/418.1 and 817.5 cm^{-1} could be assigned to Ti–O–Si bonds (O-bridged TiO_6 octahedra and SiO_4 tetrahedra) and Ti–O bonds (TiO_6 octahedra), respectively.[208] X-ray photoelectron spectroscopy (XPS) was performed to determine the elemental composition of LTSO/C. The survey scanning detects the presence of Li 1s, Si 2p, Ti 2p, O 1s, and C 1s signals (**Figure 4-7**). Specifically, the binding energy at 465.0 eV (Ti^{4+} $2p^{1/2}$) and 459.3 eV (Ti^{4+} $2p^{3/2}$) could be assigned to the O-bridged TiO_6 octahedra in LTSO (Figure 4-6d).[209, 214] As shown in Figure 4-6e, the binding energy at 102.1 eV primarily originates from the SiO_4 tetrahedra in LTSO as the characteristic peaks for SiO_2 (Si–O–Si bond) are typically reported at much higher binding energies (beyond 103.4 eV).[214-216] From the deconvoluted peaks of C 1s spectrum (Figure 4-6f), the dominate peak at 284.6 eV and minor peaks at 285.1/289.7 eV are respectively ascribed to the graphitic (C=C/C–C) and defective carbon (C=O/C–O/C–O–C/C=O–C), which are in coincidence with the Raman results.[209,217] From the deconvoluted peaks of O 1s spectra, the binding energy at 531.0 eV confirms the Ti–O–Si bonds of LTSO.[215] Moreover, oxygen-related functional groups comprising C=O (531.5 eV), C–O/C–O–C (532.4 eV), and C=O–C (533.9 eV) are in good accordance with the results from C 1s spectra (Figure 4-6f).[217,218]

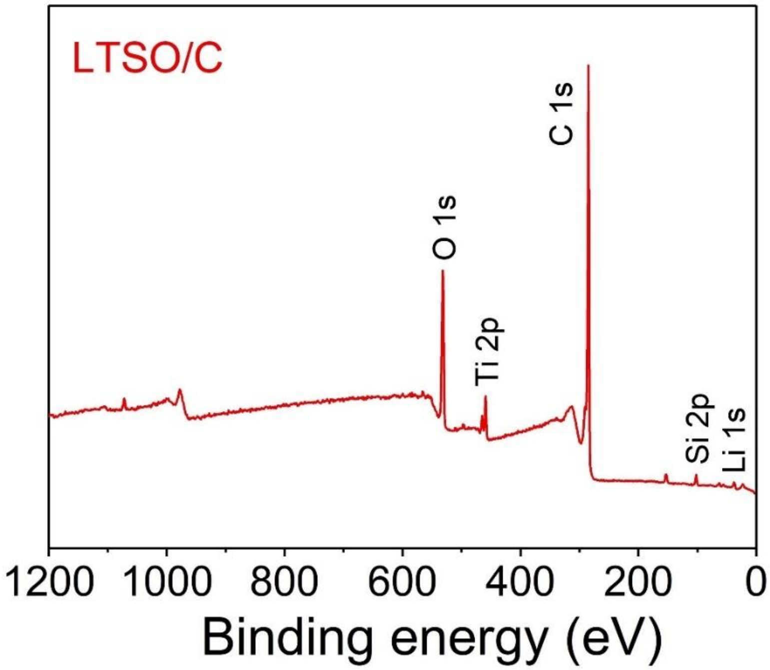

Figure 4-7. Full XPS spectra of LTSO/C.

To determine the electronic-conductivity enhanced by CVD treatment, LTSO and LTSO/C powders were densified into dimensional pellets for four-point probe resistivity measurements. The bare LTSO exhibits poor electronic conductivity of ~ 1 × 10^{-7} S m^{-1},[208] which is dramatically improved with eight magnitudes higher value of 9.8 × 10^{2} S m^{-1} for LTSO/C (**Figure 4-8a**). The electrochemical impedance spectroscopy (EIS) performed on half-cells comprising LTSO or LTSO/C as cathode and Li foil as anode supports the results from conductivity measurement. Both Nyquist plots of EIS exhibit a semicircle (or depressed semicircle) followed by a straight line (Figure 4-8b). The intercept of the semicircle at high frequency, the diameter of the semicircle, and the slope of the line (Warburg tail) are indicative of the Ohmic resistance, the charge transfer resistance, and the solid-diffusion resistance, respectively (details in Table 4-1 and Figure 4-9).[219] The substantial reduction in charge transfer resistance of LTSO/C (115.6 Ω) compared with LTSO (350.8 Ω), evidently signifies the enhanced reaction kinetic upon the introduction of a highly conductive carbonaceous coating. Moreover, the ion-diffusion coefficient (at the open circuit) derived from analyzing the Warburg part, through equation

$$D_{Li}{}^{+} = R^2\, T^2 / 2\, A^2\, n^4\, F^4\, C^2\, A_w{}^2$$

where $D_{Li}{}^{+}$ represents the Li^+ diffusion coefficient in LTSO ($cm^2\ s^{-1}$), R represents the gas constant ($8.31\ J\ mol^{-1}\ K^{-1}$), T represents the absolute temperature (298 K), A represents the surface area of the electrode ($0.785\ cm^2$), n represents the number of electrons transferred per molecule during the electrochemical reaction, F represents the Faraday constant ($96485\ C\ mol^{-1}$), C represents the molar concentration of Li^+ in LTSO, and A_w represents the Warburg coefficient associated with $Z`$ and $\omega^{-0.5}$, shows two orders of magnitude improvement (from 6.45×10^{-16} to $4.29 \times 10^{-14}\ cm^2\ s^{-1}$) after CVD treatment, which suggests that the surface carbonization of CH_4 on LTSO potentially promotes the intrinsic diffusion of Li^+ ions.

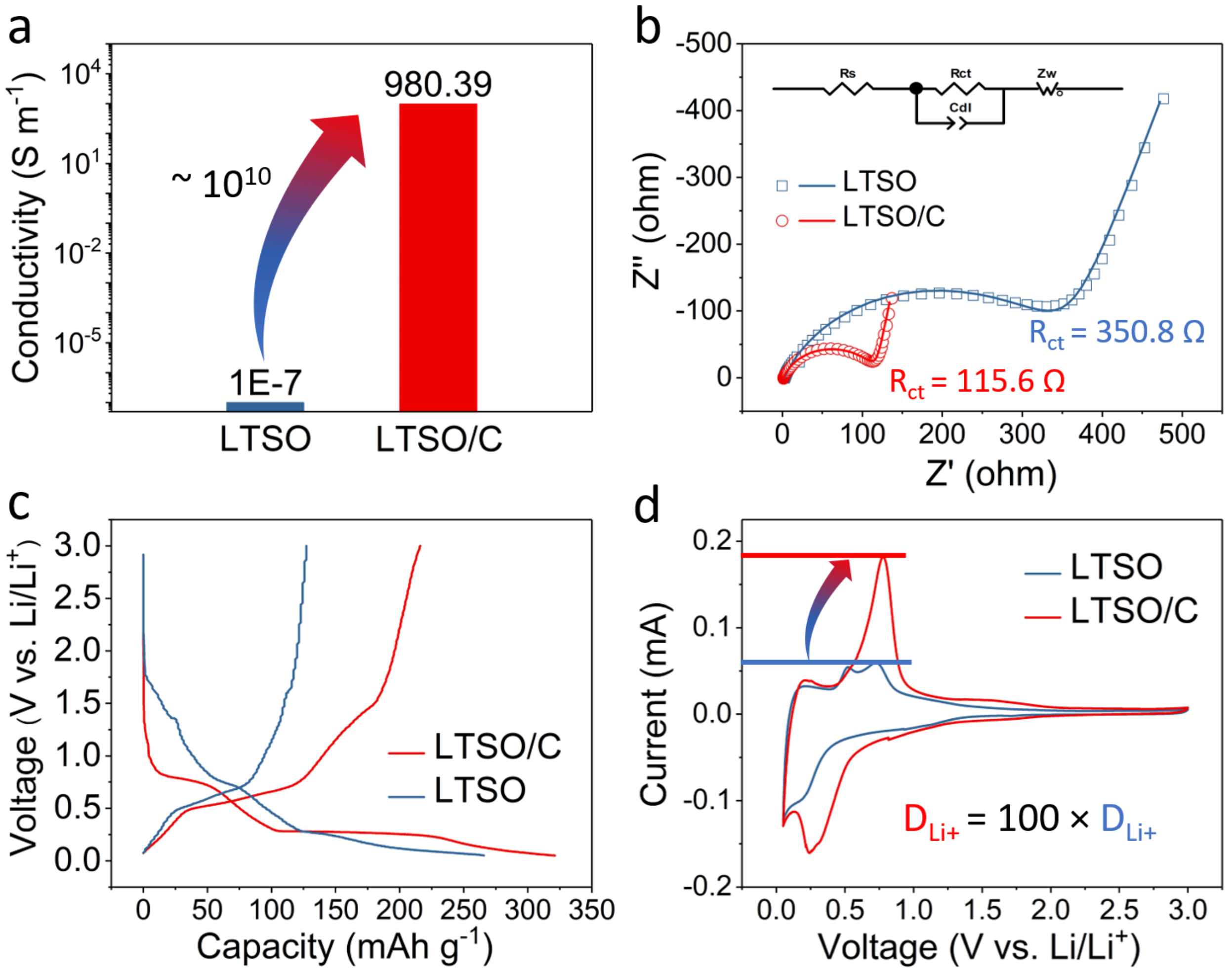

Figure 4-8. a) Electronic conductivity comparison between LTSO and LTSO/C. Electrochemical characterizations on LTSO and LTSO/C in half-cells: b) Nyquist plots of EIS (dots) and fitting (lines) of corresponding equivalent circuit (inset); c) initial discharge profiles (low voltage cutoff: 0.05 V, current density: 60 mA g-1); d) CV curves.

The galvanostatic cycling of LTSO and LTSO/C were carried out in a voltage window between 0.05 V to 3 V (*vs*. Li/Li$^+$). The initial voltage-capacity curves of LTSO/C and LTSO at the current density of 60 mA g^{-1} (0.2 C) are presented in Figure 4-8c. The LTSO/C exhibits an initial discharge capacity of 321 mAh g^{-1} and a reversible charge capacity of 216 mAh g^{-1}, corresponding to an initial Coublomic efficiency of 67%. Moreover, the cell shows a well-profiled average discharge and charge plateau at 0.3 V and 0.8 V, respectively. In sharp contrast, the bare

LTSO delivers a significantly lower reversible charge capacity of 127 mAh g^{-1} and poor initial Coublomic efficiency of 48%, which are accompanied by a large voltage hysteresis with indiscernible voltage plateaus. The cyclic voltammetry (CV) curves depicting the reaction kinetics features are in good accordance with the initial galvanostatic cycles (Figure 4-8d). The plot of LTSO/C reveals the pronounced redox peaks at ~ 0.3/0.8 V, which could be assigned to intercalation-type reaction ($Li_2TiSiO_5 + x\ Li^+ + x\ e^- \leftrightarrow Li_2Li_xTiSiO_5$, $x \leq 0.5$, 3 to 0.28 V).[85] In comparison, LTSO shows considerably lower reaction peak currents (I_p) indicative of smaller Li^+ diffusion coefficient ($D_{Li}{}^+$), according to the Randles-Sevcik equation,

$$I_p = 2.69 \times 10^5\ n^{1.5}\ A\ D_{Li}{}^{+0.5}\ C\ v^{0.5}$$

where I_p represents the peak current in amps, n represents the number of electrons transferred during the redox reaction per molecule, A represents the surface area of the electrode (cm^2), C represents the concentration of Li^+ in LTSO (mol cm^{-3}), $D_{Li}{}^+$ represents the diffusion coefficient of Li^+ in LTSO ($cm^2\ s^{-1}$), and v represents the scanning rate (V s^{-1}), where $I_p{}^2$ is proportional to $D_{Li}{}^+$.[207]

Table 4-1. Fitting results of electrochemical impedance spectroscopy (EIS).

Materials	**R_s (ohm)**	**R_{ct} (ohm)**
LTSO	2.1	350.8
LTSO/C	1.7	115.6

Note: R_s means ohmic resistance, R_{ct} means charge transfer resistance.

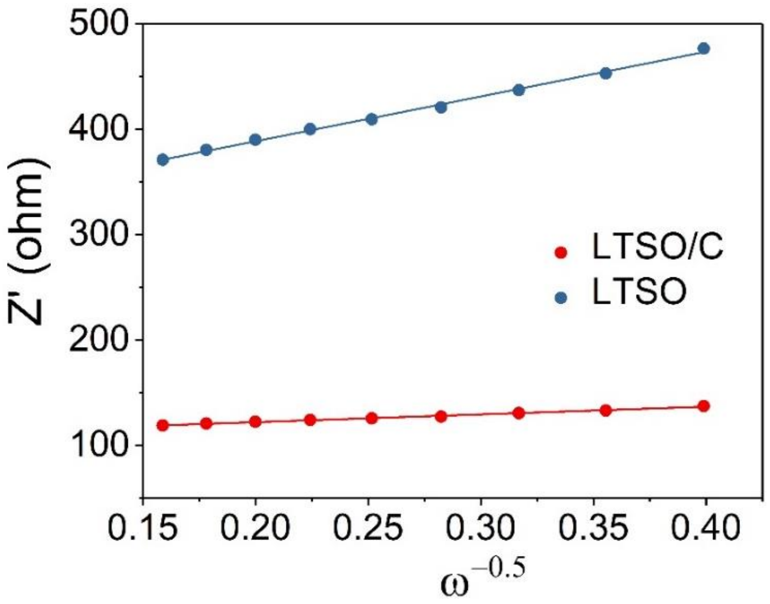

Figure 4-9. Fitting lines for calculation of Li^+ diffusion coefficient in the Warburg diffusion region.

The above results collectively demonstrate that the CVD-assisted carbonaceous coating on LTSO unambiguously facilitates the reaction kinetics by improving electronic and ionic transports. The electrochemical performances concerning rate capability and cycling stability were further evaluated. **Figure 4-10a** depicts the specific discharge capacity of LTSO, and LTSO/C plotted against consecutive rates from 0.2 C to 15 C. At a low-rate of 0.2 C, the LTSO delivers an average discharge capacity of 150 mAh g^{-1}, underlining a considerable difference with its theoretical capacity (308 mAh g^{-1}).[207] At a high-rate of 15 C, the LTSO fails to work, showing negligible capacity, which arises from the inherent low charge transport and sluggish reaction kinetics. In marked contrast, the LTSO/C could afford a notably enhanced capacity of 323 mAh g^{-1} at 0.2 C and retain 30% of the capacity at 15 C. As shown in **Figure 4-11**, the optimization of carbon content in LTSO/C indicates that a minimum 0.5% carbonaceous coating could improve rate performance. Content higher than 3.5% could be detrimental to the rate performance.

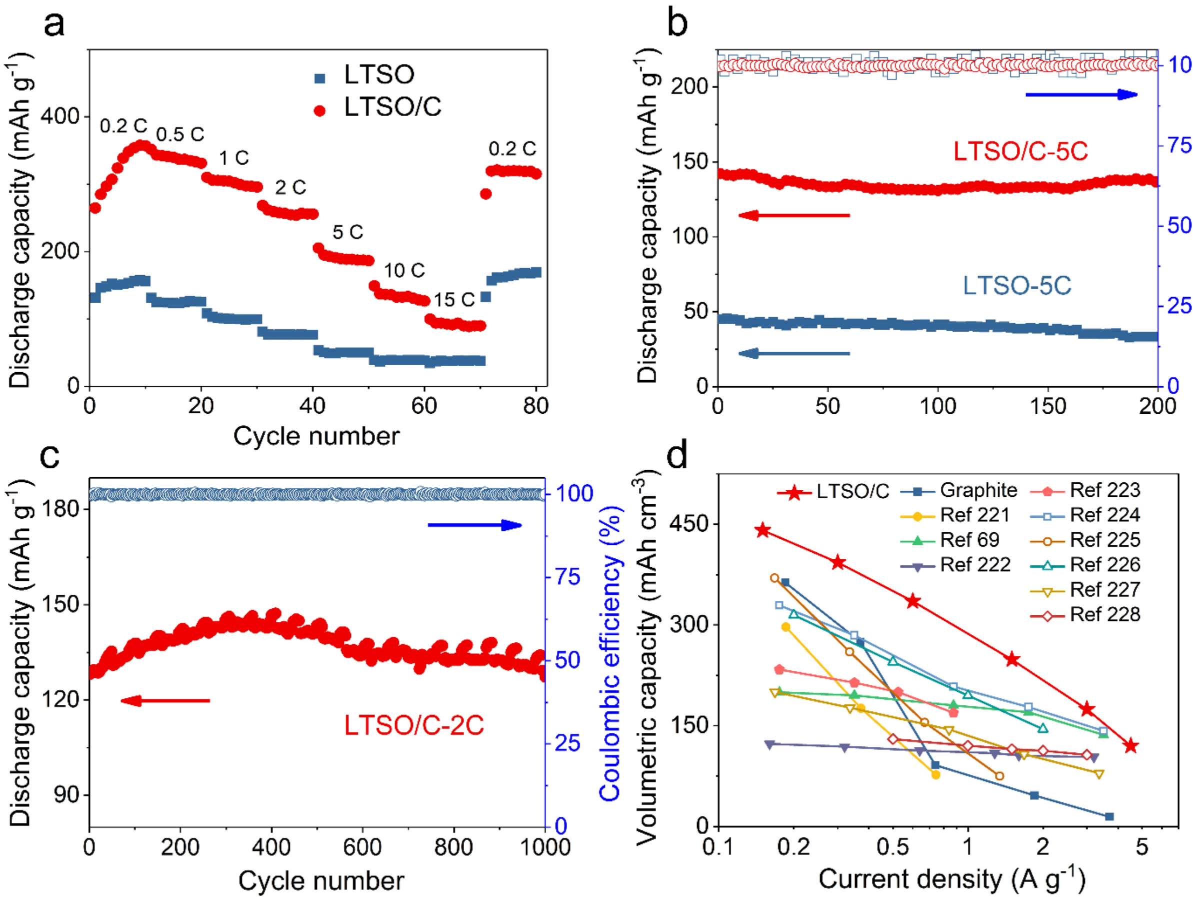

Figure 4-10. Galvanostatic cycling of half-cells: a) rate test (1 C = 300 mA g^{-1}); b) durability test at 5 C; c) long-term cycling test of LTSO/C at 2 C (low voltage cutoff: 0.1 V). d) Comparison between LTSO/C with anode counterparts (graphite, TiO_2, LTO) in volumetric capacity-current density plot.

It is noted that the LTSO/C delivers gradually increasing specific capacity that exceeds the theoretical capacity at 0.2C, which could be elucidated by its multi-step lithium-ion storage mechanism. Specifically, the first intercalation-type reaction occurs when discharge cutoff (V_{cutoff}) is higher than 0.28 V: $Li_2TiSiO_5 + x\ Li^+ + x\ e^- \leftrightarrow Li_2Li_xTiSiO_5$, $x \leq 0.5$. The second one is a conversion-type reaction: $Li_2Li_xTiSiO_5 + (2-x)\ Li^+ + (2-x)\ e^- \leftrightarrow Li_4SiO_4 + TiO$ ($0.1\ V < V_{cutoff} < 0.28\ V$). The reported theoretical capacity of 308 mAh g^{-1} is calculated based on these two steps. Once the cutoff is lower than 0.1 V, however, another intercalation reaction, $TiO + y\ Li^+ + y\ e^- \leftrightarrow$

Li_yTiO, would take place and provide additional capacity, leading to a total capacity between 350 mAh g^{-1} to 412 mAh g^{-1}.[207,209] Thus, the maximum capacity (323 mAh g^{-1}) achieved herein at a low cutoff of 0.05 V could be interpreted by the contribution from the second intercalation reaction. Moreover, as the conversion-type reactions are typically accompanied with structure changes, including phase separation and grain boundary movement, which lead to particle cracking and enlarged surface area.[207] Consequently, the observed capacity increasement in the first few cycles could be explained by the conversion-type reaction and corresponding structural evolution.[220]

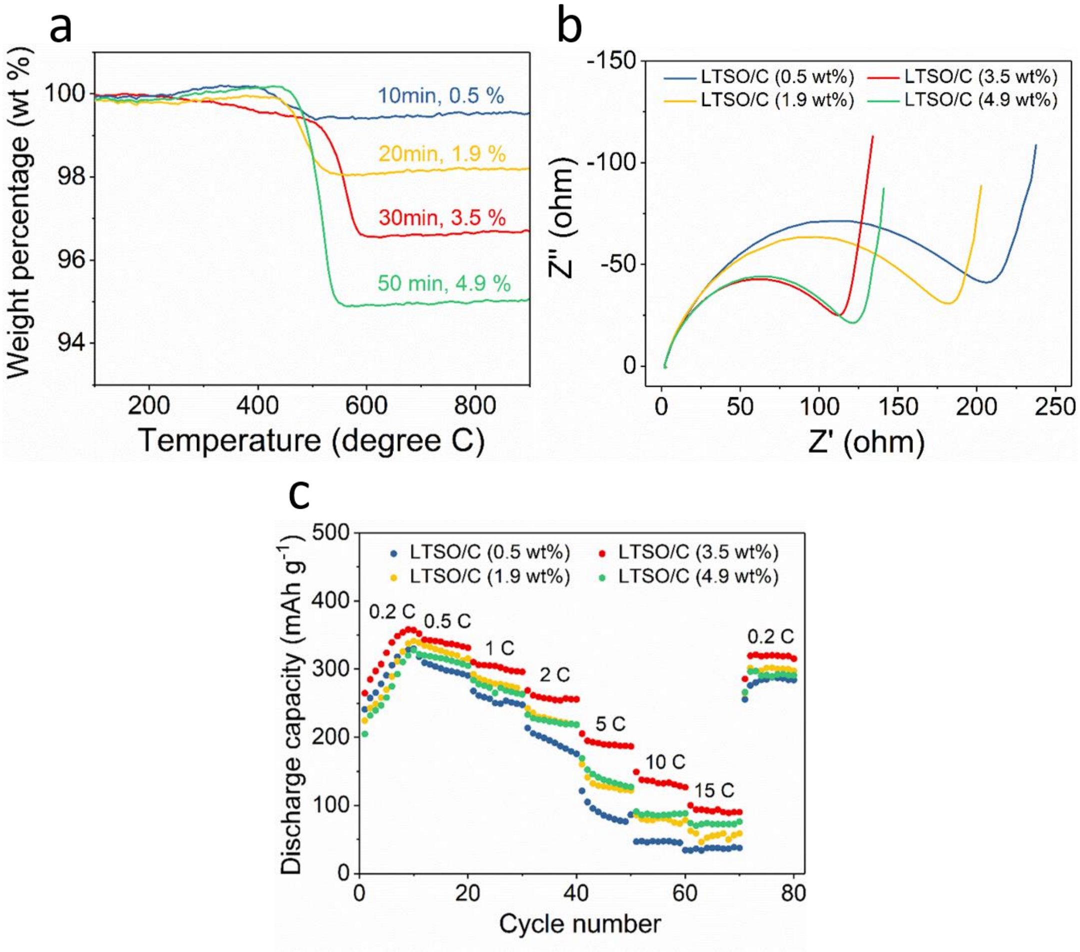

Figure 4-11. a) TG results of LTSO/C composites with different CVD treatment durations. b) Nyquist plots of LTSO/C composites with different carbon contents. c) Rate performances of LTSO/C composites with different carbon contents.

As compared in Figure 4-10b, the cycle durability was validated during high-rate operation at 5 C for 200 cycles. The LTSO/C yields an ultrastable reversible capacity of 135 mAh g^{-1}, which is more than tripled compared with bare LTSO at the same condition (40 mAh g^{-1}). Meanwhile, the preserved structural integrity of LTSO/C was confirmed by impedance measurement (**Figure 4-12a**) and diffraction pattern (Figure 4-12b) after intensive cycling at a high-rate. As shown in Figure 4-12c, a high operating cutoff voltage from 0.05 V to 0.1 V warrants outstanding prolonged 1000 cycles of LTSO/C owing to the structural stability under dominant intercalation-type lithiation (above 0.1 V).[85] Furthermore, the high tap density of LTSO/C (1.3 g mL^{-1}) benefit from the microsized particles exceeds or is comparable with its titanium-based (e.g., LTO, TiO_2) and commercial graphite anodes. As summarized in Figure 4-10d, the LTSO/C distinguishes itself from other counterparts (graphite,[221] LTO,[69,222-224] and TiO_2 [225-228]) in terms of rate capability (up to 4.5 A g^{-1}), volumetric capability (450 mAh cm^{-3}), and low discharge plateau (0.3 V). At low-rate, the high tap density of LTSO/C enables its volumetric capacity comparable commercial graphite; at high-rate, the LTSO/C could retain specific capacities comparable to the conventional high-rate anodes (LTO, TiO_2). These intriguing attributes offer a practical alternative as the high volumetric capacity and high-rate anode material.

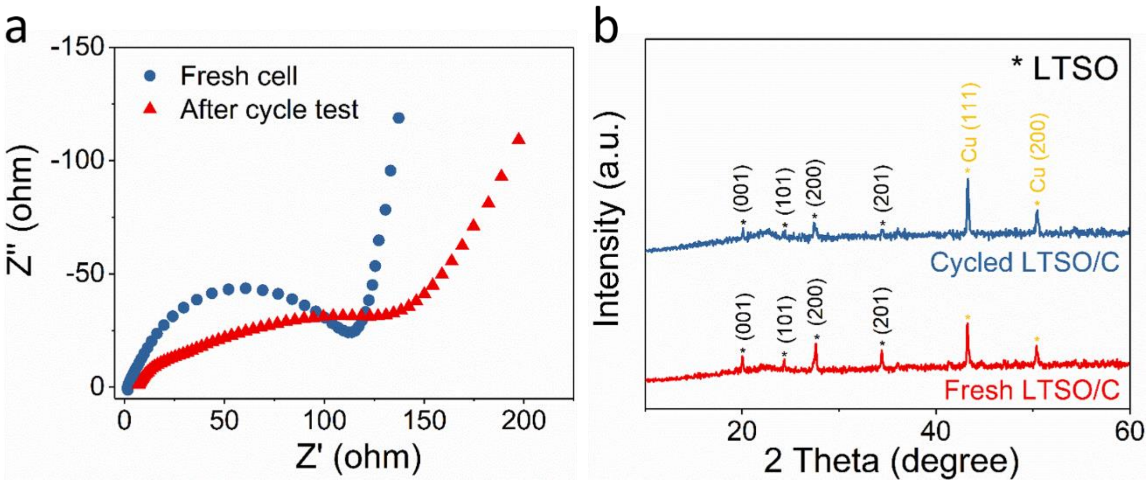

Figure 4-12. a) Electrochemical impedance spectrum results of fresh and cycled LTSO/C cells. b) XRD results of fresh and cycled LTSO/C cells.

4.4 Various efforts for making LTSO carbon composite with different benefits

As demonstrated in the previous sections, 1) using silica as both catalysts for CVD carbon-growth and precursor of forming active electrode material, and 2) using LTSO as self-catalyzed electrode material for surface CVD carbon-coating, both tactics provide decent electronic conductivity enhancement over the pure LTSO. For showing different paths of increasing the advantages of LTSO carbon composite, several attempts were conducted.

4.4.1 Applying inexpensive precursors to synthesize LTSO

The previous approaches are utilizing tetrabutyl titanate (TBT) as Ti sources. It can provide even dispersion of TiO_2 granulum after hydrolysis reaction. During the heating treatment for the formation of LTSO, the homodisperse allows solid precursors to diffuse into the bulk crystal conveniently. Otherwise, the purity of LTSO will be impacted. However, such a precursor is not economically friendly and requires particular storage conditions since it is sensitive to water. Therefore, we also developed the method using P-25 (TiO_2) as a Ti source, fumed-silica as a Si source, and ball milling as a practicable mixer for large-scale production.

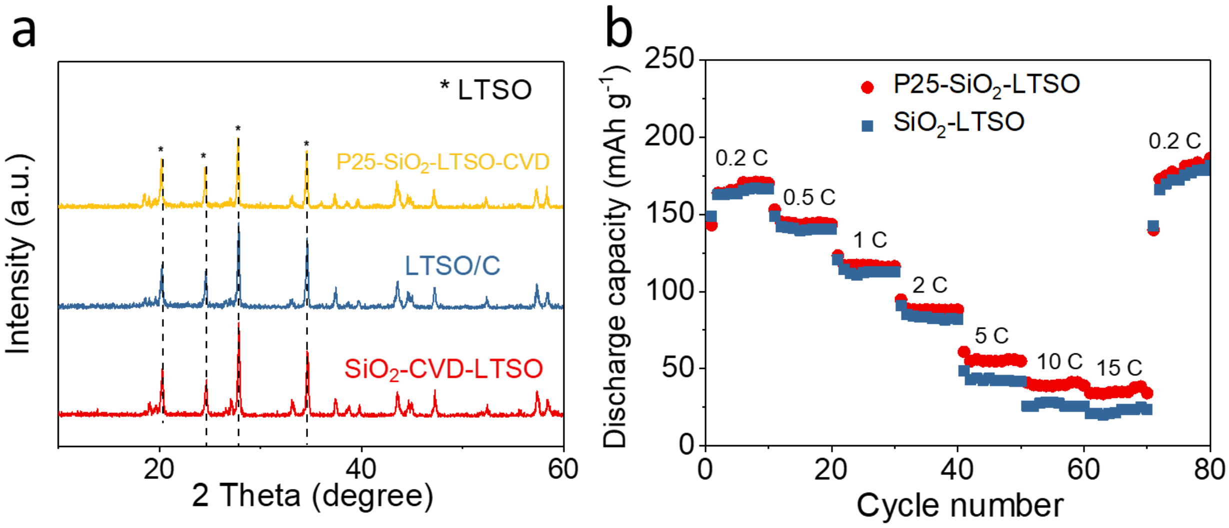

Figure 4-13. Comparison of a) XRD and b) rate performances for LTSO synthesized from a different method.

Figure 4-13a shows the XRD patterns of LTSO carbon composites with different synthetic methods. The economical one (yellow top curve) has similar purity over other tactics. It proves the feasibility of using cheap materials and cost-effective device to produce LTSO carbon composite. Furthermore, the obtained LTSO has decent rate performance even without carbon-coating. As shown in Figure 4-13b, the eco-LTSO (red dot) exhibits comparable rate performance as it of pristine LTSO synthesized from TBT.

4.4.2 Applying spray drier to synthesize LTSO carbon composite

Spray drying is a conventional large-scale production method. It requires liquid precursor solutions and creates microparticles with spherical morphology, which is benefiting to the tap density. In order to apply spray drying for producing LTSO, the internal conductivity enhancement is necessary, since the LTSO itself has insufficient electron transportation property. Therefore, we come up with a modified precursor by using graphene oxide (GO) water dispersion and fumed-silica. These solids are thoroughly pre-decentralized in deionized water before feeding in the spray drier. After collecting the ejection, the gray powder is blended with TBT suspension in the ethanol-water solution. By evaporating the solvent, the solid LTSO precursor is acquired and then heated to 870 °C for 8 hours in argon gas flow to form the LTSO carbon composite.

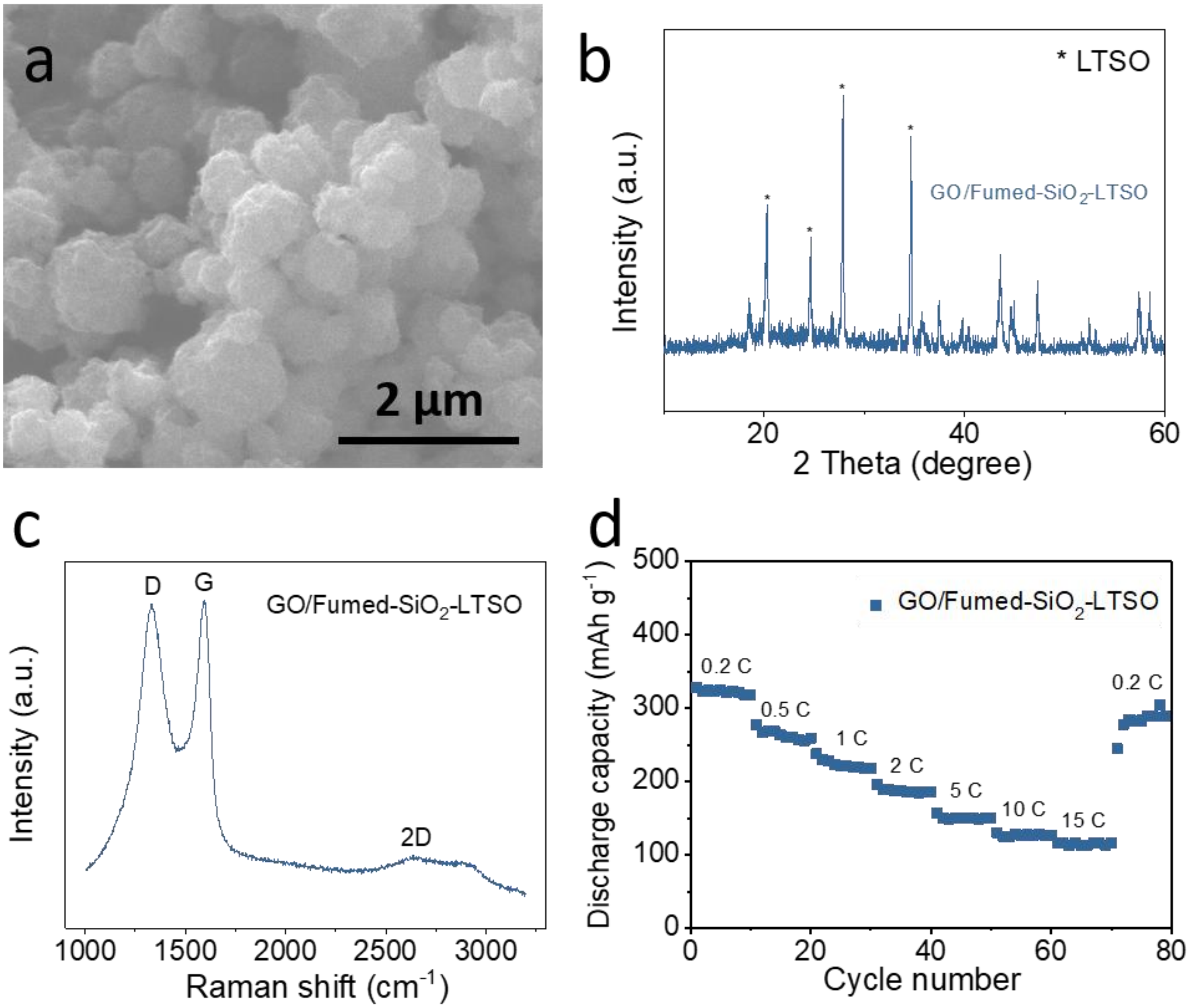

Figure 4-14. Characterizations of LTSO carbon composite synthesized by using a spray drier and GO/fumed-silica/P-25: a) SEM image; b) XRD; c) Raman spectrum; d) multi-rate performance.

Figure 4-14a indicates the morphology of LTSO carbon composite via spray drying; the expected spherical structure is observed. The particles have broad size distribution because the spray drying cannot control the size of the droplet during the spray process, where the liquid precursor is extruded by compressed air. The harvested LTSO composite shows excellent purity, which contributes to the uniform dispersion of different element sources (Figure 4-14b). The Raman characteristic of GO in the composite (Figure 4-14d) reveals the high-quality conductive carbon that consists of graphitic carbon with defects. It suggests that GO maintains the original structure after the heating process and is functional for conductivity enhancement. As a result, the rate performance of the LTSO composite is pretty decent where it gives over 100 mAh g^{-1} capacity at 15 C

4.5 Conclusion

In conclusion, a thin graphitized carbon-coated Li_2TiSiO_5 composite material (LTSO/C) was fabricated by a chemical vapor deposition treatment. The uniform and conductive coating endow the LTSO/C with exceptionally enhanced charge transport for lithium storage. Theoretical results revealed that such high-quality coating growth originated from the catalytic activity of functional groups on the parent Li_2TiSiO_5 surface. Moreover, the low content of carbonaceous coating (3.5%), mild surface area (3.4 m^2 g^{-1}), and hierarchical microparticles assembled by nanospheres collectively contribute to a tap density (1.3 g mL^{-1}) for practical anode use. The LTSO/C exhibits a comparable volumetric capacity of 441.1 mAh cm^{-3} to commercial graphite at 0.15 A g^{-1} and 120.1 mAh cm^{-3} to commercial LTO at 4.5 A g^{-1}, providing an advanced alternative anode material for durable high-rate lithium-ion batteries. Furthermore, various attempts to generate LTSO carbon composite unfold the flexibility and operability of LTSO in the industrial field.

Chapter 5. Application of silicate in sodium-ion batteries

5.1 Introduction

Sodium-ion batteries are considered as the alternative technology of lithium-ion batteries for the future energy storage system, due to their low-cost, high safety, and abundant material reserve. The current stage of sodium-ion batteries, however, indicates that seeking more appropriate electrode materials are urgent for the development of its real applications and commercialization.

Anodic materials, so far, are dominated by carbon-based materials, primarily the hard carbon. However, such carbonaceous material can not provide the outstanding rate and cycling performances and survive the high-rate process due to the sluggish reaction kinetics and sodium plating inside the layered carbon structure. The consequent structural collapse will ruin the electrode material structure and then create the failure of the battery. Even though metal oxides, Ti-based oxides specifically, provide advanced capacity under high current density, the high energy barrier of Na-ion insertion for metal oxides is still insurmountable and limiting further improvement. Besides, such metal oxides, similar to them of Li-ion batteries, are usually struggling with low electronic conductivity and slow ionic diffusivity. Without additional crystal structural and carbon composite modification, the metal oxides can hardly deliver favorable results. Therefore, many efforts have been made to overcome such drawbacks by discovering novel material with alternative ion storage mechanisms, creating hierarchical and nanosizing morphologies, and achieving effective conductive carbon-coating. Nevertheless, the current candidates still fall short for commercialization because of miserable cycling stability or complex production process.

Herein, we proposed a simple one-step synthesis of novel titanium-based silicate anode material (Na_2TiSiO_5, NTSO) with CVD catalytic ability to achieve high-quality conformal carbon-coating.

To date, the NTSO is commonly synthesized through hydrothermal reactions,[229,230] however it is not conducive for mass production with harsh requirements, especially high pressure. Jianyang Ding et al.[231] reported another approach of synthesizing NTSO with a solid-state reaction between NaOH, TiO_2, and SiO_2. They mixed all solids in an agate mortar for further annealing, and the yielded particles have average diameters around 1.6 micrometers. As an improvement for the solid-phase reaction, we applied the mild ball milling process to achieve similar mixing of reactants, and which is also suitable for large-scale production because it is environment friendly and cost-effective.[232]

Combining the advantages of silicate with excellent chemical stability and *in-situ* catalytic capacity for conductive carbon growth, and titanium-based material with decent structural stability, the NTSO is expected to show remarkable rate performance and cycling stability. Besides, exploration of applying the inexpensive precursors and scaleable production process is also considered to push the practicability of making NTSO for future commercialization.

5.2 Experimental section

5.2.1 Preparation of NTSO and NTSO carbon composite (NTSO/C)

NTSO was synthesized through a simple one-step solid-phase reaction. A certain amount of sodium hydroxide, fumed-silica, and P-25 (TiO_2) were mixing by mild ball milling, where the molar ratio of Na:Ti:Si is 2:1:1. The sizes of agate balls are various from 0.8 cm to 0.3 cm. Then the powder mixture was calcinated in the air at 850 °C for 3 hours to form white NTSO. The prepared NTSO was then placed in a tube furnace and heated to 900 °C for 30 min with a gas flow consist of Argon (500 mL min^{-1})/ Acetonitrile (150 mL min^{-1}) to obtain NTSO/C.

5.2.2 Material characterization

Powder X-ray diffractometry (XRD) was performed using a Rigaku Miniflex II diffractometer with Cu-Kα radiation at 40 kV and 40 mA. The morphology and crystal structure of as-synthesized products were identified by a field scanning electron microscopy (SEM, Nova 230 Nano) with energy-dispersive X-ray spectroscopy (EDS), and a transmission electron microscopy (TEM, HRTEM, FEI-T12). Thermogravimetric analysis (TGA, Q600 SDT, TA Instruments) was performed in the air from 20 to 1000 °C with a heating rate of 10 °C min^{-1}. Raman spectrum was collected with a Renishaw 200 System. X-ray photoelectron spectroscopy (XPS) results were carried out using an AXIS Ultra DLD instrument. Powder electronic conductivity measurement was completed using the ST2722-SZ four-point probe resistivity tester.

5.2.3 Electrochemical measurements

The NTSO and NTSO carbon composite electrodes were prepared by the slurry-coating method. Solids containing activate materials (NTSO and NTSO carbon composite), Super P (carbon black), and polyvinylidene fluoride were uniformly blended in a mass ratio of 70:20:10, correspondingly. The mixtures were subsequently dispersed in N-methyl-2-pyrrolidone, forming homogeneous slurry for doctor blade coating on an Al foil. The as-prepared electrodes were assembled in the 2032-type coin cells with Na metal foils as the counter electrode, glass fiber as the separator, and 1 M sodium perchlorate ($NaClO_4$) dissolved in a mixture of ethylene carbonate (EC) and polycarbonate (PC) (1:1, by volume) as the electrolyte. The galvanostatic charge-discharge measurements were carried out using a Land CT2001A battery tester at room temperature. The electrochemical impedance spectra were taken in a frequency range of 0.1 to 10^6 Hz with an alternating-current voltage amplitude of 20 mV by using a Solartron 1860/1287.

5.3 Results and discussion

As shown in **Figure 5-1**, NTSO and NTSO/C share similar globular morphology and particle size, which is in a range of 1 to 10 micrometers with morphology. The particle structure of NTSO/C is well preserved without further sintering after CVD treatment if compared with LTSO/C in the last chapter. It is because the treating temperature for NTSO is 900 °C, which is quite close to the calcinating temperature for forming NTSO, and the calcinating duration is relatively short, with only 3 hours. The micron-level particles, achieved by the ball milling process, are also helpful in maintaining the structure if they undergo a high-temperature heating treatment.

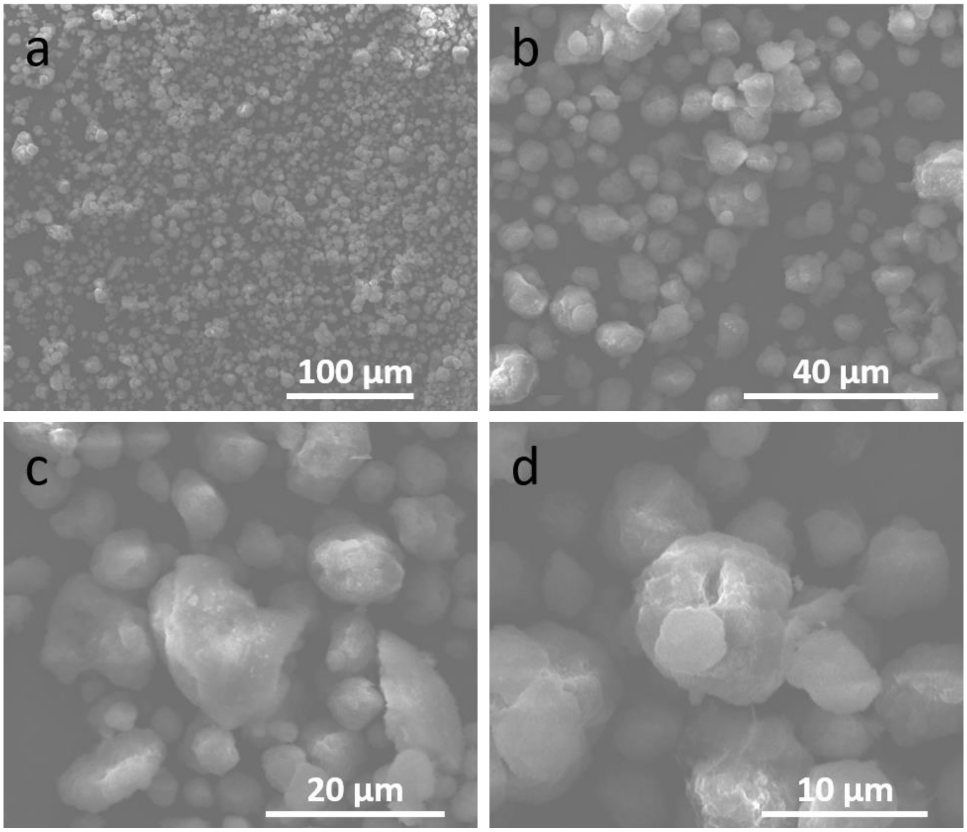

Figure 5-1. SEM images of a-c) NTSO/C, and d) NTSO.

XRD results (**Figure 5-2b**) of NTSO and NTSO/C indicates that the crystal structure remains the same after CVD treatment, which also signifies the excellent thermal and chemical stability of NTSO. Such property is observed from other silicates and ascribed from their particular structure and stable Si-O bonds. Besides, the relatively higher intensity of NTSO characteristic peaks from NTSO/C implies the heating process (during CVD treatment) is also helpful for improving the degree of crystallinity.

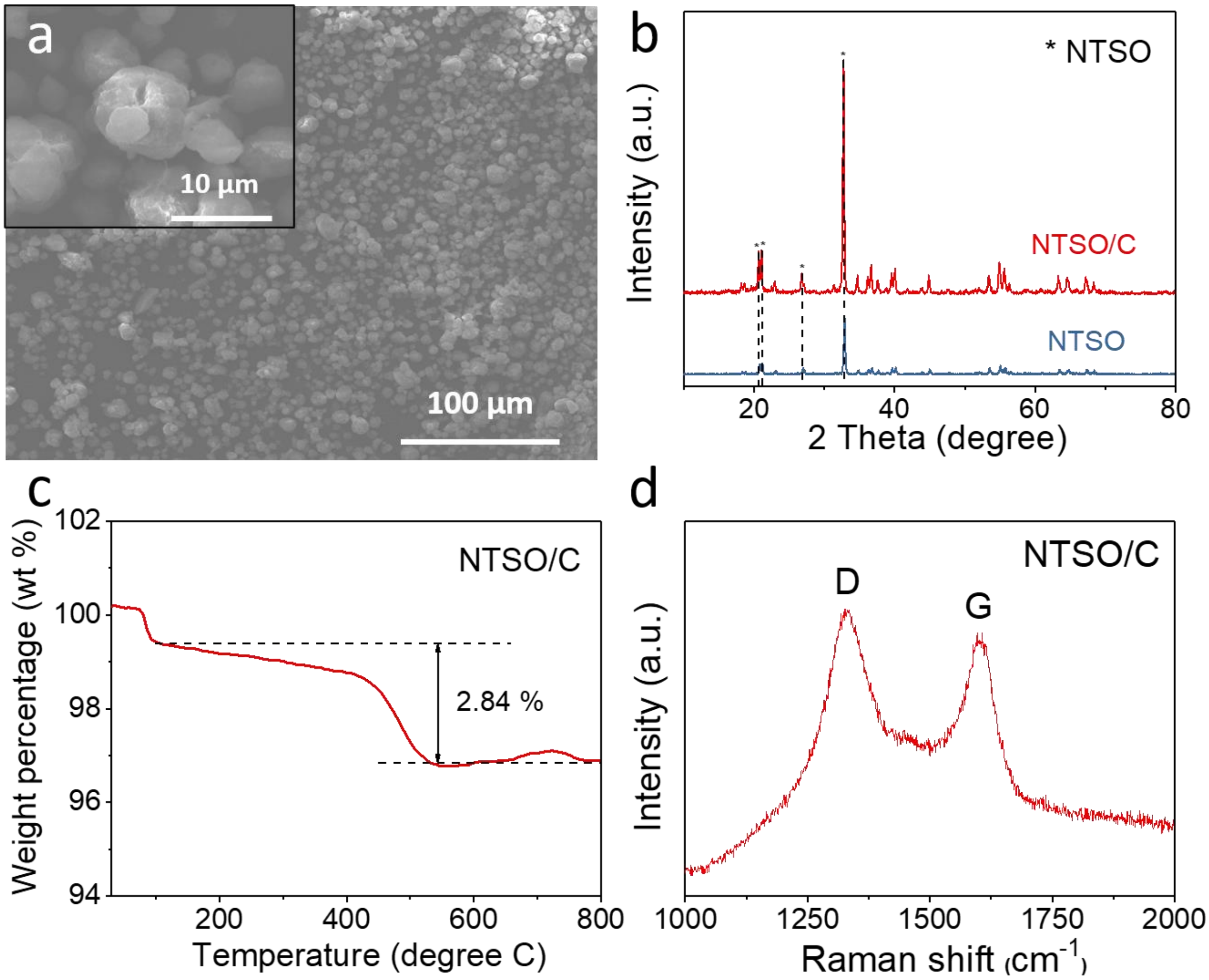

Figure 5-2. a) SEM images of NTSO/C. b) XRD results of NTSO and NTSO/C. c) TGA of NTSO/C. d) Raman spectrum of NTSO/C.

After 30 min CVD treatment, ~ 2.5 wt.% carbon material is attained (Figure 5-2c). Though the indication in the figure 5-2c is 2.84 wt.%, after deducting the amount of water that contributes to the weight loss at around 100 °C, the total mass of carbon is shown as an estimation here. Raman spectrum (Figure 5-2d) indicates the carbon material achieved by the CVD process, like LTSO/C as described in the last chapter, has a similar carbon structure (D and G peak at ~ 1300 cm^{-1} and ~ 1600 cm^{-1}, respectively) and a decent degree of graphitization

(I_D/I_G = 1.2). Therefore, we proved that NTSO also shares catalytic activity during the CVD process for achieving high-quality carbon-coating.

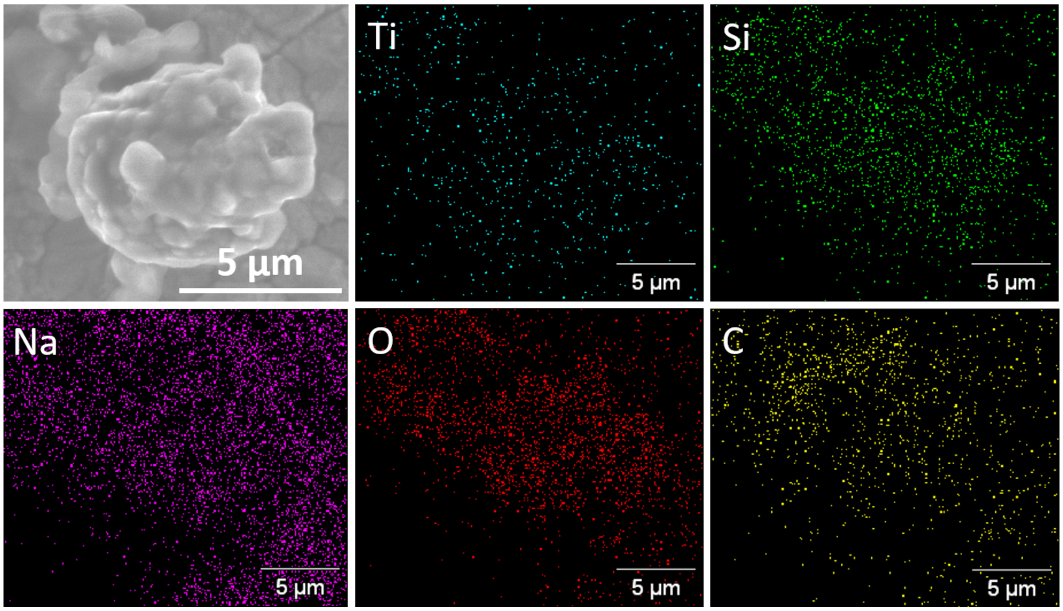

Figure 5-3. EDS element mappings (Ti, Si, Na, O, and C) of NTSO/C.

From **Figure 5-3**, the EDS mapping of NTSO/C confirms the facile carbon-coating after CVD treatment, where C element is distributed evenly over the surface.

For illustrating the enhancement of CVD-assisted carbon-coating on NTSO, multiple electrochemical measurements were conducted and summarized in **Figure 5-4**. The cyclic voltammetry curve of NTSO/C (at the first cycle) reveals the electrode reaction when discharging takes place (Figure 5-4a). Specifically speaking, the peak at around 0.55 V *vs.* Na^+/Na indicates the formation of the SEI layer, where the electrolyte reacts with the electrode material. Such a process will have an undesirable impact on the initial coulombic efficiency of NTSO/C. Even though it will fade away in a few cycles, the irreversible consumption of lithium-ion and electrolyte may cause severe failure on the full battery, where the lithium-ion source is coming from the cathode side instead of lithium metal foil. Fortunately, such a drawback could be compensated by the pre-intercalation of Na-ion, which is similar to lithiation in LIBs.

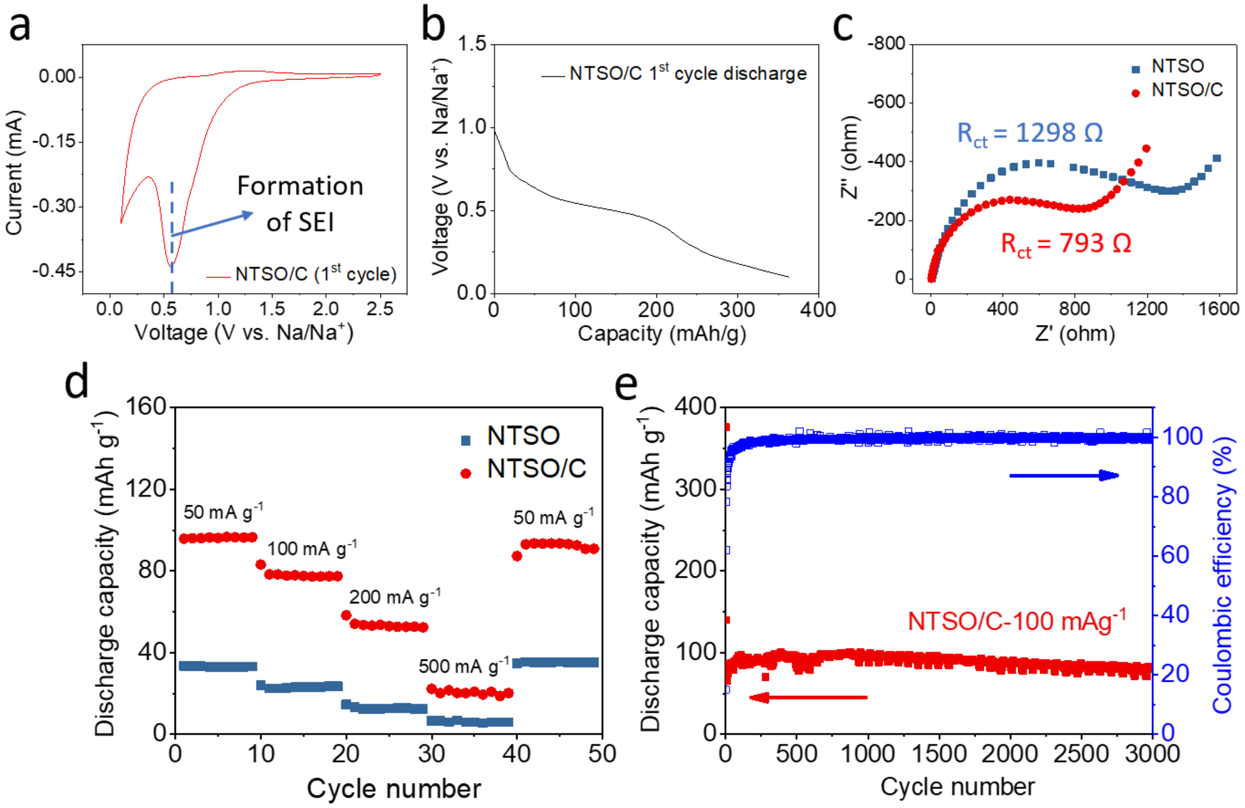

Figure 5-4. Electrochemical properties and performance measurements of NTSO and NTSO/C: a) cyclic voltammetry curve of NTSO/C (first cycle); b) discharge curve of NTSO/C (first cycle); c) electrochemical impedance spectrum of NTSO and NTSO/C; d) rate performance of NTSO and NTSO/C; e) cycling test of NTSO/C with a current density of 100 mA g^{-1}.

As shown in Figure 5-4b, the discharge cure of NTSO/C in the first cycle shows the slop at around 0.55 V *vs*. Na^+/Na, which coincides with the cyclic voltammetry results and confirms the voltage of the SEI formation. The electrochemical impedance spectrum indicates the enhancement of charge transfer resistance of NTSO/C from 1298 Ω to 793 Ω, after CVD carbon-coating (Figure 5-4c). It also demonstrates the benefit of electronic conductivity increasement.

As a result, NTSO/C exhibits superior rate performance over NTSO (Figure 5-4d). It delivers 100 mAh g^{-1} reversible capacity at a current density of 50 mA g^{-1}, where NTSO only shows less than 40 mAh g^{-1}. However, when the current density increases to 500 mAh g^{-1}, the NTSO/C starts to be lacking in strength. Such a phenomenon is understandable since the energy barrier of insertion Na-ion is much higher than it of Li-ion, as mentioned in the previous chapter. It will cause insufficient ion storage in the electrode material, especially when undergoing the high-rate charge/discharge process. Even though the carbon-coating provides the advantages of electronic and ionic transportation, but the intrinsic ionic storage mechanism still falls short.

It is worth mentioning, however, that the NTSO/C shows the excellent cycling stability (Figure 5-4e). Different from traditional carbon-based materials, NTSO/C can maintain over 90% capacity retention after 3000 cycles with a current density of 100 mA g^{-1}. Though the initial coulombic efficiency is ~20%, which ascribes to the formation of the SEI layer, the long cycle-life creates the possibility of NTSO/C for future applications.

5.4 Conclusion

In summary, we have developed a low-cost and easy-scalable tactic to produce NTSO carbon composites for anode electrode material of sodium-ion batteries. With ~ 2.5 wt.% surface carbon-coating, accomplished by 30 min acetonitrile-CVD treatment, NTSO carbon composite exhibits decent rate performance and exceptional cycling stability (over 90% capacity retention after 3000 cycles). Though the low initial coulombic efficiency requires further handling for the full battery application, the advantages still make NTSO carbon composite valuable for further development, such as the large-gride energy storage, public transportation, and building energy supply, which is not sensitive for high-power demands.

Chapter 6. Conclusion of the dissertation

Fast charge/discharge capability is a critical feature for the next generation of lithium-ion batteries because of the growing demands of the high-performance portable devices, such as electric vehicles, remote communication devices, and uncrewed transportations. The essential technical issues of the current lithium-ion batteries rest on developing electrode materials with excellent electronic conductivity, ionic diffusivity, and cycling stability.

Titanium-based materials are extensively regarded as the most promising candidate for high power lithium-ion batteries applications, especially the commercialized and well-researched $Li_4Ti_5O_{12}$, because of their outstanding structural stability. However, the insufficient theoretical capacity and high discharge voltage plateau limit the further development of titanium-based materials. Besides, the low electronic conductivity and ionic diffusivity also require additional treatments and material designs. Freely employing such materials is still challenging, particularly for high-rate adhibitions.

Thereupon, we designed a scalable synthetic strategy towards novel anode electrode material, Li_2TiSiO_5, with exceptional high-power performances. The achieved tactic employed chemical vapor deposition as an *in-situ* carbon growth method to accomplish high-quality conformal carbon-coating over the surface of Li_2TiSiO_5. Benefited from the catalytic activity of Li_2TiSiO_5, the low optimized content of carbonaceous coating (3.5 wt.%), mild surface area (3.4 m^2 g^{-1}), and hierarchical microparticles assembled by nanospheres collectively contribute to a tap density (1.3 g mL^{-1}) for practical anode use. The resulting Li_2TiSiO_5 carbon composite exhibits a comparable volumetric capacity of 441.1 mAh cm^{-3} to commercial graphite at 0.15 A g^{-1} and 120.1 mAh cm^{-3} to commercial $L_{i4}Ti_5O_{12}$ at 4.5 A g^{-1}, providing an advanced alternative anode material for durable high-rate lithium-ion batteries.

Furthermore, the exploration of titanium-based silicate for sodium-ion batteries also reveals a talented candidate, Na_2TiSiO_5, which shares similar catalytic activity as it of Li_2TiSiO_5. The accomplished Na_2TiSiO_5 carbon composite exhibits admirable rate performance with 100 mAh g^{-1} at a current density of 50 mA g^{-1}, and 60 mAh g^{-1} at a current density of 200 mA g^{-1}. The remarkable cycling stability with 90% capacity retention after 3000 cycles further affirming the potential value of developing the Na_2TiSiO_5 as anode material for sodium-ion batteries.

To conclude, we hope this dissertation could elucidate the function of titanium-based silicate in lithium-ion and sodium-ion batteries and inspire a new path for designing carbon composites with the help of chemical vapor deposition.

Chapter 7. Reference

1. Scott, A. C.; Chaloner, W. G.; Belcher, C. M.; Roos, C. I., The interaction of fire and mankind: Introduction. The Royal Society: 2016.

2. Smil, V., World history and energy. *Encyclopedia of energy* **2004,** *6*, 549-561.

3. Koohi-Fayegh, S.; Rosen, M., A review of energy storage types, applications and recent developments. *Journal of Energy Storage* **2020,** *27*, 101047.

4. Christen, T.; Carlen, M. W., Theory of Ragone plots. *J. Power Sources* **2000,** *91* (2), 210-216.

5. Hall, P. J.; Bain, E. J., Energy-storage technologies and electricity generation. *Energy policy* **2008,** *36* (12), 4352-4355.

6. Baker, J., New technology and possible advances in energy storage. *Energy Policy* **2008,** *36* (12), 4368-4373.

7. Hou, J.; Shao, Y.; Ellis, M. W.; Moore, R. B.; Yi, B., Graphene-based electrochemical energy conversion and storage: fuel cells, supercapacitors and lithium ion batteries. *PCCP* **2011,** *13* (34), 15384-15402.

8. Nitta, N.; Wu, F.; Lee, J. T.; Yushin, G., Li-ion battery materials: present and future. *Mater. Today* **2015,** *18* (5), 252-264.

9. Girishkumar, G.; McCloskey, B.; Luntz, A. C.; Swanson, S.; Wilcke, W., Lithium− air battery: promise and challenges. *The Journal of Physical Chemistry Letters* **2010,** *1* (14), 2193-2203.

10. Zhang, L.-L.; Wang, Z.-L.; Xu, D.; Zhang, X.-B.; Wang, L.-M., The development and challenges of rechargeable non-aqueous lithium–air batteries. *International Journal of Smart and Nano Materials* **2013,** *4* (1), 27-46.

11. Bruce, P. G.; Freunberger, S. A.; Hardwick, L. J.; Tarascon, J.-M., Li–O 2 and Li–S batteries with high energy storage. *Nature materials* **2012,** *11* (1), 19.

12. Thackeray, M. M.; Wolverton, C.; Isaacs, E. D., Electrical energy storage for transportation—approaching the limits of, and going beyond, lithium-ion batteries. *Energy Environ. Sci.* **2012,** *5* (7), 7854-7863.

13. Verma, P.; Maire, P.; Novák, P., A review of the features and analyses of the solid electrolyte interphase in Li-ion batteries. *Electrochim. Acta* **2010,** *55* (22), 6332-6341.

14. Chayambuka, K.; Mulder, G.; Danilov, D. L.; Notten, P. H., Sodium-ion battery materials and electrochemical properties reviewed. *Adv. Energy Mater.* **2018,** *8* (16), 1800079.

15. Palomares, V.; Serras, P.; Villaluenga, I.; Hueso, K. B.; Carretero-González, J.; Rojo, T., Na-ion batteries, recent advances and present challenges to become low cost energy storage systems. *Energy Environ. Sci.* **2012,** *5* (3), 5884-5901.

16. Watanabe, M.; Thomas, M. L.; Zhang, S.; Ueno, K.; Yasuda, T.; Dokko, K., Application of ionic liquids to energy storage and conversion materials and devices. *Chem. Rev.* **2017,** *117* (10), 7190-7239.

17. Ru, Y.; Zheng, S.; Xue, H.; Pang, H., Different positive electrode materials in organic and aqueous systems for aluminium ion batteries. *J. Mater. Chem. A* **2019,** *7* (24), 14391-14418.

18. Dresselhaus, M.; Thomas, I., Alternative energy technologies. *Nature* **2001,** *414* (6861), 332-337.

19. Pacala, S.; Socolow, R., Stabilization wedges: solving the climate problem for the next 50 years with current technologies. *science* **2004,** *305* (5686), 968-972.

20. Vikström, H.; Davidsson, S.; Höök, M., Lithium availability and future production outlooks. *Appl. Energy* **2013,** *110*, 252-266.

21. Gruber, P. W.; Medina, P. A.; Keoleian, G. A.; Kesler, S. E.; Everson, M. P.; Wallington, T. J., Global lithium availability: A constraint for electric vehicles? *Journal of Industrial Ecology* **2011,** *15* (5), 760-775.

22. Speirs, J.; Contestabile, M.; Houari, Y.; Gross, R., The future of lithium availability for electric vehicle batteries. *Renew. Sustain. Energy Rev.* **2014,** *35*, 183-193.

23. Grosjean, C.; Miranda, P. H.; Perrin, M.; Poggi, P., Assessment of world lithium resources and consequences of their geographic distribution on the expected development of the electric vehicle industry. *Renew. Sustain. Energy Rev.* **2012,** *16* (3), 1735-1744.

24. Lowe, M.; Tokuoka, S.; Trigg, T.; Gereffi, G., Lithium-ion batteries for electric vehicles. *The US Value Chain, Contributing CGGC researcher: Ansam Abayechi* **2010**.

25. Nelson, P. A.; Gallagher, K. G.; Bloom, I. D.; Dees, D. W. *Modeling the performance and cost of lithium-ion batteries for electric-drive vehicles*; Argonne National Lab.(ANL), Argonne, IL (United States): 2012.

26. Greenwood, N. N.; Earnshaw, A., *Chemistry of the Elements*. Elsevier: 2012.

27. Kim, T.; Song, W.; Son, D.-Y.; Ono, L. K.; Qi, Y., Lithium-ion batteries: outlook on present, future, and hybridized technologies. *J. Mater. Chem. A* **2019,** *7* (7), 2942-2964.

28. Wang, F.; Xiao, S.; Chang, Z.; Yang, Y.; Wu, Y., Nanoporous LiNi 1/3 Co 1/3 Mn 1/3 O 2 as an ultra-fast charge cathode material for aqueous rechargeable lithium batteries. *Chem. Commun.* **2013,** *49* (80), 9209-9211.

29. Notten, P. H.; het Veld, J. O.; Van Beek, J., Boostcharging Li-ion batteries: A challenging new charging concept. *J. Power Sources* **2005,** *145* (1), 89-94.

30. Anseán, D.; Dubarry, M.; Devie, A.; Liaw, B.; García, V.; Viera, J.; González, M., Fast charging technique for high power LiFePO4 batteries: A mechanistic analysis of aging. *J. Power Sources* **2016,** *321*, 201-209.

31. Tarascon, J.; Armand, M., Nature 414: 359 Crossref. *Medline, Google Scholar* **2001**.

32. Cheng, X.-B.; Yan, C.; Zhang, X.-Q.; Liu, H.; Zhang, Q., Electronic and ionic channels in working interfaces of lithium metal anodes. *ACS Energy Letters* **2018,** *3* (7), 1564-1570.

33. Zhang, X. Q.; Cheng, X. B.; Zhang, Q., Energy Storage: Advances in Interfaces between Li Metal Anode and Electrolyte (Adv. Mater. Interfaces 2/2018). *Advanced Materials Interfaces* **2018,** *5* (2), 1870005.

34. Shen, X.; Liu, H.; Cheng, X.; Yan, C.; Huang, J., Energy Storage Mater. 2018, 12, 161; d) L. *Wang, Z. Zhou, X. Yan, F. Hou, L. Wen, W. Luo, J. Liang, SX Dou, Energy Storage Mater* **2018,** *14*, 22.

35. Anseán, D.; González, M.; Viera, J.; García, V.; Blanco, C.; Valledor, M., Fast charging technique for high power lithium iron phosphate batteries: A cycle life analysis. *J. Power Sources* **2013,** *239*, 9-15.

36. Lee, S.; Cho, Y.; Song, H. K.; Lee, K. T.; Cho, J., Carbon-coated single-crystal LiMn2O4 nanoparticle clusters as cathode material for high-energy and high-power lithium-ion batteries. *Angew. Chem.* **2012,** *124* (35), 8878-8882.

37. Morrissey, P.; Weldon, P.; O'Mahony, M., Future standard and fast charging infrastructure planning: An analysis of electric vehicle charging behaviour. *Energy Policy* **2016,** *89*, 257-270.

38. Neubauer, J.; Pesaran, A.; Bae, C.; Elder, R.; Cunningham, B., Updating United States Advanced Battery Consortium and Department of Energy battery technology targets for battery electric vehicles. *J. Power Sources* **2014,** *271*, 614-621.

39. Botsford, C.; Szczepanek, A. In *Fast charging vs. slow charging: Pros and cons for the new age of electric vehicles*, International Battery Hybrid Fuel Cell Electric Vehicle Symposium, 2009.

40. Meintz, A.; Zhang, J.; Vijayagopal, R.; Kreutzer, C.; Ahmed, S.; Bloom, I.; Burnham, A.; Carlson, R. B.; Dias, F.; Dufek, E. J., Enabling fast charging–Vehicle considerations. *J. Power Sources* **2017,** *367*, 216-227.

41. Okubo, M.; Hosono, E.; Kim, J.; Enomoto, M.; Kojima, N.; Kudo, T.; Zhou, H.; Honma, I., Nanosize effect on high-rate Li-ion intercalation in LiCoO2 electrode. *J. Am. Chem. Soc.* **2007,** *129* (23), 7444-7452.

42. Dunn, B.; Kamath, H.; Tarascon, J.-M., Electrical energy storage for the grid: a battery of choices. *Science* **2011,** *334* (6058), 928-935.

43. Li, N.; Chen, Z.; Ren, W.; Li, F.; Cheng, H.-M., Flexible graphene-based lithium ion batteries with ultrafast charge and discharge rates. *Proceedings of the National Academy of Sciences* **2012,** *109* (43), 17360-17365.

44. Kang, B.; Ceder, G., Battery materials for ultrafast charging and discharging. *Nature* **2009,** *458* (7235), 190-193.

45. Vetter, J.; Novák, P.; Wagner, M. R.; Veit, C.; Möller, K.-C.; Besenhard, J.; Winter, M.; Wohlfahrt-Mehrens, M.; Vogler, C.; Hammouche, A., Ageing mechanisms in lithium-ion batteries. *J. Power Sources* **2005,** *147* (1-2), 269-281.

46. Zhang, S. S., The effect of the charging protocol on the cycle life of a Li-ion battery. *J. Power Sources* **2006,** *161* (2), 1385-1391.

47. Yu, X.; Manthiram, A., Electrode–electrolyte interfaces in lithium-based batteries. *Energy Environ. Sci.* **2018,** *11* (3), 527-543.

48. Thangadurai, V.; Narayanan, S.; Pinzaru, D., Garnet-type solid-state fast Li ion conductors for Li batteries: critical review. *Chem. Soc. Rev.* **2014,** *43* (13), 4714-4727.

49. Janek, J.; Zeier, W. G., A solid future for battery development. *Nat. Energy* **2016,** *1* (9), 1-4.

50. Chen, W.; Lei, T.; Wu, C.; Deng, M.; Gong, C.; Hu, K.; Ma, Y.; Dai, L.; Lv, W.; He, W., Designing Safe Electrolyte Systems for a High-Stability Lithium–Sulfur Battery. *Adv. Energy Mater.* **2018,** *8* (10), 1702348.

51. Tian, H.; Gao, T.; Li, X.; Wang, X.; Luo, C.; Fan, X.; Yang, C.; Suo, L.; Ma, Z.; Han, W., High power rechargeable magnesium/iodine battery chemistry. *Nat. Commun.* **2017,** *8* (1), 1-8.

52. Liu, C.; Liu, X.; Tan, J.; Wang, Q.; Wen, H.; Zhang, C., Nitrogen-doped graphene by all-solid-state ball-milling graphite with urea as a high-power lithium ion battery anode. *J. Power Sources* **2017,** *342*, 157-164.

53. Lee, S. W.; Yabuuchi, N.; Gallant, B. M.; Chen, S.; Kim, B.-S.; Hammond, P. T.; Shao-Horn, Y., High-power lithium batteries from functionalized carbon-nanotube electrodes. *Nature nanotechnology* **2010,** *5* (7), 531-537.

54. Chung, S., Nature Materials. *Mater* **2002,** *1*, 123.

55. Chen, H.; Grey, C. P., Molten Salt Synthesis and High Rate Performance of the “Desert-Rose” form of LiCoO2. *Adv. Mater.* **2008,** *20* (11), 2206-2210.

56. Zhu, G. L.; Zhao, C. Z.; Huang, J. Q.; He, C.; Zhang, J.; Chen, S.; Xu, L.; Yuan, H.; Zhang, Q., Fast Charging Lithium Batteries: Recent Progress and Future Prospects. *Small* **2019,** *15* (15), 1805389.

57. Sivakkumar, S. R.; Nerkar, J.; Pandolfo, A., Rate capability of graphite materials as negative electrodes in lithium-ion capacitors. *Electrochim. Acta* **2010,** *55* (9), 3330-3335.

58. Guo, B.; Wang, X.; Fulvio, P. F.; Chi, M.; Mahurin, S. M.; Sun, X. G.; Dai, S., Soft-templated mesoporous carbon-carbon nanotube composites for high performance lithium-ion batteries. *Adv. Mater.* **2011,** *23* (40), 4661-4666.

59. Liang, Y.; Chen, L.; Cai, L.; Liu, H.; Fu, R.; Zhang, M.; Wu, D., Strong contribution of pore morphology to the high-rate electrochemical performance of lithium-ion batteries. *Chem. Commun.* **2016,** *52* (4), 803-806.

60. Zhou, H.; Zhu, S.; Hibino, M.; Honma, I.; Ichihara, M., Lithium storage in ordered mesoporous carbon (CMK-3) with high reversible specific energy capacity and good cycling performance. *Adv. Mater.* **2003,** *15* (24), 2107-2111.

61. Hu, Y. S.; Adelhelm, P.; Smarsly, B. M.; Hore, S.; Antonietti, M.; Maier, J., Synthesis of hierarchically porous carbon monoliths with highly ordered microstructure and their application in rechargeable lithium batteries with high-rate capability. *Adv. Funct. Mater.* **2007,** *17* (12), 1873-1878.

62. Wu, Z.-S.; Ren, W.; Xu, L.; Li, F.; Cheng, H.-M., Doped graphene sheets as anode materials with superhigh rate and large capacity for lithium ion batteries. *ACS nano* **2011,** *5* (7), 5463-5471.

63. Qie, L.; Chen, W. M.; Wang, Z. H.; Shao, Q. G.; Li, X.; Yuan, L. X.; Hu, X. L.; Zhang, W. X.; Huang, Y. H., Nitrogen-doped porous carbon nanofiber webs as anodes for

lithium ion batteries with a superhigh capacity and rate capability. *Adv. Mater.* **2012,** *24* (15), 2047-2050.

64. Wang, Y.-Q.; Gu, L.; Guo, Y.-G.; Li, H.; He, X.-Q.; Tsukimoto, S.; Ikuhara, Y.; Wan, L.-J., Rutile-TiO2 nanocoating for a high-rate Li4Ti5O12 anode of a lithium-ion battery. *J. Am. Chem. Soc.* **2012,** *134* (18), 7874-7879.

65. Wagemaker, M.; van Eck, E. R.; Kentgens, A. P.; Mulder, F. M., Li-ion diffusion in the equilibrium nanomorphology of spinel Li4+ x Ti5O12. *The Journal of Physical Chemistry B* **2009,** *113* (1), 224-230.

66. Ohzuku, T.; Ueda, A.; Yamamoto, N., Zero-strain insertion material of Li [Li1/3Ti5/3] O 4 for rechargeable lithium cells. *J. Electrochem. Soc.* **1995,** *142* (5), 1431.

67. Shen, L.; Uchaker, E.; Zhang, X.; Cao, G., Hydrogenated Li4Ti5O12 nanowire arrays for high rate lithium ion batteries. *Adv. Mater.* **2012,** *24* (48), 6502-6506.

68. Park, K.-S.; Benayad, A.; Kang, D.-J.; Doo, S.-G., Nitridation-driven conductive Li4Ti5O12 for lithium ion batteries. *J. Am. Chem. Soc.* **2008,** *130* (45), 14930-14931.

69. Zhu, G.-N.; Liu, H.-J.; Zhuang, J.-H.; Wang, C.-X.; Wang, Y.-G.; Xia, Y.-Y., Carbon-coated nano-sized Li 4 Ti 5 O 12 nanoporous micro-sphere as anode material for high-rate lithium-ion batteries. *Energy Environ. Sci.* **2011,** *4* (10), 4016-4022.

70. Huang, R.; Ikuhara, Y. H.; Mizoguchi, T.; Findlay, S. D.; Kuwabara, A.; Fisher, C. A.; Moriwake, H.; Oki, H.; Hirayama, T.; Ikuhara, Y., Oxygen-Vacancy Ordering at Surfaces of Lithium Manganese (III, IV) Oxide Spinel Nanoparticles. *Angew. Chem.* **2011,** *123* (13), 3109-3113.

71. Hwang, H.; Kim, H.; Cho, J., MoS2 nanoplates consisting of disordered graphene-like layers for high rate lithium battery anode materials. *Nano Lett.* **2011,** *11* (11), 4826-4830.

72. Luo, J.; Liu, J.; Zeng, Z.; Ng, C. F.; Ma, L.; Zhang, H.; Lin, J.; Shen, Z.; Fan, H. J., Three-dimensional graphene foam supported Fe3O4 lithium battery anodes with long cycle life and high rate capability. *Nano Lett.* **2013,** *13* (12), 6136-6143.

73. Li, Y.; Tan, B.; Wu, Y., Mesoporous Co3O4 nanowire arrays for lithium ion batteries with high capacity and rate capability. *Nano Lett.* **2008,** *8* (1), 265-270.

74. Wu, H.; Chan, G.; Choi, J. W.; Ryu, I.; Yao, Y.; McDowell, M. T.; Lee, S. W.; Jackson, A.; Yang, Y.; Hu, L., Stable cycling of double-walled silicon nanotube battery anodes through solid–electrolyte interphase control. *Nature nanotechnology* **2012,** *7* (5), 310-315.

75. Tang, C.; Wang, H.-F.; Huang, J.-Q.; Qian, W.; Wei, F.; Qiao, S.-Z.; Zhang, Q., 3d hierarchical porous graphene-based energy materials: Synthesis, functionalization, and application in energy storage and conversion. *Electrochemical Energy Reviews* **2019,** *2* (2), 332-371.

76. Yan, L.; Rui, X.; Chen, G.; Xu, W.; Zou, G.; Luo, H., Recent advances in nanostructured Nb-based oxides for electrochemical energy storage. *Nanoscale* **2016,** *8* (16), 8443-8465.

77. Deng, Q.; Fu, Y.; Zhu, C.; Yu, Y., Niobium-based oxides toward advanced electrochemical energy storage: recent advances and challenges. *Small* **2019,** *15* (32), 1804884.

78. Hu, M.; Jiang, Y.; Sun, W.; Wang, H.; Jin, C.; Yan, M., Reversible conversion-alloying of Sb2O3 as a high-capacity, high-rate, and durable anode for sodium ion batteries. *ACS Appl. Mater. Interfaces* **2014,** *6* (21), 19449-19455.

79. Zhao, Y.; Li, X.; Yan, B.; Xiong, D.; Li, D.; Lawes, S.; Sun, X., Recent developments and understanding of novel mixed transition-metal oxides as anodes in lithium ion batteries. *Adv. Energy Mater.* **2016,** *6* (8), 1502175.

80. Jang, J.-H.; Chae, B.-M.; Oh, H.-J.; Lee, Y.-K., Understanding conversion mechanism of NiO anodic materials for Li-ion battery using in situ X-ray absorption near edge structure spectroscopy. *J. Power Sources* **2016,** *304,* 189-195.

81. Chae, B.-M.; Oh, E.-S.; Lee, Y.-K., Conversion mechanisms of cobalt oxide anode for Li-ion battery: In situ X-ray absorption fine structure studies. *J. Power Sources* **2015,** *274,* 748-754.

82. Li, J.; Hwang, S.; Guo, F.; Li, S.; Chen, Z.; Kou, R.; Sun, K.; Sun, C.-J.; Gan, H.; Yu, A., Phase evolution of conversion-type electrode for lithium ion batteries. *Nat. Commun.* **2019,** *10* (1), 1-10.

83. Su, Q.; Wang, S.; Yao, L.; Li, H.; Du, G.; Ye, H.; Fang, Y., Study on the electrochemical reaction mechanism of ZnFe 2 O 4 by in situ transmission electron microscopy. *Scientific reports* **2016,** *6* (1), 1-9.

84. Li, S.; Li, A.; Zhang, R.; He, Y.; Zhai, Y.; Xu, L., Hierarchical porous metal ferrite ball-in-ball hollow spheres: General synthesis, formation mechanism, and high performance as anode materials for Li-ion batteries. *Nano Res.* **2014,** *7* (8), 1116-1127.

85. Liu, J.; Pang, W. K.; Zhou, T.; Chen, L.; Wang, Y.; Peterson, V. K.; Yang, Z.; Guo, Z.; Xia, Y., Li 2 TiSiO 5: a low potential and large capacity Ti-based anode material for Li-ion batteries. *Energy Environ. Sci.* **2017,** *10* (6), 1456-1464.

86. Aravindan, V.; Gnanaraj, J.; Lee, Y.-S.; Madhavi, S., Insertion-type electrodes for nonaqueous Li-ion capacitors. *Chem. Rev.* **2014,** *114* (23), 11619-11635.

87. Zhai, Y.; Dou, Y.; Zhao, D.; Fulvio, P. F.; Mayes, R. T.; Dai, S., Carbon materials for chemical capacitive energy storage. *Adv. Mater.* **2011,** *23* (42), 4828-4850.

88. Dai, L.; Chang, D. W.; Baek, J. B.; Lu, W., Carbon nanomaterials for advanced energy conversion and storage. *small* **2012,** *8* (8), 1130-1166.

89. Yang, Z.; Ren, J.; Zhang, Z.; Chen, X.; Guan, G.; Qiu, L.; Zhang, Y.; Peng, H., Recent advancement of nanostructured carbon for energy applications. *Chem. Rev.* **2015,** *115* (11), 5159-5223.

90. Liang, C.; Li, Z.; Dai, S., Mesoporous carbon materials: synthesis and modification. *Angew. Chem. Int. Ed.* **2008,** *47* (20), 3696-3717.

91. Fang, Y.; Lv, Y.; Che, R.; Wu, H.; Zhang, X.; Gu, D.; Zheng, G.; Zhao, D., Two-dimensional mesoporous carbon nanosheets and their derived graphene nanosheets: synthesis and efficient lithium ion storage. *J. Am. Chem. Soc.* **2013,** *135* (4), 1524-1530.

92. Huang, X.; Qian, K.; Yang, J.; Zhang, J.; Li, L.; Yu, C.; Zhao, D., Functional nanoporous graphene foams with controlled pore sizes. *Adv. Mater.* **2012,** *24* (32), 4419-4423.

93. Fang, Y.; Gu, D.; Zou, Y.; Wu, Z.; Li, F.; Che, R.; Deng, Y.; Tu, B.; Zhao, D., A low-concentration hydrothermal synthesis of biocompatible ordered mesoporous carbon nanospheres with tunable and uniform size. *Angew. Chem.* **2010,** *122* (43), 8159-8163.

94. Guo, X.; Sun, B.; Su, D.; Liu, X.; Liu, H.; Wang, Y.; Wang, G., Recent developments of aprotic lithium-oxygen batteries: functional materials determine the electrochemical performance. *Science Bulletin* **2017,** *62* (6), 442-452.

95. Liu, H.; Liu, X.; Li, W.; Guo, X.; Wang, Y.; Wang, G.; Zhao, D., Porous carbon composites for next generation rechargeable lithium batteries. *Adv. Energy Mater.* **2017,** *7* (24), 1700283.

96. Wan, Y.; Shi, Y.; Zhao, D., Supramolecular aggregates as templates: ordered mesoporous polymers and carbons. *Chem. Mater.* **2008,** *20* (3), 932-945.

97. Stein, A.; Wang, Z.; Fierke, M. A., Functionalization of porous carbon materials with designed pore architecture. *Adv. Mater.* **2009,** *21* (3), 265-293.

98. Jun, S.; Joo, S. H.; Ryoo, R.; Kruk, M.; Jaroniec, M.; Liu, Z.; Ohsuna, T.; Terasaki, O., Synthesis of new, nanoporous carbon with hexagonally ordered mesostructure. *J. Am. Chem. Soc.* **2000,** *122* (43), 10712-10713.

99. Gu, D.; Li, W.; Wang, F.; Bongard, H.; Spliethoff, B.; Schmidt, W.; Weidenthaler, C.; Xia, Y.; Zhao, D.; Schüth, F., Controllable synthesis of mesoporous peapod-like Co3O4@ carbon nanotube arrays for high-performance lithium-ion batteries. *Angew. Chem.* **2015,** *127* (24), 7166-7170.

100. Han, F.; Li, W.-C.; Li, M.-R.; Lu, A.-H., Fabrication of superior-performance SnO 2@ C composites for lithium-ion anodes using tubular mesoporous carbon with thin carbon walls and high pore volume. *J. Mater. Chem.* **2012,** *22* (19), 9645-9651.

101. Meng, Y.; Gu, D.; Zhang, F.; Shi, Y.; Yang, H.; Li, Z.; Yu, C.; Tu, B.; Zhao, D., Ordered mesoporous polymers and homologous carbon frameworks: amphiphilic surfactant templating and direct transformation. *Angew. Chem. Int. Ed.* **2005,** *44* (43), 7053-7059.

102. Meng, Y.; Gu, D.; Zhang, F.; Shi, Y.; Cheng, L.; Feng, D.; Wu, Z.; Chen, Z.; Wan, Y.; Stein, A., A family of highly ordered mesoporous polymer resin and carbon structures from organic− organic self-assembly. *Chem. Mater.* **2006,** *18* (18), 4447-4464.

103. Xue, C.; Tu, B.; Zhao, D., Facile fabrication of hierarchically porous carbonaceous monoliths with ordered mesostructure via an organic organic self-assembly. *Nano Res.* **2009,** *2* (3), 242-253.

104. Liu, H.; Li, W.; Shen, D.; Zhao, D.; Wang, G., Graphitic carbon conformal coating of mesoporous TiO2 hollow spheres for high-performance lithium ion battery anodes. *J. Am. Chem. Soc.* **2015,** *137* (40), 13161-13166.

105. Li, W.; Yang, J.; Wu, Z.; Wang, J.; Li, B.; Feng, S.; Deng, Y.; Zhang, F.; Zhao, D., A versatile kinetics-controlled coating method to construct uniform porous TiO2 shells for multifunctional core–shell structures. *J. Am. Chem. Soc.* **2012,** *134* (29), 11864-11867.

106. Petkovich, N. D.; Stein, A., Controlling macro-and mesostructures with hierarchical porosity through combined hard and soft templating. *Chem. Soc. Rev.* **2013,** *42* (9), 3721-3739.

107. Kim, H.; Cho, J., Superior lithium electroactive mesoporous Si@ Carbon core− shell nanowires for lithium battery anode material. *Nano Lett.* **2008,** *8* (11), 3688-3691.

108. Liu, H.; Chen, S.; Wang, G.; Qiao, S. Z., Ordered Mesoporous Core/Shell SnO2/C Nanocomposite as High-Capacity Anode Material for Lithium-Ion Batteries. *Chemistry–A European Journal* **2013,** *19* (50), 16897-16901.

109. Kwasi-Effah, C. C.; Rabczuk, T., Dimensional analysis and modelling of energy density of lithium-ion battery. *Journal of Energy Storage* **2018,** *18*, 308-315.

110. Tarascon, J.; Armand, M., Issues and challenges facing rechargeable lithium batteries' Nature, 414, 359 (2001).

111. Bin, D.; Wen, Y.; Wang, Y.; Xia, Y., The development in aqueous lithium-ion batteries. *Journal of energy chemistry* **2018,** *27* (6), 1521-1535.

112. Kim, J.-H.; Jung, M.-J.; Kim, M.-J.; Lee, Y.-S., Electrochemical performances of lithium and sodium ion batteries based on carbon materials. *Journal of industrial and engineering chemistry* **2018,** *61*, 368-380.

113. Wang, J.; Zhang, C.; Kang, F., Nitrogen-enriched porous carbon coating for manganese oxide nanostructures toward high-performance lithium-ion batteries. *ACS Appl. Mater. Interfaces* **2015,** *7* (17), 9185-9194.

114. Ji, L.; Lin, Z.; Alcoutlabi, M.; Zhang, X., Recent developments in nanostructured anode materials for rechargeable lithium-ion batteries. *Energy Environ. Sci.* **2011,** *4* (8), 2682-2699.

115. Xiao, Z.; Ning, G.; Ma, X.; Li, W.; Xu, C., MnO-encapsulated graphene cubes derived from homogeneous MnCO3-C cubes as high performance anode material for Li ion batteries. *Carbon* **2018,** *139*, 750-758.

116. Wang, C.-Y.; Yi, Y.-H.; Chang, W.-C.; Kao, T.-L.; Tuan, H.-Y., Multi-walled carbon nanotube-wrapped SiP2 as a superior anode material for lithium-ion and sodium-ion batteries. *J. Power Sources* **2018,** *399*, 49-58.

117. Canal-Rodríguez, M.; Arenillas, A.; Menéndez, J. A.; Beneroso, D.; Rey-Raap, N., Carbon xerogels graphitized by microwave heating as anode materials in lithium-ion batteries. *Carbon* **2018,** *137*, 384-394.

118. Novoselov, K. S.; Geim, A. K.; Morozov, S. V.; Jiang, D.; Zhang, Y.; Dubonos, S. V.; Grigorieva, I. V.; Firsov, A. A., Electric field effect in atomically thin carbon films. *science* **2004,** *306* (5696), 666-669.

119. Allen, M. J.; Tung, V. C.; Kaner, R. B., Honeycomb carbon: a review of graphene. *Chem. Rev.* **2010,** *110* (1), 132-145.

120. Singh, R. K.; Kumar, R.; Singh, D. P., Graphene oxide: strategies for synthesis, reduction and frontier applications. *RCS Adv.* **2016,** *6* (69), 64993-65011.

121. Chen, D.; Feng, H.; Li, J., Graphene oxide: preparation, functionalization, and electrochemical applications. *Chem. Rev.* **2012,** *112* (11), 6027-6053.

122. Kumar, R.; Sahoo, S.; Joanni, E.; Singh, R. K.; Tan, W. K.; Kar, K. K.; Matsuda, A., Recent progress in the synthesis of graphene and derived materials for next generation electrodes of high performance lithium ion batteries. *Prog. Energy Combust. Sci.* **2019,** *75*, 100786.

123. Tour, J. M., Top-down versus bottom-up fabrication of graphene-based electronics. *Chem. Mater.* **2014,** *26* (1), 163-171.

124. Buzaglo, M.; Ruse, E.; Levy, I.; Nadiv, R.; Reuveni, G.; Shtein, M.; Regev, O., Top-down, scalable graphene sheets production: It is all about the precipitate. *Chem. Mater.* **2017,** *29* (23), 9998-10006.

125. Huang, Y.; Sutter, E.; Shi, N. N.; Zheng, J.; Yang, T.; Englund, D.; Gao, H.-J.; Sutter, P., Reliable exfoliation of large-area high-quality flakes of graphene and other two-dimensional materials. *ACS nano* **2015,** *9* (11), 10612-10620.

126. Park, S.; Ruoff, R. S., Chemical methods for the production of graphenes. *Nature nanotechnology* **2009,** *4* (4), 217-224.

127. Leon, V.; Rodriguez, A. M.; Prieto, P.; Prato, M.; Vazquez, E., Exfoliation of graphite with triazine derivatives under ball-milling conditions: preparation of few-layer graphene via selective noncovalent interactions. *ACS nano* **2014,** *8* (1), 563-571.

128. Russo, P.; Hu, A.; Compagnini, G.; Duley, W. W.; Zhou, N. Y., Femtosecond laser ablation of highly oriented pyrolytic graphite: a green route for large-scale production of porous graphene and graphene quantum dots. *Nanoscale* **2014,** *6* (4), 2381-2389.

129. Russo, P.; Liang, R.; Jabari, E.; Marzbanrad, E.; Toyserkani, E.; Zhou, Y. N., Single-step synthesis of graphene quantum dots by femtosecond laser ablation of graphene oxide dispersions. *Nanoscale* **2016,** *8* (16), 8863-8877.

130. Aussems, D.; Bal, K.; Morgan, T.; van de Sanden, M.; Neyts, E., Mechanisms of elementary hydrogen ion-surface interactions during multilayer graphene etching at high surface temperature as a function of flux. *Carbon* **2018,** *137*, 527-532.

131. Kosynkin, D. V.; Higginbotham, A. L.; Sinitskii, A.; Lomeda, J. R.; Dimiev, A.; Price, B. K.; Tour, J. M., Longitudinal unzipping of carbon nanotubes to form graphene nanoribbons. *Nature* **2009,** *458* (7240), 872-876.

132. Dimiev, A. M.; Khannanov, A.; Vakhitov, I.; Kiiamov, A.; Shukhina, K.; Tour, J. M., Revisiting the mechanism of oxidative unzipping of multiwall carbon nanotubes to graphene nanoribbons. *ACS nano* **2018,** *12* (4), 3985-3993.

133. Cai, J.; Ruffieux, P.; Jaafar, R.; Bieri, M.; Braun, T.; Blankenburg, S.; Muoth, M.; Seitsonen, A. P.; Saleh, M.; Feng, X., Atomically precise bottom-up fabrication of graphene nanoribbons. *Nature* **2010,** *466* (7305), 470-473.

134. Zhang, Y.; Li, Z.; Kim, P.; Zhang, L.; Zhou, C., Anisotropic hydrogen etching of chemical vapor deposited graphene. *ACS nano* **2012,** *6* (1), 126-132.

135. Chen, B.; Huang, H.; Ma, X.; Huang, L.; Zhang, Z.; Peng, L.-M., How good can CVD-grown monolayer graphene be? *Nanoscale* **2014,** *6* (24), 15255-15261.

136. Speyer, L.; Fontana, S.; Cahen, S.; Hérold, C., Simple production of high-quality graphene foams by pyrolysis of sodium ethoxide. *Mater. Chem. Phys.* **2018,** *219*, 57-66.

137. Huang, H.; Chen, W.; Chen, S.; Wee, A. T. S., Bottom-up growth of epitaxial graphene on 6H-SiC (0001). *ACS nano* **2008,** *2* (12), 2513-2518.

138. Raccichini, R.; Varzi, A.; Passerini, S.; Scrosati, B., The role of graphene for electrochemical energy storage. *Nature materials* **2015,** *14* (3), 271-279.

139. Kim, C.; Kim, J. W.; Kim, H.; Kim, D. H.; Choi, C.; Jung, Y. S.; Park, J., Graphene oxide assisted synthesis of self-assembled zinc oxide for lithium-ion battery anode. *Chem. Mater.* **2016,** *28* (23), 8498-8503.

140. Sun, H.; Sun, X.; Hu, T.; Yu, M.; Lu, F.; Lian, J., Graphene-wrapped mesoporous cobalt oxide hollow spheres anode for high-rate and long-life lithium ion batteries. *J. Phys. Chem. C* **2014,** *118* (5), 2263-2272.

141. Liu, H.-p.; Wen, G.-w.; Bi, S.-f.; Wang, C.-y.; Hao, J.-m.; Gao, P., High rate cycling performance of nanosized Li4Ti5O12/graphene composites for lithium ion batteries. *Electrochim. Acta* **2016,** *192*, 38-44.

142. Zhang, J.; Cai, Y.; Wu, J.; Yao, J., Graphene oxide-confined synthesis of Li4Ti5O12 microspheres as high-performance anodes for lithium ion batteries. *Electrochim. Acta* **2015,** *165*, 422-429.

143. Tian, H.; Wang, T.; Zhang, F.; Zhao, S.; Wan, S.; He, F.; Wang, G., Tunable porous carbon spheres for high-performance rechargeable batteries. *J. Mater. Chem. A* **2018,** *6* (27), 12816-12841.

144. Zhong, Y.; Zhen, Z.; Zhu, H., Graphene: Fundamental research and potential applications. *FlatChem* **2017,** *4*, 20-32.

145. Ambrosi, A.; Chua, C. K.; Latiff, N. M.; Loo, A. H.; Wong, C. H. A.; Eng, A. Y. S.; Bonanni, A.; Pumera, M., Graphene and its electrochemistry–an update. *Chem. Soc. Rev.* **2016,** *45* (9), 2458-2493.

146. Han, T.-H.; Kim, H.; Kwon, S.-J.; Lee, T.-W., Graphene-based flexible electronic devices. *Materials Science and Engineering: R: Reports* **2017,** *118*, 1-43.

147. Chen, K.; Wang, Q.; Niu, Z.; Chen, J., Graphene-based materials for flexible energy storage devices. *Journal of energy chemistry* **2018,** *27* (1), 12-24.

148. Kairi, M. I.; Zuhan, M. K. N. M.; Khavarian, M.; Vigolo, B.; Bakar, S. A.; Mohamed, A. R., Co-synthesis of large-area graphene and syngas via CVD method from greenhouse gases. *Mater. Lett.* **2018,** *227*, 132-135.

149. Di Gaspare, L.; Scaparro, A.; Fanfoni, M.; Fazi, L.; Sgarlata, A.; Notargiacomo, A.; Miseikis, V.; Coletti, C.; De Seta, M., Early stage of CVD graphene synthesis on Ge (001) substrate. *Carbon* **2018,** *134*, 183-188.

150. Ge, X.; Zhang, Y.; Chen, L.; Zheng, Y.; Chen, Z.; Liang, Y.; Hu, S.; Li, J.; Sui, Y.; Yu, G., Mechanism of SiOx particles formation during CVD graphene growth on Cu substrates. *Carbon* **2018,** *139*, 989-998.

151. Bayev, V.; Fedotova, J.; Kasiuk, J.; Vorobyova, S.; Sohor, A.; Komissarov, I.; Kovalchuk, N.; Prischepa, S.; Kargin, N.; Andrulevičius, M., CVD graphene sheets electrochemically decorated with “core-shell” Co/CoO nanoparticles. *Appl. Surf. Sci.* **2018,** *440*, 1252-1260.

152. Dhall, S.; Kumar, M.; Bhatnagar, M.; Mehta, B., Dual gas sensing properties of graphene-Pd/SnO2 composites for H2 and ethanol: role of nanoparticles-graphene interface. *Int. J. Hydrogen Energy* **2018,** *43* (37), 17921-17927.

153. Yu, J.; Li, J.; Zhang, W.; Chang, H., Synthesis of high quality two-dimensional materials via chemical vapor deposition. *Chemical science* **2015,** *6* (12), 6705-6716.

154. Yan, Z.; Lin, J.; Peng, Z.; Sun, Z.; Zhu, Y.; Li, L.; Xiang, C.; Samuel, E. L.; Kittrell, C.; Tour, J. M., Toward the synthesis of wafer-scale single-crystal graphene on copper foils. *ACS nano* **2012,** *6* (10), 9110-9117.

155. Li, X.; Cai, W.; Colombo, L.; Ruoff, R. S., Evolution of graphene growth on Ni and Cu by carbon isotope labeling. *Nano Lett.* **2009,** *9* (12), 4268-4272.

156. López, G.; Mittemeijer, E., The solubility of C in solid Cu. *Scripta Mater.* **2004,** *51* (1), 1-5.

157. Muñoz, R.; Gómez-Aleixandre, C., Review of CVD synthesis of graphene. *Chem. Vap. Deposition* **2013,** *19* (10-11-12), 297-322.

158. Lenz-Solomun, P.; Wu, M.-C.; Goodman, D. W., Methane coupling at low temperatures on Ru (0001) and Ru (11 20) catalysts. *Catal. Lett.* **1994,** *25* (1-2), 75-86.

159. Reina, A.; Jia, X.; Ho, J.; Nezich, D.; Son, H.; Bulovic, V.; Dresselhaus, M. S.; Kong, J., Large area, few-layer graphene films on arbitrary substrates by chemical vapor deposition. *Nano Lett.* **2009,** *9* (1), 30-35.

160. Jerng, S.; Yu, D.; Kim, Y.; Ryou, J.; Hong, S.; Kim, C.; Yoon, S.; Efetov, D.; Kim, P.; Chun, S., Nanocrystalline graphite growth on sapphire by carbon molecular beam epitaxy. *J. Phys. Chem. C* **2011,** *115* (11), 4491-4494.

161. Kim, K.-B.; Lee, C.-M.; Choi, J., Catalyst-free direct growth of triangular nano-graphene on all substrates. *J. Phys. Chem. C* **2011,** *115* (30), 14488-14493.

162. Lee, C. M.; Choi, J., Direct growth of nanographene on glass and postdeposition size control. *Appl. Phys. Lett.* **2011,** *98* (18), 183106.

163. Zhang, L.; Shi, Z.; Wang, Y.; Yang, R.; Shi, D.; Zhang, G., Catalyst-free growth of nanographene films on various substrates. *Nano Res.* **2011,** *4* (3), 315-321.

164. Rummeli, M. H.; Bachmatiuk, A.; Scott, A.; Borrnert, F.; Warner, J. H.; Hoffman, V.; Lin, J.-H.; Cuniberti, G.; Buchner, B., Direct low-temperature nanographene CVD synthesis over a dielectric insulator. *ACS nano* **2010,** *4* (7), 4206-4210.

165. Ellis, B.; Makahnouk, W.; Makimura, Y.; Toghill, K.; Nazar, L., A multifunctional 3.5 V iron-based phosphate cathode for rechargeable batteries. *Nature materials* **2007,** *6* (10), 749-753.

166. Wadia, C.; Albertus, P.; Srinivasan, V., Resource constraints on the battery energy storage potential for grid and transportation applications. *J. Power Sources* **2011,** *196* (3), 1593-1598.

167. Ellis, B. L.; Makahnouk, W. M.; Rowan-Weetaluktuk, W.; Ryan, D.; Nazar, L. F., Crystal Structure and Electrochemical Properties of A2MPO4F Fluorophosphates (A= Na, Li; M= Fe, Mn, Co, Ni). *Chem. Mater.* **2010,** *22* (3), 1059-1070.

168. Ong, S. P.; Chevrier, V. L.; Hautier, G.; Jain, A.; Moore, C.; Kim, S.; Ma, X.; Ceder, G., Voltage, stability and diffusion barrier differences between sodium-ion and lithium-ion intercalation materials. *Energy Environ. Sci.* **2011,** *4* (9), 3680-3688.

169. Stevens, D.; Dahn, J., The mechanisms of lithium and sodium insertion in carbon materials. *J. Electrochem. Soc.* **2001,** *148* (8), A803.

170. Ge, P.; Fouletier, M., Electrochemical intercalation of sodium in graphite. *Solid State Ionics* **1988,** *28*, 1172-1175.

171. Kang, H.; Liu, Y.; Cao, K.; Zhao, Y.; Jiao, L.; Wang, Y.; Yuan, H., Update on anode materials for Na-ion batteries. *J. Mater. Chem. A* **2015,** *3* (35), 17899-17913.

172. Wen, Y.; He, K.; Zhu, Y.; Han, F.; Xu, Y.; Matsuda, I.; Ishii, Y.; Cumings, J.; Wang, C., Expanded graphite as superior anode for sodium-ion batteries. *Nat. Commun.* **2014,** *5* (1), 1-10.

173. Cao, Y.; Xiao, L.; Sushko, M. L.; Wang, W.; Schwenzer, B.; Xiao, J.; Nie, Z.; Saraf, L. V.; Yang, Z.; Liu, J., Sodium ion insertion in hollow carbon nanowires for battery applications. *Nano Lett.* **2012,** *12* (7), 3783-3787.

174. Liu, Y.; Merinov, B. V.; Goddard, W. A., Origin of low sodium capacity in graphite and generally weak substrate binding of Na and Mg among alkali and alkaline earth metals. *Proceedings of the National Academy of Sciences* **2016,** *113* (14), 3735-3739.

175. Simone, V.; Boulineau, A.; de Geyer, A.; Rouchon, D.; Simonin, L.; Martinet, S., Hard carbon derived from cellulose as anode for sodium ion batteries: Dependence of electrochemical properties on structure. *Journal of energy chemistry* **2016,** *25* (5), 761-768.

176. Stevens, D.; Dahn, J., High capacity anode materials for rechargeable sodium-ion batteries. *J. Electrochem. Soc.* **2000,** *147* (4), 1271.

177. Ponrouch, A.; Goñi, A.; Palacin, M. R., High capacity hard carbon anodes for sodium ion batteries in additive free electrolyte. *Electrochem. Commun.* **2013,** *27,* 85-88.

178. Jin, B.; Gao, F.; Zhu, Y.-F.; Lang, X.-Y.; Han, G.-F.; Gao, W.; Wen, Z.; Zhao, M.; Li, J.-C.; Jiang, Q., Facile synthesis of non-graphitizable polypyrrole-derived carbon/carbon nanotubes for lithium-ion batteries. *Scientific Reports* **2016,** *6*, 19317.

179. Irisarri, E.; Ponrouch, A.; Palacin, M., Hard carbon negative electrode materials for sodium-ion batteries. *J. Electrochem. Soc.* **2015,** *162* (14), A2476.

180. Doeff, M. M.; Ma, Y.; Visco, S. J.; De Jonghe, L. C., Electrochemical insertion of sodium into carbon. *J. Electrochem. Soc.* **1993,** *140* (12), L169.

181. Alcántara, R.; Jiménez-Mateos, J. M.; Lavela, P.; Tirado, J. L., Carbon black: a promising electrode material for sodium-ion batteries. *Electrochem. Commun.* **2001,** *3* (11), 639-642.

182. Alcántara, R.; Lavela, P.; Ortiz, G. F.; Tirado, J. L., Carbon microspheres obtained from resorcinol-formaldehyde as high-capacity electrodes for sodium-ion batteries. *Electrochemical and Solid State Letters* **2005,** *8* (4), A222.

183. Wenzel, S.; Hara, T.; Janek, J.; Adelhelm, P., Room-temperature sodium-ion batteries: improving the rate capability of carbon anode materials by templating strategies. *Energy Environ. Sci.* **2011,** *4* (9), 3342-3345.

184. Myung, S. T.; Takahashi, N.; Komaba, S.; Yoon, C. S.; Sun, Y. K.; Amine, K.; Yashiro, H., Nanostructured TiO2 and Its Application in Lithium-Ion Storage. *Adv. Funct. Mater.* **2011,** *21* (17), 3231-3241.

185. Chen, J. S.; Luan, D.; Li, C. M.; Boey, F. Y. C.; Qiao, S.; Lou, X. W., TiO 2 and SnO 2@ TiO 2 hollow spheres assembled from anatase TiO 2 nanosheets with enhanced lithium storage properties. *Chem. Commun.* **2010,** *46* (43), 8252-8254.

186. Chen, Z.; Belharouak, I.; Sun, Y. K.; Amine, K., Titanium-based anode materials for safe lithium-ion batteries. *Adv. Funct. Mater.* **2013,** *23* (8), 959-969.

187. Yang, Z.; Choi, D.; Kerisit, S.; Rosso, K. M.; Wang, D.; Zhang, J.; Graff, G.; Liu, J., Nanostructures and lithium electrochemical reactivity of lithium titanites and titanium oxides: A review. *J. Power Sources* **2009,** *192* (2), 588-598.

188. Xu, Y.; Lotfabad, E. M.; Wang, H.; Farbod, B.; Xu, Z.; Kohandehghan, A.; Mitlin, D., Nanocrystalline anatase TiO 2: a new anode material for rechargeable sodium ion batteries. *Chem. Commun.* **2013,** *49* (79), 8973-8975.

189. Wu, L.; Buchholz, D.; Bresser, D.; Chagas, L. G.; Passerini, S., Anatase TiO2 nanoparticles for high power sodium-ion anodes. *J. Power Sources* **2014,** *251*, 379-385.

190. Yabuuchi, N.; Kubota, K.; Dahbi, M.; Komaba, S., Research development on sodium-ion batteries. *Chem. Rev.* **2014,** *114* (23), 11636-11682.

191. Senguttuvan, P.; Rousse, G.; Seznec, V.; Tarascon, J.-M.; Palacin, M. R., Na2Ti3O7: lowest voltage ever reported oxide insertion electrode for sodium ion batteries. *Chem. Mater.* **2011,** *23* (18), 4109-4111.

192. Yang, D.; Zheng, Z.; Liu, H.; Zhu, H.; Ke, X.; Xu, Y.; Wu, D.; Sun, Y., Layered titanate nanofibers as efficient adsorbents for removal of toxic radioactive and heavy metal ions from water. *J. Phys. Chem. C* **2008,** *112* (42), 16275-16280.

193. Chiba, K.; Kijima, N.; Takahashi, Y.; Idemoto, Y.; Akimoto, J., Synthesis, structure, and electrochemical Li-ion intercalation properties of Li2Ti3O7 with Na2Ti3O7-type layered structure. *Solid State Ionics* **2008,** *178* (33-34), 1725-1730.

194. Rudola, A.; Saravanan, K.; Mason, C. W.; Balaya, P., Na 2 Ti 3 O 7: an intercalation based anode for sodium-ion battery applications. *J. Mater. Chem. A* **2013,** *1* (7), 2653-2662.

195. Xu, J.; Ma, C.; Balasubramanian, M.; Meng, Y. S., Understanding Na 2 Ti 3 O 7 as an ultra-low voltage anode material for a Na-ion battery. *Chem. Commun.* **2014,** *50* (83), 12564-12567.

196. Shirpour, M.; Cabana, J.; Doeff, M., New materials based on a layered sodium titanate for dual electrochemical Na and Li intercalation systems. *Energy Environ. Sci.* **2013,** *6* (8), 2538-2547.

197. Rudola, A.; Saravanan, K.; Devaraj, S.; Gong, H.; Balaya, P., Na 2 Ti 6 O 13: a potential anode for grid-storage sodium-ion batteries. *Chem. Commun.* **2013,** *49* (67), 7451-7453.

198. Liang, Z.; Hui-Lin, P.; Yong-Sheng, H.; Hong, L.; Li-Quan, C., Spinel lithium titanate (Li4Ti5O12) as novel anode material for room-temperature sodium-ion battery. *Chinese Physics B* **2012,** *21* (2), 028201.

199. Sun, Y.; Zhao, L.; Pan, H.; Lu, X.; Gu, L.; Hu, Y.-S.; Li, H.; Armand, M.; Ikuhara, Y.; Chen, L., Direct atomic-scale confirmation of three-phase storage mechanism in Li 4 Ti 5 O 12 anodes for room-temperature sodium-ion batteries. *Nat. Commun.* **2013,** *4* (1), 1-10.

200. Zhao, F.; Xue, P.; Ge, H.; Li, L.; Wang, B., Na-doped Li4Ti5O12 as an anode material for sodium-ion battery with superior rate and cycling performance. *J. Electrochem. Soc.* **2016,** *163* (5), A690.

201. Gao, L.; Wang, L.; Dai, S.; Cao, M.; Zhong, Z.; Shen, Y.; Wang, M., Li4Ti5O12-TiO2 nanowire arrays constructed with stacked nanocrystals for high-rate lithium and sodium ion batteries. *J. Power Sources* **2017,** *344*, 223-232.

202. Xu, G.; Tian, Y.; Wei, X.; Yang, L.; Chu, P. K., Free-standing electrodes composed of carbon-coated Li4Ti5O12 nanosheets and reduced graphene oxide for advanced sodium ion batteries. *J. Power Sources* **2017,** *337*, 180-188.

203. Son, I. H.; Park, J. H.; Park, S.; Park, K.; Han, S.; Shin, J.; Doo, S.-G.; Hwang, Y.; Chang, H.; Choi, J. W., Graphene balls for lithium rechargeable batteries with fast charging and high volumetric energy densities. *Nat. Commun.* **2017,** *8* (1), 1-11.

204. Opra, D. P.; Gnedenkov, S. V.; Sinebryukhov, S. L., Recent efforts in design of TiO2 (B) anodes for high-rate lithium-ion batteries: A review. *J. Power Sources* **2019,** *442*, 227225.

205. Liu, J.; Liu, Y.; Hou, M.; Wang, Y.; Wang, C.; Xia, Y., Li2TiSiO5 and expanded graphite nanocomposite anode material with improved rate performance for lithium-ion batteries. *Electrochim. Acta* **2018,** *260*, 695-702.

206. Zhou, L.; Zhang, K.; Hu, Z.; Tao, Z.; Mai, L.; Kang, Y. M.; Chou, S. L.; Chen, J., Recent Developments on and Prospects for Electrode Materials with Hierarchical Structures for Lithium-Ion Batteries. *Adv. Energy Mater.* **2018,** *8* (6), 1701415.

207. Jin, L.; Gong, R.; Zheng, J.; Zhang, C.; Xia, Y.; Zheng, J. P., Fabrication of Dual-Modified Carbon Network Enabling Improved Electronic and Ionic Conductivities for Fast and Durable Li2TiSiO5 Anodes. *ChemElectroChem* **2019,** *6* (12), 3020-3029.

208. Wang, S.; Wang, R.; Bian, Y.; Jin, D.; Zhang, Y.; Zhang, L., In-situ encapsulation of pseudocapacitive Li2TiSiO5 nanoparticles into fibrous carbon framework for ultrafast and stable lithium storage. *Nano Energy* **2019,** *55*, 173-181.

209. Jin, L.; Gong, R.; Zhang, W.; Xiang, Y.; Zheng, J.; Xiang, Z.; Zhang, C.; Xia, Y.; Zheng, J. P., Toward high energy-density and long cycling-lifespan lithium ion capacitors: a 3D carbon modified low-potential Li 2 TiSiO 5 anode coupled with a lignin-derived activated carbon cathode. *J. Mater. Chem. A* **2019,** *7* (14), 8234-8244.

210. Yi, T.-F.; Yang, S.-Y.; Xie, Y., Recent advances of Li 4 Ti 5 O 12 as a promising next generation anode material for high power lithium-ion batteries. *J. Mater. Chem. A* **2015,** *3* (11), 5750-5777.

211. Nozawa, K.; Gailhanou, H.; Raison, L.; Panizza, P.; Ushiki, H.; Sellier, E.; Delville, J.; Delville, M., Smart control of monodisperse Stöber silica particles: effect of reactant addition rate on growth process. *Langmuir* **2005,** *21* (4), 1516-1523.

212. Zhao, L.; Yu, J.-G.; Cheng, B.; Zhao, X.-J., Preparation and formation mechanisms of monodispersed silicon dioxide spherical particles. *Acta Chim. Sin.* **2003,** *61* (4), 562-566.

213. Wu, J.-B.; Lin, M.-L.; Cong, X.; Liu, H.-N.; Tan, P.-H., Raman spectroscopy of graphene-based materials and its applications in related devices. *Chem. Soc. Rev.* **2018,** *47* (5), 1822-1873.

214. Ziadi, A.; Thiele, G.; Elouadi, B., The crystal structure of Li2TiSiO5. *J. Solid State Chem.* **1994,** *109* (1), 112-115.

215. Brassard, D.; Sarkar, D.; El Khakani, M.; Ouellet, L., Tuning the electrical resistivity of pulsed laser deposited TiSiO x thin films from highly insulating to conductive behaviors. *Appl. Phys. Lett.* **2004,** *84* (13), 2304-2306.

216. Zhang, J.; Grabstanowicz, L. R.; Gao, S.; Hosmane, N. S.; Huang, B.; Dai, Y.; Liu, D.-j.; Xu, T., Visible-light photocatalytic SiO 2/TiO 2− x C x/C nanoporous composites using TiCl 4 as the precursor for TiO 2 and polyhydroxyl tannin as the carbon source. *Catal. Sci. Technol.* **2012,** *2* (2), 390-399.

217. Chen, C.; Yu, D.; Zhao, G.; Du, B.; Tang, W.; Sun, L.; Sun, Y.; Besenbacher, F.; Yu, M., Three-dimensional scaffolding framework of porous carbon nanosheets derived from plant wastes for high-performance supercapacitors. *Nano Energy* **2016,** *27*, 377-389.

218. Liu, B.; Liu, Y.; Chen, H.; Yang, M.; Li, H., Oxygen and nitrogen co-doped porous carbon nanosheets derived from Perilla frutescens for high volumetric performance supercapacitors. *J. Power Sources* **2017,** *341*, 309-317.

219. Bredar, A. R.; Chown, A. L.; Burton, A. R.; Farnum, B. H., Electrochemical Impedance Spectroscopy of Metal Oxide Electrodes for Energy Applications. *ACS Appl. Mater.* **2020**.

220. Shen, L.; Liu, F.; Chen, G.; Zhou, H.; Le, Z.; Wu, H. B.; Wang, G.; Lu, Y., Encapsulation of SnO 2 nanocrystals into hierarchically porous carbon by melt infiltration for high-performance lithium storage. *J. Mater. Chem. A* **2016,** *4* (48), 18706-18710.

221. Billaud, J.; Bouville, F.; Magrini, T.; Villevieille, C.; Studart, A. R., Magnetically aligned graphite electrodes for high-rate performance Li-ion batteries. *Nat. Energy* **2016,** *1* (8), 1-6.

222. Ma, J.; Wei, Y.; Gan, L.; Wang, C.; Xia, H.; Lv, W.; Li, J.; Li, B.; Yang, Q.-H.; Kang, F., Abundant grain boundaries activate highly efficient lithium ion transportation in high rate Li 4 Ti 5 O 12 compact microspheres. *J. Mater. Chem. A* **2019,** *7* (3), 1168-1176.

223. Ren, J.; Ming, H.; Jia, Z.; Zhang, Y.; Ming, J.; Zhou, Q.; Zheng, J., High Tap Density Li4Ti5O12 Microspheres: Synthetic Conditions and Advanced Electrochemical Performance. *Energy Technol.* **2017,** *5* (9), 1680-1686.

224. Zheng, L.; Wang, X.; Xia, Y.; Xia, S.; Metwalli, E.; Qiu, B.; Ji, Q.; Yin, S.; Xie, S.; Fang, K., Scalable in situ synthesis of Li4Ti5O12/carbon nanohybrid with supersmall Li4Ti5O12 nanoparticles homogeneously embedded in carbon matrix. *ACS Appl. Mater. Interfaces* **2018,** *10* (3), 2591-2602.

225. Huang, C.; Young, N. P.; Zhang, J.; Snaith, H. J.; Grant, P. S., A two layer electrode structure for improved Li ion diffusion and volumetric capacity in Li ion batteries. *Nano Energy* **2017,** *31*, 377-385.

226. Hong, Z.; Hong, J.; Xie, C.; Huang, Z.; Wei, M., Hierarchical rutile TiO2 with mesocrystalline structure for Li-ion and Na-ion storage. *Electrochim. Acta* **2016,** *202*, 203-208.

227. Li, Y.; Wang, S.; He, Y.-B.; Tang, L.; Kaneti, Y. V.; Lv, W.; Lin, Z.; Li, B.; Yang, Q.-H.; Kang, F., Li-ion and Na-ion transportation and storage properties in various sized TiO 2 spheres with hierarchical pores and high tap density. *J. Mater. Chem. A* **2017,** *5* (9), 4359-4367.

228. Qiu, J.; Lai, C.; Wang, Y.; Li, S.; Zhang, S., Resilient mesoporous TiO2/graphene nanocomposite for high rate performance lithium-ion batteries. *Chem. Eng. J.* **2014,** *256*, 247-254.

229. Liu, J.; Liu, Y.; Wang, Y.; Wang, C.; Xia, Y., Li/Na Ion Intercalation Process into Sodium Titanosilicate as Anode Material. *Batteries & Supercaps* **2019,** *2* (10), 867-873.

230. He, D.; Wu, T.; Wang, B.; Yang, Y.; Zhao, S.; Wang, J.; Yu, H., Novel Na 2 TiSiO 5 anode material for lithium ion batteries. *Chem. Commun.* **2019,** *55* (15), 2234-2237.

231. Ding, J.; Li, Y.; Wu, Q.; Long, Q.; Wang, Y.; Wang, Y., A novel self-activated white-light-emitting phosphor of Na 2 TiSiO 5 with two Ti sites of TiO 5 and TiO 6. *RCS Adv.* **2016,** *6* (11), 8605-8611.

232. Moazzen, M. A. M.; Borghei, S. M.; Taleshi, F., Change in the morphology of ZnO nanoparticles upon changing the reactant concentration. *Applied Nanoscience* **2013,** *3* (4), 295-302.